Dissertation
submitted to the
Combined Faculties for the Natural Sciences and for Mathematics
of the Ruperto-Carola University of Heidelberg, Germany
for the degree of
Doctor of Natural Sciences

Presented by
Master of Science: Zhuhua Cheng
born in Shangdong, China

Oral examination: 16th June, 2004

Characterization of Water Flow and Solute Transport in Coarse Textured Materials

Referees: Prof. Dr. Kurt Roth
Prof. Dr. William Shotyk

Zusammenfassung

In der vorliegenden Arbeit wurden verschiedene grob texturierte Materialien hinsichtlich ihrer hydraulischen Eigenschaften und ihrer Transporteigenschaften untersucht. Durch die Inversion eines Multi-Step Outflow Experiments konnten die hydraulischen Eigenschaften bestimmt werden. Die Anwendbarkeit dieser Methode wurde durch die Analyse der Differenzen zwischen gemessenen und simulierten Werten, der Konfidenzintervalle und Korrelationsmatrix der bestimmten Parameter und der χ^2-Flächen der modellierten Ausflussdaten bewertet. Für Feinsand und Grobsand zeigte das Modell die größten Abweichungen im Zustand hoher Wassersättigungen. Die weniger empfindlichen Parameter K_s und τ können durch Inversion nicht gut bestimmt werden. Bimodale hydraulische Modelle ergaben eine bessere Anpassung an die Ausflusskurve des Mischmaterials aufgrund ihrer höheren Flexibilität. In einer abschließenden Diskussion werden die Abweichungen des Modells darauf zurückgeführt, dass die experimentellen Bedingungen nicht in der Lage sind, die Voraussetzungen des Prozessmodells, der Richards-Gleichung, zu erfüllen. Außerdem war die Parameterisierung der hydraulischen Eigenschaften ungeeignet. Durch stationäre Transportexperimente bei zwei verschiednen, konstanten Fließraten wurde der Stofftransport durch die grob strukturierten Materialien untersucht. Bei diesen Experimenten wurden asymmetrische Durchbruchskurven beobachtet. Das "hysteretische" Verhalten im Transportprozess sowie der Einfluss der Strömungsgeschwindigkeit auf die Wechselwirkung zwischen gelöstem Stoff und Matrix wurde ebenfalls untersucht und die beteiligten Modelle mit Hilfe berechneter Güteparameter der Simulationen beurteilt.

Summary

In the present work, several coarse textured materials were investigated with respect to their hydraulic and transport properties. Hydraulic properties were estimated using a state-of-the-art method: the inversion of multi-step outflow experiments. The applicability of the adopted method is evaluated through analysis of the structure of the residuals, the parameter confidence interval and correlation matrix, and the χ^2 surfaces for outflow. The model errors are larger at higher saturations than those at lower saturations for the fine sand and the coarse sand. The insensitive parameters like K_s and τ cannot be determined correctly by inversion of the currently used experiments. With higher flexibility, bimodal hydraulic models yielded a better fit for the outflow for the mixed material. In a final discussion, the deviations of the model from the measurements were attributed to the experimental conditions that could not satisfy the assumptions of the process model, Richards equation, and the unsuitable parametric model for hydraulic properties. Through stationary breakthrough

experiments at two distinct fluxes, solute transport through the coarse textured materials were investigated and asymmetric breakthrough curves were obtained. The "hysteresis" phenomenon in transport process and influence of the flow rate on the interaction between the solute and the matrix were analyzed and the models were evaluated with the calculated goodness-of-fit.

Contents

1 Introduction **1**

1.1 Objective of this Study 2

1.2 Outline of this Thesis 3

2 The Method of Inverse Modeling **5**

2.1 Fundamental Theory–Buckingham-Darcy's Law and Richards Equation 5

2.2 Parameterization of Hydraulic Properties 8

2.2.1 Parameterization of unsaturated hydraulic conductivity . . . 8

2.2.2 Parameterization of water characteristic 9

2.3 Outflow Experiments and Inverse Modeling 13

2.3.1 One-step method and the nonuniqueness problem 13

2.3.2 multi-step method 14

2.3.3 Pressure and suction desorption in outflow experiments . . . 15

2.3.4 Posedness of the inverse modeling 15

3 Materials and Methods **17**

3.1 Materials 17

3.1.1 Grain size distribution 17

3.1.2 Total porosity 18

3.1.3 Saturation hydraulic conductivity 18

3.1.4 pH value 20

3.2 Experimental Setup and Measurement Procedure for MSO Experiment 21

3.2.1 Experimental setup 21

3.2.2 Measurement procedure 22

3.3 Formulation of the Inverse Problem 23

3.4 Experimental Setup and Measurement Procedure for Transport Experiment 24

3.4.1 Experimental setup 24

3.4.2 Sprinkler 25

3.4.3 Pump and balance–the flux control unit 25

3.4.4 Stationary transport experiment with the tracer–Brilliant Blue 26

4 Estimation of Hydraulic Parameters from MSO Experiments by Inversion 29
4.1 The Coarse Sand 29
4.2 The Fine Sand 36
4.3 The Mixed Material 41
4.4 Sources for the Deviation between Simulations and Measurements . 46
4.4.1 From Navier-Stokes equation to Darcy's law–the effect of simplification 46
4.4.2 Multiphase phenomena 49
4.4.3 Dynamic effect in the capillary pressure-saturation relationship 50
4.4.4 Heterogeneity 51
4.4.5 Parameterizations of hydraulic properties 53
4.5 Summary 54

5 Single Phase Chemical Transport through Coarse Materials with Stationary Water Flux 55
5.1 Transport Models Employed 55
5.1.1 The convection-dispersion model 55
5.1.2 The mobile-immobile Model 57
5.1.3 Solute transport process with linear kinetic interaction 58
5.2 Fitting of Model Functions 58
5.2.1 Characterization of BTCs of Brilliant Blue through the coarse media 60
5.2.2 Performance of the CD model and the MIM model in fitting BTCs of Brilliant Blue 62
5.2.3 Effect of flow rate on the interaction between Brilliant Blue and the porous media 62
5.2.4 Solute breakthrough and elution 65
5.2.5 Fitting with different models 68
5.2.6 Dye transport with low flow rate through the fine sand column 74
5.2.7 Confidence intervals for estimated parameters and estimation of goodness-of-fit for the model 74
5.3 Summary 77

6 Summary and Outlook 79
6.1 Hydraulic Parameter Estimation with Inversion 79
6.2 Transport Behavior of Brilliant Blue with Stationary Water Flux . . 80
6.3 Outlook 81

Bibliography **83**

Appendix **A–6**

List of Figures

2.1 Flow chart of inverse parameter estimation approach 6

3.1 Sketch of falling head permeameter. 19
3.2 Experimental setup of MSO measurement 21
3.3 Experimental setup for transport measurement 24
3.4 Distribution of needles on the sprinkler 25
3.5 Measured adsorption isotherm of the fine sand with linear sorption isotherm. 28

4.1 Simulated outflow curve with K_s fitted compared with the measured outflow curve with the coarse sand 30
4.2 Simulated outflow curve with K_s fixed compared with the measurement with the coarse sand. 31
4.3 χ^2 surfaces for the coarse sand 33
4.4 χ^2 surface for cumulative outflow in the θ_s-τ-K_s three dimensional space for the coarse sand 35
4.5 Reproducibility of multi-step outflow experiments with the fine sand—the outflow curves 36
4.6 Hydraulic functions estimated from two MSO repeats with the fine sand 37
4.7 Simulated outflow curve with K_s fixed compared with the measurement for the fine sand 38
4.8 χ^2 surfaces for the fine sand 39
4.9 Simulated outflow curves with unimodal and bimodal hydraulic functions for the mixed material 42
4.10 Estimated hydraulic functions for the mixed material 42
4.11 Equivalent pore size distribution of the mixed material 43
4.12 χ^2 surfaces for the mixed material 45
4.13 Fluid velocity calculated for the coarse sand 49
4.14 REV concept 52
4.15 Effect of local heterogeneity 52

4.16 Sketch of possible sources for deviation between the model and measurement 53

5.1 CD model with different boundary conditions 59
5.2 Breakthrough limb of BTCs of Brilliant Blue effluent for different materials under different flow rates 61
5.3 Measured versus simulated relative concentration of Brilliant Blue effluent from the fine sand column under high flow rate condition using the CD model and the MIM model 62
5.4 Deviations of the simulated and the measured Brilliant Blue concentration in the effluent from the fine sand column under high flow rate–comparison of performance of the MIM and CD models 63
5.5 Sketch of distinct flow regions under different flow rates for steady state flow 64
5.6 Breakthrough and elution limbs of a BTC for Brilliant Blue effluent from the coarse sand column 65
5.7 Fits of the breakthrough limb (left) and the elution limb (right) of the BTC for Brilliant Blue effluent from the **mixed material** column at high flow rate with the cdfts-rl model and the residual curves 66
5.8 Fits of the breakthrough limb (left) and the elution limb (right) of the BTC for Brilliant Blue effluent from the **fine sand** column at high flow rate with the cdfts-rl model fixed 67
5.9 Fits of the breakthrough limb (left) and the elution limb (right) of the BTC for Brilliant Blue effluent from the **coarse sand** column at high flow rate with the cdfts-rl model and C_0 fixed 67
5.10 Fits of the breakthrough limb (left) and the elution limb (right) of the BTC for Brilliant Blue effluent from the **gravel** column at high flow rate with the cdfts-rl model and initial concentration fixed at C_0 67
5.11 Illustration of the differences in solute breakthrough and elution during application of a pulse of solute flux 69
5.12 Generation of input data for the cdftd-rl model, mixed material . . . 70
5.13 Fitting the cdftp-rl model to the BTC of Brilliant Blue effluent from the gravel column with high flow rate, initial concentration is fitted and the sensitivity of the parameters 71
5.14 Parameter obtained using different flux concentration input for the gravel at high flow rate 72
5.15 Fits of the breakthrough limb (left) and the elution limb (right) of the BTC for Brilliant Blue effluent from the mixed material column at high flow rate with the cdftd-rl model and C_0 fixed 73

5.16 Parameters obtained using different flux concentration input for the mixed material at high flow rate 73
5.17 Dye transport through the fine sand column with low flow rate, fitted with the cdfts model with C_0 fitted and the cdfts-rl model with C_0 fixed 74

A–1 Fit of the whole BTC for Brilliant Blue effluent from the coarse sand column at high flow rate with the cdftp-rl model, C_0 fixed A–1
A–2 Fits of the breakthrough limb (left) and the elution limb (right) of the BTC for Brilliant Blue effluent from the coarse sand column at high flow rate with the cdftd-rl model C_0 fixed—more noises generated especially for the breakthrough limb A–1
A–3 Fit of the breakthrough limb of the BTC for Brilliant Blue effluent from the coarse sand column at low flow rate with the cdfts-rl model C_0 fixed, the solid line denoting the input concentration A–2
A–4 Fit of the breakthrough limb of the BTC for Brilliant Blue effluent from the gravel column at low flow rate with the cdfts-rl model, C_0 fixed A–2
A–5 Fit of the elution limb of the BTC for Brilliant Blue effluent from the gravel column at low flow rate with the cdfts-rl model, C_0 fixed . . . A–3
A–6 Fit of the whole BTC for Brilliant Blue effluent from the mixed material column at low flow rate with the cdftp-rl model, C_0 fixed, solid line denoting the input concentration and the disturbance are caused by external disturbance A–3
A–7 Fit of the breakthrough limb (left) and the elution limb (right) of the BTC for Brilliant Blue effluent from the gravel column at high flow rate with the cdftd-rl model, C_0 fixed A–4
A–8 Dye transport in the mixed material with low flow rate, fitted with cdfts-rl model, C_0 fitted A–4
A–9 Dye transport in the mixed material with high flow rate, deviations of the MIM and CD model from the measurement, C_0 fitted A–5
A–10 Measured versus simulated relative concentration of Brilliant Blue effluent from the mixed material column under high flow rate condition using the CD model and the MIM model A–5

List of Tables

3.1 Grain size distribution (by weight) of the gravel, coarse sand and mixed material 18
3.2 Some independently measured material properties 20

4.1 Estimated MvG parameters for the coarse sand with Ks fitted and fixed 30
4.2 Optimized MvG parameters with K_s fitted for the coarse sand. . . 32
4.3 Correlation matrix for optimized MvG parameters with K_s fitted for the coarse sand 34
4.4 Estimated MvG parameters for the fine sand with K_s fixed 37
4.5 Correlation matrix for estimated MvG parameters for the fine sand with K_s fixed 38
4.6 Effect of data selection on the parameter estimation. 40
4.7 Estimated MvG parameters for the mixed material using the bimodal model with K_s fixed 44
4.8 Correlation matrix for the optimized MvG parameters with K_s fixed for the mixed material 44

5.1 Estimated Parameters with cdfts-rl model for the rate limited interaction model for the four materials under different flow rates 63
5.2 Comparison of Parameters estimated with the cdfts-rl model for the breakthrough and elution limbs of BTCs of Brilliant Blue under high flow rate 66
5.3 Statistical information excerpted from output of Levenberg-Marquardt algorithm on parameters estimated from fit of a BTC of Brilliant Blue effluent from the gravel column at high flow rate with cdfts-rl model 75
5.4 Correlation matrix for the optimized parameters from a fit of the BTC of Brilliant Blue effluent from the gravel column at high flow rate with cdfts-rl model 75
5.5 Calculated Goodness-of-Fit for Different Models ("/": concentration data not available; "†": value is too small) 76

1 Introduction

Elucidating and quantifying water flow and solute transport in variably saturated porous media is a strong emphasis in many scientific disciplines and management applications which still remains an important challenge. The intricate task in such research is to acquire knowledge of hydraulic properties, namely the water characteristic function $\theta(\psi)$ and the hydraulic conductivity function $K(\theta)$, both of which are highly nonlinear functions of pressure head and water content, respectively.

Currently, many laboratory and field methods exist to determine the hydraulic properties represented by these two functions. The traditional direct measurements in laboratory with hanging water column, a pressure membrane, or equilibration over salt solutions require restrictive initial and boundary conditions and are time consuming, range-limited and expensive (Jury et al. 1991). Advanced methods introduce new technical apparatus such as Nuclear Magnetic Resonance Imaging (NMRI), X-ray computed tomography (CT), Time Domain Reflectometry (TDR), and Ground-Penetrating Radar (GPR) to measure water content at different scales. Both CT and NMRI can be applied to the direct 3-D measurement of flow at micro-scale. These high resolution measurements provide the possibility to resolve the individual pores and to delineate air-water interfacial contacts (Rogasik et al. 1999, Wildenschild et al. 2002, Dijk and Berkowitz 1999). TDR and GPR methods are applications of electromagnetic waves in the same frequency range. TDR is usually used at small scale, localized and non-destructive measurements with high resolution (Robinson et al. 2003) and GPR yields 2-D profiles and can measure water content at larger scale non-destructively. According to a recent report, GPR even shows the potential to detect the heterogeneity of structure and water content in small scale (Stoffregen et al. 2002). Combinations of these techniques with tensiometer measurement will eventually yield water retention data.

In many applications such as land mapping, the direct measurement of hydraulic properties in laboratory and field is time-consuming, costly, hence next to impossible. Since the resolution of the measurement is not high in such case, as an alternative to direct methods, an indirect method is introduced to deduce hydraulic properties from other soil properties like bulk density, fraction of silt, clay, organic matter etc.using purely statistical regression analysis, which is so-called pedotransfer func-

tion method (PTFs). By analysing existing databases containing measured data, hydraulic characteristics are predicted from measured soil data. Good predictions instead of direct measurements may be accurate enough for such applications.

Since $K(\theta)$ varies drastically, usually several orders of magnitude over narrow water content range, the precise and fast measurement is even more difficult than that of water retention.

With the aid of improved computing power, the inverse technique is now widely used to determine hydraulic parameters by matching observations and simulation results for a particular unsaturated event using a parameter optimization code. The inverse method is a parameter estimation technique that involves the indirect estimation of soil physical properties by repeated numerical solution of the governing transient flow equation. In this procedure, first of all, the water dynamics of the system is assumed to be adequately described, e.g. by Richards equation. Then soil hydraulic functions, which are needed to predict the flow behavior of the system, are expressed by analytical models with yet unknown parameter values. To determine these unknown parameters, an outflow experiment is set up under controlled initial and boundary conditions. During the experiment one or more flow-controlled variables are measured. Subsequently, the Richards equation is solved numerically using the parameterized hydraulic functions with initial estimates for their parameters. These parameters are optimized by minimization of an objective function containing the sums of squared deviations between observed and predicted flow variables, using repeated numerical simulation of the flow process (Hopmans and Šimůnek 1999). Two attractive features of the evaluation of outflow/inflow experiments by inverse modeling are that experimentation and modeling goes hand-in-hand and $\theta(\psi)$ and $K(\theta)$ can be estimated from one single experiment. The method yields not only hydraulic parameters, but provides at the same time a plausibility control for the whole measurement process (Durner et al. 1999b).

1.1 Objective of this Study

Inverse modeling in combination with multi-step outflow (MSO) experiments have been widely used to estimate hydraulic parameters of porous media. However, at the same time, issues such as posedness of the problem and dynamic effects problem emerged. Some phenomena are still not understood well. While previous work has mainly studied natural soils and fine sand, little effort has been spent on the applicability of the MSO method to identify hydraulic parameters of coarse media. Coarse materials like sand or even gravel are often included in environmental or engineered structures like road covers or disposal sites and they are an important component of many fluvial deposits. Water flow and chemical transport in such

media account for much of the environmental and engineering quality. In order to predict water flow and solute transport in such porous media, material properties like hydraulic conductivity or dispersion characteristics must be known. This work is a small part of BMBF-verbund-Forschungsvorhaven "Sickerwasserprognose". The coarse textured materials are taken from this project. Using the multi-step outflow experimental setup, this work follows two parallel lines. One is to investigate the possibility of identifying hydraulic parameters of such coarse textured media from inverse modeling of the outflow and tensiometer data of MSO measurements. On this line, the work will look closely at the magnitude and structure of the model errors and the possible sources for these errors specially for the coarse materials. The other line is the study of transport properties of the coarse materials which will focus on whether Brilliant Blue, known as a cost-effective tracer, can be used to study transport properties of these materials and whether the conventional transport models are sufficient to describe the breakthrough curves of Brilliant Blue.

1.2 Outline of this Thesis

The remainder of this thesis is organized as follows: In the following chapter 2, an overview of the theoretical background of the inverse method used in this work is given. First, in section 2.1, the conventional fundamental theory for the inverse modeling applied in this work is reviewed. In the following section 2.2 the frequently used parameterization models of hydraulic properties are given. In section 2.3, the one-step and multi-step outflow methods and the related posedness problem of the inverse modeling are reviewed.

Material information and detailed method descriptions are given in chapter 3. Here, the related material properties measured independently are listed. Experimental setup and measurement procedures of the MSO experiments and transport experiments are described.

MSO experiments with these coarse materials have been carried out and results are shown in chapter 4. The first three sections show the simulated outflow data with hydraulic parameters estimated from the inverse modeling in comparison with those measured data and especially the residuals of the inverse simulation are plotted and scrutinized. Parameter identifiability with the combination of MSO and inverse methods is evaluated by examining the χ^2 surfaces for outflow in different parameter combination planes. In section 4.4, the possible sources for model errors are discussed in detail.

Chapter 5 investigates Brilliant Blue transport with stationary water flux through these coarse materials. Section 5.1 describes the models employed including the conventional convection-dispersion (CD) model, the mobile-immobile (MIM) model

and the CD model coupled with the linear adsorption interaction model. In section 5.2, the results of fitting the transport models are shown which include the depiction of the general features of the breakthrough curves (BTCs), performance of the CD model, the combination of the CD model with linear interaction model, the effect of flow rate on the interaction between Brilliant Blue and the solid matrix, fits with the models to the breakthrough and the elution limbs of the BTCs, influence of different flux input conditions on the fit and the calculated goodness-of-fit for different models as an indicator for a "correct model".

The last chapter summarizes the whole work and gives an outlook for the future research.

2 The Method of Inverse Modeling

The method of inverse modeling is the state-of-the-art in hydraulic parameter estimation. Since in this work, the hydraulic properties of the coarse textured materials are estimated with this method, here in this chapter the fundamental principles and progress of inverse modeling in combination with outflow methods to identify hydraulic parameters will be presented as a review.

The whole procedure of applying the inverse method to determine hydraulic functions can be illustrated with a chart shown in Figure 2.1. Outflow experiments with desired initial and boundary conditions produce experimental data which may be cumulative outflow data or soil water potential data. The parameterized hydraulic functions with initial estimates for their parameters are used in inverse solution of the governing function of water flow. With nonlinear optimization, the parameters for the hydraulic functions are estimated.

In the following, each part of the inverse procedure will be reviewed in detail.

2.1 Fundamental Theory–Buckingham-Darcy's Law and Richards Equation

Before applying inverse method to estimate hydraulic parameters, a governing equation is assumed to adequately describe water movement in porous media. Conventionally, the Richards equation is chosen as the governing equation. Hence, in this first section, we will have a review on the history of Richards equation.

Early in 1856, Henry Darcy, an engineer working for the city of Dijon, developed the following relationship (Jury et al. 1991):

$$j_w = -K^* \frac{\Delta H}{\Delta z} \tag{2.1}$$

where j_w is the volumetric water flux, K^* the saturated hydraulic conductivity, H the hydraulic head, z vertical distance taken positive upward, $\Delta H/\Delta z$ the driving force. Eq. 2.1 is so-called *Darcy's law* which describes the water movement in saturated materials.

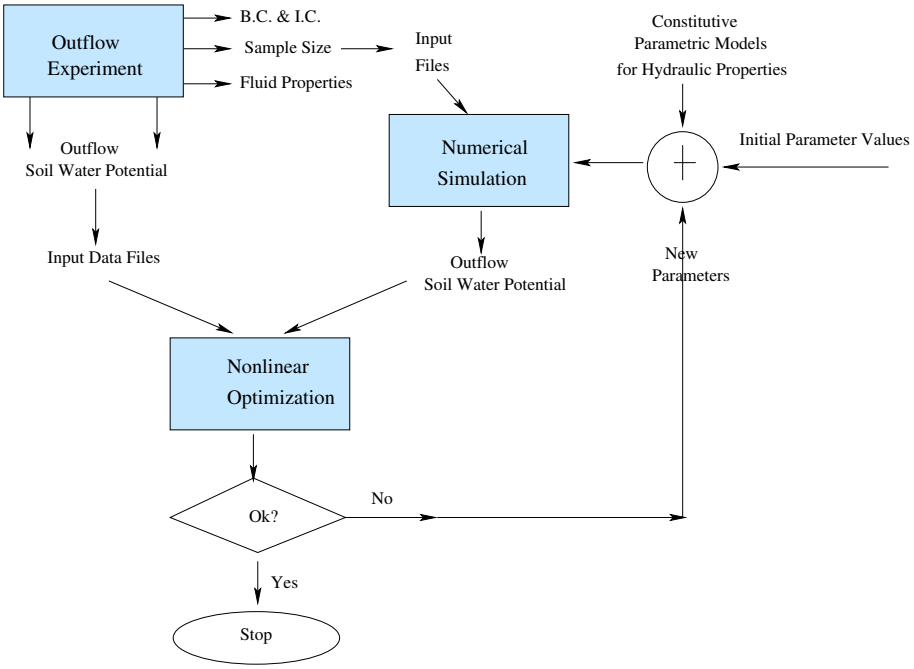

Figure 2.1: Flow chart of inverse parameter estimation approach (after Hopmans et al.1999)

In 1907, Edgar Buckingham put forward a more general form of Darcy's law (Eq. 2.1) to describe flow through unsaturated soil:

$$j_w = -K(\theta)\frac{d\psi_w}{dz} \tag{2.2}$$

where $K(\theta)$ is the hydraulic conductivity function, ψ_w water potential. Eq. 2.2 is called the *Buckingham-Darcy flux law* today. The modification rested primarily on two assumptions:

1. The driving force for water flow in isothermal, rigid, unsaturated soil contains no solute membranes and zero air pressure. Potential ψ_w is the sum of the matric and gravitational potentials.

2. The hydraulic conductivity of unsaturated soil is a function of the water content (Jury et al. 1991).

These conditions must be satisfied when applying the Buckingham-Darcy's law. Under many situations the reason that causes deviation of application of theory from reality is the lack of necessary conditions required by the theory as discussed later in chapter 4.

Steady-state downward water flow, while never actually achieved in the field, is nevertheless an approximation of certain flows, such as subsurface drainage in environments under high-frequency irrigation or frequent rainfall. Under these condi-

tions, the Buckingham-Darcy flux low (Eq. 2.2) may be replaced by a far simpler-expression. Under stationary state, when water is flowing downward at a constant rate, matric potential gradients $d\psi_m/dz$ approach zero and water flows under the influence of gravity alone. Thus, provided that the water table is far below the surface, one may approximate the Buckingham-Darcy law (Eq. 2.2) for downward flow as

$$j_w \approx -K(\psi_m) \tag{2.3}$$

where $K(\psi_m)$ is the unsaturated hydraulic conductivity. This approximation is known as *gravity flow* (Jury et al. 1991).

Under natural conditions, water flow through soils is not stationary but varies in time as well as in space which is called *transient water flow*. To describe transient flow in soils, both the Buckingham-Darcy law and the mass balance equation must be satisfied. A general form of water conservation is given by

$$\frac{\partial}{\partial t}\theta + \frac{\partial}{\partial z}j_w + r_w = 0 \tag{2.4}$$

where r_w is the root water uptake rate. For a further simplification form, r_w is neglected.

Combining Eq. 2.2 and Eq. 2.4 and applying the chain rule of differentiation to $\partial_t\theta$, we finally obtain (Roth 1996b)

$$C_w(\psi_m)\frac{\partial}{\partial t}\psi_m - \frac{\partial}{\partial z}\left[K(\psi_m)\left[\frac{\partial}{\partial z}\psi_m - \rho_w g\right]\right] = 0\ . \tag{2.5}$$

Eq. 2.5 is the so-called *Richards equation* in potential form. When matric potential is expressed in water head form, Eq. 2.5 changes into

$$C(h)\frac{\partial}{\partial t}h - \frac{\partial}{\partial z}\left[K(h)\left[\frac{\partial}{\partial z}h - 1\right]\right] = 0\ . \tag{2.6}$$

Since Richards equation is a nonlinear partial differential equation, it generally cannot be solved exactly but only by some approximation method. It is very often solved numerically. For the case of constant water flux through the soil surface, the state variables θ and ψ_m are also stationary, nothing changes in time. So that all temporal derivatives are zero and the Richards equation Eq. 2.5 is simplified to

$$\frac{d}{dz}\left[K(\psi_m)\left[\frac{d}{dz}\psi_m - \rho_w g\right]\right] = 0\ . \tag{2.7}$$

2.2 Parameterization of Hydraulic Properties

To describe unsaturated flow, hydraulic properties of porous media expressed with the constitutive relationships of unsaturated hydraulic conductivity K vs. pressure head ψ and effective water content θ_e vs. ψ must be specified. Three conventional models are commonly used to describe these functional relationships: the Mualem-van Genuchten model (MvG) (van Genuchten 1980), the Burdine-Brooks-Corey model (Brooks and Corey 1966), and the Gardner-Russo model (Gardner 1958, Russo 1988). Most existing stochastic analyzes utilize the Gardner-Russo model because of its simplicity. On the other hand, the more complex van Genuchten-Mualem and Burdine-Brooks-Corey models usually fit measured $K(\psi)$ and $\theta(\psi)$ data better. More recently, the lognormal distribution model (LDM) has been proposed and spline functions have also been applied to parameterize soil water characteristic.

2.2.1 Parameterization of unsaturated hydraulic conductivity

Direct measurement of unsaturated hydraulic conductivity is a very intricate task hence only a small number of measurements can be handled. The aim of parameterization of unsaturated hydraulic conductivity is then to interpolate and very often also extrapolate these measurements, which requires a correct representation of the physical structure of the water filled pore space (Roth 1996b).

The model of Mualem

The most comprehensive and mostly used model currently is proposed by Mualem (1976) (Roth 1996b). It was supposed that the pore space consists of a set of capillaries and the water characteristic describes the distribution of their radii. Stacks of thin slices from parallel capillary bundles are considered to be reconnected which is called stack model. The unsaturated hydraulic conductivity of such a model is calculated through integration of the water characteristic with the following form as proposed by Mualem,

$$K(\Theta) = K_s \Theta^{\tau} \left[\frac{\int_0^{\Theta} h^{-1} d\Theta}{\int_0^{1} h^{-1} d\Theta} \right]^2 \tag{2.8}$$

where K_s is the saturated hydraulic conductivity, τ is a free parameter.

The exponential model of Gardner

Gardner (1958) suggested a simple exponential model to describe the relationship of unsaturated conductivity and water potential,

$$K(h) = K_s \exp(-\alpha|h|) \tag{2.9}$$

where α is a soil parameter. This only parameter α represents the relative rate of decrease of K with decreasing h, it is related to the width of the soil pore size distribution. The reciprocation of α, α^{-1}, can be interpreted as the air entry value of h or as the length of the capillary fringe (Russo 1988).

2.2.2 Parameterization of water characteristic

Compared with measurements of unsaturated hydraulic conductivity, measurements of water characteristic of a porous medium is relatively of less labor. The aim of parameterization of water characteristic is then to obtain a simple description of a comprehensive set of measurements. In this case, the parameterization need not have a physical basis (Roth 1996b).

The Brooks-Corey model

Brooks and Corey (1966) proposed a model (Eq. 2.10) for parameterizing soil water characteristic. They assumed water saturation Θ to remain constant until the matric head exceeds $h_0 = -\psi_m^0 \rho_w g$ which physically corresponds to the air-entry value of the porous medium. When $h > h_0$, the saturation decreases as a power of h

$$\Theta(h) = \frac{\theta - \theta_r}{\theta_s - \theta_r} = \begin{cases} [h/h_0]^{-\lambda} & ; \quad h > h_0 \\ 1 & ; \quad h \leq h_0 \end{cases} \tag{2.10}$$

where λ is a positive parameter which is related to the texture of the pore space, θ_s and θ_r are saturated and residual water content respectively.

Inserting Eq. 2.10 into the Mualem model Eq. 2.8, the parameterization form of hydraulic conductivity function can be written as

$$K(h) = \begin{cases} K_s \, [h/h_0]^{-2-\lambda[a+2]} & ; \quad h > h_0 \\ K_s & ; \quad h \leq h_0 \end{cases} \tag{2.11}$$

Parameterizations Eq. 2.10 and Eq. 2.11 are referred to as the Burdine-Brooks-Corey model (Roth 1996b).

The van Genuchten model

Based on the Burdine-Brooks-Corey model, van Genuchten (1980) proposed another form for parameterizing water characteristic written as

$$\Theta(\psi) = \frac{\theta - \theta_r}{\theta_s - \theta_r} = [1 + [\alpha\psi]^n]^{-m} \tag{2.12}$$

where α, n and m are empirical parameters with positive values. The residual water content θ_r represents the small amount of water which is adsorbed in thin films at low water potentials and which is barely mobile. The parameter α scales ψ and thus determines the position of the curve relative to the axis of matric potential and the parameter n determines the shape of the curve. Thus, α is related to the mean pore size and n to the width of the pore size distribution. However, both parameters are fitting parameters without immediate physical meaning. When Eq. 2.12 is combined with the Mualem model (Eq. 2.8), very often $m = 1 - 1/n$ is taken.

The Mualem-van Genuchten parameterization form for the hydraulic conductivity function can be written as

$$K(\Theta) = K_s \Theta^{\tau} \left[1 - \left[1 - \Theta^{n/[n-1]}\right]^{1-1/n}\right]^2 \tag{2.13}$$

where now the conductivity is given as a function of the relative water content Θ. Note that the shape of the curve is determined by the same shape parameter n as for the soil water characteristic. The hydraulic conductivity at water saturation, K_s is introduced as a parameter to fix the absolute height of the curve. Moreover, an additional parameter τ which is termed as "tortuosity" is used and is thought to account for the change in the topology of the water phase with decreasing water content. At this point, we arrive at the complete set of hydraulic parameters, describing the hydraulic properties of porous media.

The Burdine-Brooks-Corey (BC) model and the Mualem-van Genuchten (MvG) model are both widely used to parameterize the hydraulic properties. The former is applicable to C-shaped relationships while the latter to S-shaped relationships (Kastanek and Nielson 2001).

The Gardner-Russo model

Attracted by the simplicity of Gardner's model (Eq. 2.9) for unsaturated hydraulic conductivity, Russo (1988) derived a model of water characteristic which can produce Gardner's model when incorporated into Mualem's model to be consistent with the Burdine-Brooks-Corey model and the Mualem-van Genuchten model. The model is given as

$$S(h) = \left(e^{-0.5\alpha|h|}\left(1 + 0.5\alpha|h|\right)\right)^{2/(\tau+2)} \quad . \tag{2.14}$$

This relationship together with Eq. 2.9 is referred to as the Gardner-Russo (GR) model. Russo (1988) compared the performance of the BC, MvG, and GR models and found that the MvG model is the most accurate and most consistent with the data. The BC and GR models are less accurate but similar with each other.

The lognormal distribution model

The lognormal distribution model (LDM) for hydraulic functions was proposed by Kosugi (1996). It was developed through applying a lognormal distribution law to the soil pore radius distribution function. Parameters of this retention model have physical significance on the water content θ–capillary pressure ψ curve and are related directly to the statistics of the pore radius distribution.

The two-parameter LDM for soil water retention is

$$\Theta = Q\left[ln\left(\psi/\psi_m\right)/\sigma\right] \tag{2.15}$$

when it is combined with the Mualem model (Eq. 2.8), the relative hydraulic conductivity is written as

$$K_r(\Theta) = \Theta^{0.5}\left\{Q\left[Q^{-1}(\Theta) + \sigma\right]\right\}^2 \tag{2.16}$$

where ψ_m and σ are parameters related to pore size distribution and Q is the complementary normal distribution function. Hwang and Powers (2003) investigated the capability of several soil hydraulic functions to provide unique parameter sets from multi-step outflow data for sandy soils and found that the LDM, because of its parameters with physical significance on retention function, provided the best unique parameter sets.

Using spline functions to describe water characteristic

To increase the flexibility of the hydraulic function model, spline function interpolation is chosen as an alternative for the analytical models mentioned above to describe soil water characteristic. Kastanek and Nielson (2001) applied third order polynomial functions, i.e., the cubic spline function, with the aid of virtual points to yield proposed mathematical representation of the soil water characteristic. To interpolate n data points with the independent data x_i and the dependent data $y_i = f(x_i)$ inside the closed interval $[x_1, x_n]$ and with $x_1 < x_2 < ...x_n$, the cubic polynomials P_i between each subinterval $[x_i, x_{i+1}]$ are chosen as

$$P_i(x) = a_i + b_i(x - x_i) + c_i(x - x_i)^2 + d_i(x - x_i)^3 \quad i = 1, 2, ..., (n-1)\ . \tag{2.17}$$

The first and second derivatives of Eq. 2.17 are written in the following respectively:

$$P_i^{'}(x) = b_i + 2c_i(x - x_i) + 3d_i(x - x_i)^2 \tag{2.18}$$

$$P_i^{''}(x) = 2c_i + 6d_i(x - x_i) \ . \tag{2.19}$$

In order to get smooth transitions, at the junctions of the intervals, the spline function and its derivatives must satisfy the following conditions:

$$P_i(x_i) = y_i \qquad i = 1, 2, ..., (n-1) \tag{2.20}$$

$$P_{n-1}(x_n) = y_n \tag{2.21}$$

$$P_i(x_{i+1}) = P_{i+1}(x_{i+1}) \qquad i = 1, 2, ..., (n-2) \tag{2.22}$$

$$P_i^{'}(x_{i+1}) = P_{i+1}^{'}(x_{i+1}) \qquad i = 1, 2, ..., (n-2) \tag{2.23}$$

$$P_i^{''}(x_{i+1}) = P_{i+1}^{''}(x_{i+1}) \qquad i = 1, 2, ..., (n-2) \tag{2.24}$$

For a unique solution, two further conditions need to be specified:

$$P_1^{''}(x_1) = P_{n-1}^{''}(x_n) = 0 \tag{2.25}$$

Solving the equations above yields $4(n-1)$ coefficients of all polynomials of order three. Obviously, there are too many parameters to handle which is impossible without computer. Furthermore, because of the high flexibility of spline functions, to extrapolate the estimated curve beyond the fitted range might produce unrealistic shape.

2.3 Outflow Experiments and Inverse Modeling

Once the forms of parameterized hydraulic properties are chosen, which contain unknown parameters (e.g. n, α, θ_s, θ_r, K_s, and τ for the MvG hydraulic functions), we need to set up an outflow experiment with specific initial and boundary conditions to measure one or two flow-controlled variables that can afford necessary information related to unknown parameters. The boundary conditions of an outflow experiment must be carefully selected to guarantee parameter identifiability. Since the first studies on the identification of unsaturated hydraulic properties by inverse simulation of transient flow experiments, two decades ago, significant progress has been made in the development of numerical codes and in automating devices for inflow/outflow measurements.

2.3.1 One-step method and the nonuniqueness problem

Gardner (1956) introduced the pressure plate outflow method to measure outflow induced by a series of step increases in air pressure from an initially saturated soil sample to analytically determine the soil water diffusivity and unsaturated hydraulic conductivity. Later, this method was modified in a one-step experiment by Doering (1965) in order to save time. Zachman et al. (1981) applied inverse techniques to their numerical experiments in which an initially saturated sample was allowed to drain and the cumulative outflow as a function of time, soil water pressure head as a function of time at one location, and water content as a function of time at a single location were measured. It was found that hydraulic functions determined by inverse modeling using cumulative outflow as a function of time was closest to the real hydraulic functions.

Kool et al. (1985) and Parker et al. (1985) were the first to apply the inverse approach by numerical solution of the Richards equation for the transient one-step outflow process, the former through a numerical study and the latter through an experimental one. Kool et al. (1985) concluded that with the one-step outflow (OSO) experiment designed to cover a wide range in water content, the initial parameter values close to their true values and the small errors in outflow measurement, unique parameter set can be better determined. Parker et al. (1985) concluded that with the OSO experiment coupled with the inverse method the hydraulic functions can be simultaneously optimized and they further suggested to include an independently measured point of the soil water retention curve in the objective function which allows extrapolation of the hydraulic functions to water content range beyond that achieved with one-step pressure change. Later, Kool and Parker (1988) demonstrated with synthetic experimental data the advantage of simultaneously measuring tensiometer data and outflow data.

These works lead to widely application of the inverse method to laboratory OSO measurement to identify hydraulic parameters. However, in parallel to its advantages, e.g. transient experimental conditions, time-saving procedure, relatively cheap experimental setup, the nonuniqueness problem was encountered (Parker et al. 1985, Kool et al. 1985), i.e., more than one set of parameters yield minimum for the objective function. Toorman et al. (1992), with also synthetic data sets evaluated this problem for the one-step method by looking at response surfaces. It was found that there were long valleys in the different parameter planes which indicates that many combinations of $\alpha - n$, $\alpha - K_s$ or $n - K_s$ will predict similar cumulative outflow curves. Furthermore, their results showed that if both cumulative outflow and matric potential at some distance away from the lower boundary are measured, the parameter estimation sensitivity will be greatly improved. These results were later demonstrated by van Dam et al. (1992). It was found that including additional $\theta(\psi)$ or tensiometer data in the objective function improves parameter estimation.

Except the numerical difficulties, another major problem with application of the one-step method has always been that the quick change of the boundary condition does not represent natural conditions and may lead to non-uniform flow in the soil sample. Hopmans et al. (1992), by visualizing water content distributions in a soil during an one-step outflow experiment with X-ray tomography, showed that flow induced by a large pressure step on an initially saturated soil sample, could not be described by Richards equation when preferential flow occurs. Therefore, they recommended using the method only with initially unsaturated samples. Furthermore, when a sharp pressure change is applied, under the high pneumatic pressure or low suction, soil near the ceramic plate starts to loose its water in larger pores. Due to the lower water content, it has a relatively high resistance compared with the remaining part of the sample (van Dam et al. 1992). This very thin drained soil layer near the porous plate will then control the outflow flux to a large extent which will result in a low sensitivity of the method.

2.3.2 multi-step method

To improve the outflow experiment and inverse procedure, the multi-step outflow (MSO) method which induces drainage of the soil core by a sequence of smaller pneumatic pressure increments was introduced (Eching and Hopmans 1993, Eching et al. 1994, van Dam et al. 1994). Using only outflow data in the objective function, van Dam et al. (1994) found that the MSO method resulted in unique estimates of hydraulic functions and that for the same experimental conditions the OSO method often yielded nonunique solutions. In this sense, they concluded that the MSO method has theoretical and practical advantages above the OSO approach. This conclusion was based on only a single loam soil. To explore the feasibility of using

both cumulative outflow and soil water pressure head data in the inverse procedure, Eching and Hopmans (1993) compared the water retention curves optimized from cumulative outflow only and those obtained from outflow and soil water pressure head measurements for both OSO and MSO experiments. They found that the optimization was greatly improved when both outflow and soil water pressure head data were used. The addition of soil water pressure head values in the optimization procedure provides unique parameters for the hydraulic functions under their experimental conditions. Generally speaking, the estimation of parameter values of soil hydraulic functions were improved. And the MSO experiments were found to match the equilibrium data better than the OSO experiments. Many other researchers also found that the multi-step method is superior to the one-step method because the hydraulic parameters are weakly correlated and all parameters can be identified simultaneously (Crescimanno and Iovino 1995, Zurmühl 1996). Therefore, the application of MSO has been expanded dramatically in both the laboratory experiments and field experiments (Weerts et al. 1999, Inoue et al. 1998).

2.3.3 Pressure and suction desorption in outflow experiments

To induce drainage from a saturated soil column in an outflow experiment, either a step increase of pneumatic pressure is applied from the upper boundary of the column (van Dam et al. 1994, Eching et al. 1994), or a step decrease of suction is applied from the bottom of the column (Zurmühl 1996, Inoue et al. 1998). It is usually assumed that these two methods have the same effects on soil water flow. However, the difference between the soil water retention data obtained by these two methods has been noticed by Peck (1960) and Chahal and Yong (1965) several decades ago. Discrepancies were attributed to changes in trapped air volumes while releasing the pressure, thereby causing the assumed soil water potential for equilibrated pressurized soil samples to be lower than for soil equilibrated under suction. Also in the work of Eching and Hopmans (1993), differences between the measured soil water retention data determined from desorption under pressure and suction were found, however, not significant.

2.3.4 Posedness of the inverse modeling

For an inverse problem, most important of all, it should be "correctly posed". The ill-posedness of an inverse solution is generally characterized by the non-uniqueness, non-identifiability, and instability of the identified parameters and will result in all cases to a non-unique or divergent solution (Yeh 1986). The instability stems from the fact that small errors in the measured variable may result in large changes of the optimized parameters. While non-uniqueness means that a given response leads

to more than one set of parameters. Non-uniqueness can be caused by local minima or more than one single global optimum in the response surface of the objective function. Non-uniqueness can also be caused by a lack of sensitivity of the flow variables in the objective function to certain parameter combinations. Nonidentifiability means that more than one parameter set lead to the same response. If a parameter set is nonidentifiable, the inverse problem is also non-unique (Hopmans and Šimůnek 1999). Identifiability, uniqueness and stability of an inverse problem depend on porous media under investigation, the type and range of boundary conditions used, the model for the hydraulic funcitons chosen (hence the number of parameters to be determined) and the measurement error (Durner et al. 1999a). Large measurement errors might result in non-uniqueness of parameter estimation. Insensitive parameters should be measured independently if possible. As for type of boundary conditions, although pressure changes at smaller steps, i.e., MSO boundary conditions, have been proved to be superior to OSO, they are stepwise which seldom happen in nature. Therefore, a continuous change of pressure at the lower boundary was investigated by Zurmühl (1996). However, parameter θ_s and K_s were found highly correlated to each other and in the K_s-θ_s parameter plane, a global minimum cannot be found. While this problem did not happen for the MSO case. So currently, MSO is still preferred.

A severe drawback of any outflow/inflow method will remain a problem: the low sensitivity towards the conductivity function near saturation. Sometimes the range of pressures that can be studied is limited by the experimental setup used. If suction is applied, a theoretical limit exists at atmospheric pressure. In a pressure plate apparatus, where higher pressures can be applied, the resistance of a porous plate with high enough air entry pressure will be so high that it limits the outflow rate in the wet stage and therefore screen the hydraulic properties of soils near saturation.

3 Materials and Methods

In this chapter, some properties related to flow and transport characteristics of the five materials investigated in this project are described and the experimental setup together with detailed procedures of the MSO experiments and transport experiments are given in detail.

In the following section 3.1, the independently measured material properties are presented. Section 3.2 describes the experimental setup and measurement procedures for the multi-step outflow experiments. Section 3.3 is about the formulation of our inverse problems, and section 3.4 is focused on the experimental setup and measurement procedures for the transport experiments.

3.1 Materials

Grain size distribution of the porous medium has an influential impact on its hydraulic and transport properties. Such information can help us understand the experimental results shown in following chapters. Total porosity of the porous media was measured here to get a rough estimation of saturated water content θ_s. Saturated hydraulic conductivity K_s, one of the important hydraulic parameters, was measured independently to provide a model input and a criterion for evaluation of the results obtained from the inverse estimation. pH value of the materials was measured additionally because it is an important factor related to the adsorption of Brilliant Blue used as a tracer for the transport measurements,

3.1.1 Grain size distribution

Five materials with varied-coarse texture have different grain size distributions and were taken from different sources.

Construction waste consists of grains (by weight): 4-2 mm 14.9% , 2-0.63 mm 29%, 0.63-0.2 mm 36.5%, 0.2-0.063 mm 17.5%, $<$ 0.063 mm 1.9%.

Fine sand: the fine sand has a narrow grain size distribution ranging from 0.1-0.5 mm and an average of 0.25 mm;

As shown in Table 3.1, the **coarse sand**, the **gravel** and the **mixed material** are

Table 3.1: Grain size distribution (by weight) of the gravel, coarse sand and mixed material

Grain size [mm]	< 0.06	0.06 – 0.13	0.13 – 0.25	0.25 – 0.5	0.5 – 1	1 – 2	2 – 4	4 – 8	8 – 16	16 – 32
Gravel	–	–	–	–	–	–	0.07	0.78	0.15	–
Coarse sand	0.01	0.02	0.10	0.25	0.23	0.18	0.19	0.02	–	–
Mixed material	–	0.02	0.05	0.11	0.10	0.07	0.09	0.18	0.36	0.02

all coarse materials.
The coarse sand consists of little fine sand (<0.25 mm 13%) and the rest is a large portion of coarse sand and fine gravel.
"Grains" that make up the material gravel are real gravels. This material consists of mainly fine gravels and only 15% by weight are gravels with middle size.
The mixed material is in fact a mixture of sand and gravel with a large range. It consists of grains from fine sand to large gravels (about 32 mm).

3.1.2 Total porosity

The total porosity of the materials was determined using a steel cylinder with a precise volume of 100 cm^3. The material was filled into the cylinder completely full and three such repeats for each material were dried at 105^oC to a constant weight and were weighted afterwards. The bulk density of the material can be calculated by dividing the weight of the dry material in the cylinder by the volume of the cylinder. The porosity was calculated according to

$$\phi = 1 - \frac{\rho_s}{\rho_r} \tag{3.1}$$

where ϕ is the total porosity of the material, ρ_s the soil bulk density, and ρ_r the real density of the soil matrix (2.65 g cm^{-3} for mineral media). Table 3.2 shows the total porosity of these five materials.

3.1.3 Saturation hydraulic conductivity

Saturated hydraulic conductivities K_s of the porous media were independently measured using a falling head permeameter (Figure 3.1) (Klute and Dirksen 1986) (cited by Roth (1996b)). The porous medium was filled into a PVC column to a depth of L with water level slowly rising from the metal mesh at the bottom of the column in the same way as filling an MSO column as described in the following section, in

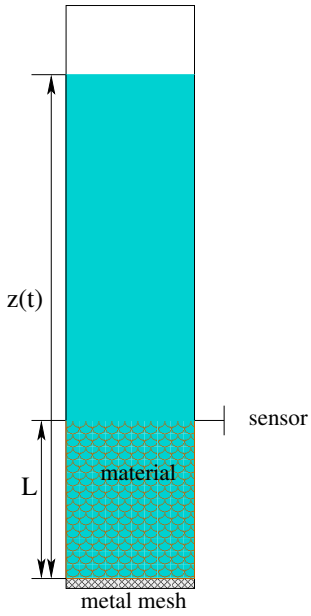

Figure 3.1: Sketch of falling head permeameter.

order to approach a stable state. After the porous medium was completely saturated the water level inside the column was raised to $z(0)$ at time $t = 0$. Then water was allowed to drain freely through the metal mesh due to gravity. The height of the water level $z(t)$ is registered with time by a pressure sensor installed at depth L. When $z(t) > L$, the height of the water level $z(t)$ decreases exponentially with time, i.e.,

$$z(t) = z(0)e^{-\frac{K_s t}{L}} \quad . \tag{3.2}$$

Then, the saturated hydraulic conductivity can be deduced as the slope by plotting $log(z(t)/z(0))$ versus time, i.e.,

$$K_s = -\frac{L}{t} log\left(\frac{z(t)}{z_0}\right) \quad . \tag{3.3}$$

Table 3.2 shows the saturated hydraulic conductivity of the five materials measured with this falling head method. For different materials, depending on the grain size, metal meshes with different mesh size are used to hold the materials without influencing the water flow. Experimentally, the measurement was repeated several times and there was good reproducibility. Therefore, the results shown here will be compared with those obtained from inverse modeling in the following chapter.

Table 3.2: Some independently measured material properties

Material	K_s [a] [cm h^{-1}]	pH	ϕ
Construction waste	51	12	16.5%
Coarse sand	362	7.7	31.5%
Fine sand	93	6.4	40.0%
Mixed material	612	7.9	23.5 %
Gravel	1.4×10^4	8.1	-

[a] measured by falling head method

3.1.4 pH value

According to Flury and Flühler (1995), the properties of Brilliant Blue, the tracer chosen for the transport experiment, depend on the pH value of the porous medium, which will be discussed in detail in the following section. Thereby, a pH meter was used to measure the pH values of the suspensions prepared with 0.01M $CaCl_2$ and the porous media (water:material=5:1). The results are also shown in Table 3.2. As one can find that pH values of all the materials except the construction waste are between 6 and 8. While the construction waste showed an alkali property with a pH value up to 12, under which condition, there might be problems to use Brilliant Blue as a tracer, as will be discussed in the following chapter.

3.2 Experimental Setup and Measurement Procedure for MSO Experiment

3.2.1 Experimental setup

As mentioned already in chapter 2 (section 2.3.2), the multi-step outflow (MSO) method which induces drainage of the soil core by a sequence of smaller pneumatic pressure increments or step decrease of suction was introduced and considered to be superior to the OSO method (Eching and Hopmans 1993, Eching et al. 1994, van Dam et al. 1994, Crescimanno and Iovino 1995, Zurmühl 1996). With an automated soil water matric head measurement during drainage of soil cores in MSO measurements, Eching et al. (1994) and Eching and Hopmans (1993) found that the estimation of parameter values of soil hydraulic functions were improved. In their experiments, the water saturated sample was mounted on a ceramic plate and stepwise increasing pneumatic pressures were applied to the surface of the column to induce outflow. By connecting the bottom of the column to a burette, volume of outflow could be recorded in high temporal resolution.

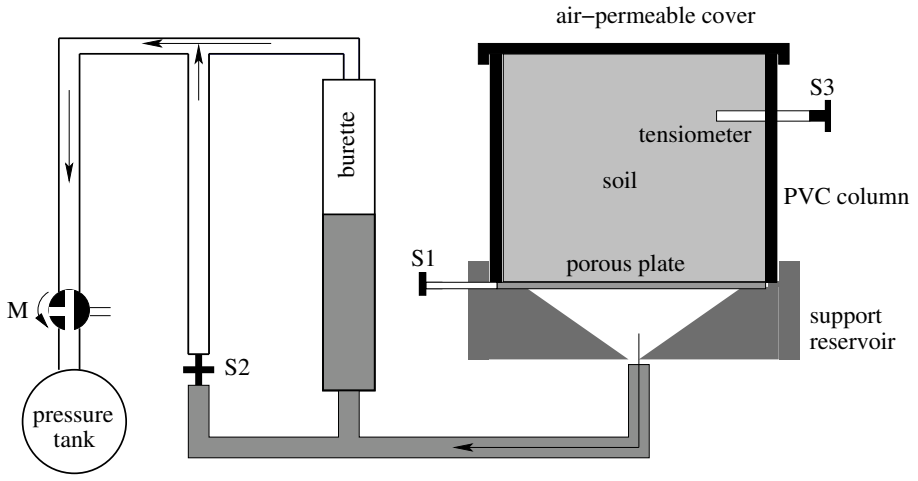

Figure 3.2: Experimental setup of MSO measurement

In the experiments carried out in this study, instead of pneumatic pressure, step decrease of suction is applied at the lower boundary by connecting the column to a negative pressure tank together with magnetic valves to control the pressure. As shown in Figure 3.2 the experimental setup for an MSO experiment consists of four basic elements:

(i) a PVC column together with a ceramic plate and a reservoir below that to

hold and support the sample and water,

(ii) the pressure tank in combination with magnetic valve (M) and pressure sensor S1 to control pressure at the lower boundary,

(iii) the burette to collect the induced outflow and with the sensor S2 connected to it to record the amount of outflow, and

(iv) the control program and computer.

Besides those mentioned above, a ceramic tensiometer is installed 2 cm below the surface horizontally and the additional sensor S3 connected to it can measure the change of matric head at that depth.

The PVC column is 10 cm high and 16.3 cm in diameter with a volume of 2060 cm^3. To keep the system air tight under low tension conditions but still water permeable at the bottom, a membrane is put on the ceramic plate. Pore size is about 10 μm for the membrane and about 250 μm for the porous plate. Thickness of the membrane is about 0.1 mm and that of the porous plate is about 1 cm. The saturated hydraulic conductivity of the membrane and porous plate system, which usually ranges around 20 cm h^{-1}, was measured before each experiment as an input parameter for the inverse simulation. Depending on the saturated water concent of each material (roughly estimated from porosity shown in Table 3.2), in order to get high enough resolution of outflow record, plastic sticks with varied diameters can be used to raise the water level in the burette.

3.2.2 Measurement procedure

For a typical multi-step outflow experiment, first, all the sensors are calibrated and their stability is also tested before each measurement. The ceramic plate and the membrane above it are completely saturated and put on the water-filled reservoir. The PVC column is then fixed on the plate. From the membrane to the plate, it must be air-tight. Air bubbles below the membrane, in the porous plate or below it in the reservoir should be removed from the system, e.g., by suction from the additional outlet at the bottom of the reservoir. After that, the porous media are filled into the column carefully with slowly increasing water table connected to the bottom of the column. The material is moistened by capillary rise. Efforts are taken to fill the column uniformly. After the column is filled, the external water table is kept a little higher than the surface for some time to guarantee that the material is completely saturated. Piecewise suction steps are then applied to the lower boundary. The time interval between subsequent pressure steps is chosen such that the system is expected to get equilibrated and the outflow ceases within a pressure step.

Pressure steps, i.e., rates of pressure decrease should be also small enough to avoid disconnection of flow paths at higher flow rates according to Wildenschild et al. (2001). Cumulative outflow and water matric head are measured as a function of time. By inversely solving Richards Equation, the parameters of the models chosen for hydraulic functions $K(\theta)$ and $\psi(\theta)$ can be estimated.

3.3 Formulation of the Inverse Problem

As described in chapter 2, when applying inverse method to identify hydraulic parameters, it is tacitly assumed that Richards equation and the formulated constitutive relationships K–ψ and θ–ψ in the chosen forms can describe the physical behavior of the porous medium in question.

In our case, the Mualem-van Genuchten models (Eq. 2.12 and Eq. 2.8) are chosen to parameterize the hydraulic properties of the porous media. Hence the hydraulic functions are defined by the parameter vector $b = \{\theta_s, \theta_r, \alpha, K_s, n, \tau\}^T$. If hysteresis is to be investigated, an additional parameter α_w for the imbibition process is required.

Deviations between measurements and simulations are expressed by an objective function $O(b)$, $b = \{b_1, ..., b_p\}^T$, where p is the number of parameters. Using an ordinary weighted least square method, the objective function is given by

$$O(b) = \sum_{i=1}^{N} W_i (Q_{mi} - Q_{si})^2 + \sum_{j=1}^{M} W_i V_j (h_m(t_j) - h_s(t_j, b)) \ , \tag{3.4}$$

where the variable Q denotes the cumulative outflow, h is the matric potential, W and V are weighting coefficients, N and M are the numbers of cumulative outflow measurements and matric potential measurements respectively. Since in our experiments, these two variables are measured simultaneously, so that N and M are equal.

With given starting values of the parameter vector $b = \{\theta_s, \theta_r, \alpha, K_s, n, \tau\}^T$, the program (ESHPIM 3.2) (Zurmühl, 1996) calculates the objective function iteratively to find the "best set" of parameters which results in a global minimum of the objective function.

3.4 Experimental Setup and Measurement Procedure for Transport Experiment

3.4.1 Experimental setup

The experimental setup for the transport experiments is shown in Figure 3.3.

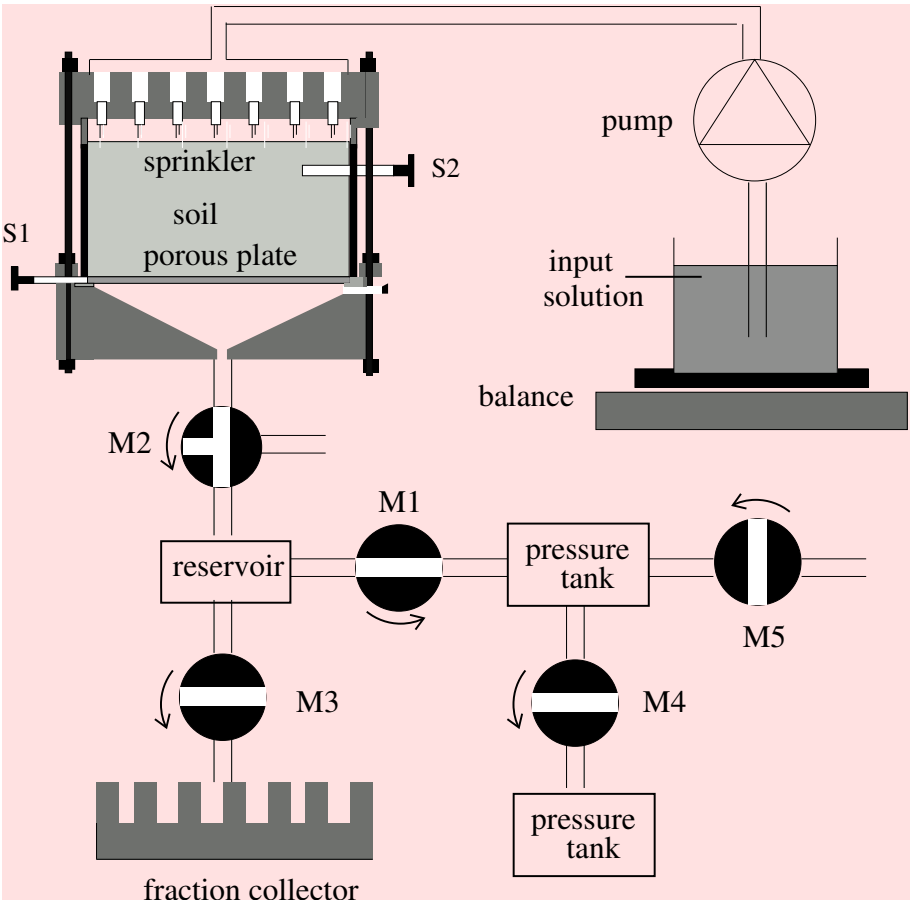

Figure 3.3: Experimental setup for transport measurement

It consists of four basic parts:

(i) the supporting unit similar to that of MSO experimental setup,

(ii) the infiltration generation unit which includes a balance (Precisa XB 10200D), a reservoir with input solution, a pump (meredos TL) and a plate with needles installed on it (the sprinkler),

(iii) the pressure regulating unit which includes sensor S1, the magnetic valves M1, M2, M4, M5 and two pressure tanks,

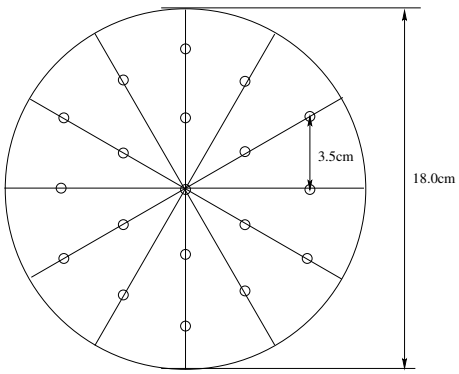

Figure 3.4: Distribution of needles on the sprinkler

(iv) the outflow collection unit including the magnetic valves M2, M3 and a fraction collector (RediFrac) and

(v) the control program and computer

The PVC column is of the same size as that used in MSO measurement. Porous plate and a membrane are also used to keep the system below the membrane air-tight. In the following part, we will have a close look at the infiltration generation and control unit to see how the instruments operate together.

3.4.2 Sprinkler

To generate homogeneous infiltration in the laboratory is obviously a difficult task. In our experimental design (Figure 3.4), 19 needles (needle out-diameter 0.4 mm, effective needle length 20 mm) are distributed uniformly. While apparently, drops from the needles are far from homogeneous infiltration. The reason why we still prefer this design is that at one hand, it is globally uniform and at the other hand, we know the local heterogeneity.

3.4.3 Pump and balance–the flux control unit

Before each experiment, the pump needs to be calibrated to set the right pump gain. The pump is calibrated in the following way. A beaker with water is put on the balance. A plastic tube with one end in the beaker under the water surface connects the pump with the other end. The pump runs at a fixed pump speed (50% of the full speed in our case) for a fixed time period. The flux during this period is calculated by deviding weight loss on the balance by time. Deviding the pump speed by the flux results in the real pump gain.

During the experiment, the control program checks the real flux from time to time and if the error is larger than a permitted value, the pump gain or even the running mode (continuous or interrupted mode) is adjusted to obtain a more precise infiltration rate. With this control procedure, the error of infiltration rate can be limited within 2%.

For our transport experiments, two distinct flow rates are investigated. One is set at 1 cm h^{-1} and the other extreme is 0.01 cm h^{-1}. For the low flow rate, difficulty was encountered with continuous running mode of the pump. Even with the lowest pump speed and thinner pipe, the real flux generated was still higher than the defined value. Hence an interruption mode was chosen in such a way that the pump is allowed to run at higher pump rate for a certain period and then it is interrupted and wait until the average flux for the whole circle is equal to the desired flow rate. Since the flux is really low, the flow regime will not be too much different from the continuous mode at the same flow rate.

3.4.4 Stationary transport experiment with the tracer–Brilliant Blue

The ideal tracer for water flow should have the following properties,

(i) no retardation,

(ii) no chemical and biological degradation during the time of interest,

(iii) absence of background concentration.

HDO and $H_2{}^{18}O$ satisfy these conditions but it is too expensive to analyse them (Kasteel et al. 2002). Bromide is also a good candidate and is used very often. However, large amount of measurements are still restricted because of the cost.

The food dye Brilliant Blue has been widely used as a tracer for visualizing the flow pathways of water in soils in the last decades (Flury et al. 1994, Perillo et al. 1998). And recently, Brilliant Blue has been used to determine absolute solute concentration, both in the laboratory and in the field (Aeby et al. 1997, Jawitz et al. 1998, Forrer et al. 2000). Compared with these ideal tracers, analysis of Brilliant Blue is apparently cost-effective. Especially when Brilliant Blue is used in field experiments to visualize the flow paths, photographs of the soil profile offer a high spatial resolution of the concentration distribution. The disadvantage with using Brilliant Blue as a tracer for water flow is that it can be adsorbed by the soil matrix (Kasteel et al. 2002). However, for small concentration ranges of typically less than 5 mg l^{-1} and low pH, linear adsorption of Brilliant Blue was found by Flury and Flühler (1995) for their soils and Perillo et al. (1998) also found that linearized Freundlich model fit the adsorption isotherm of Brilliant Blue with a concentration up to 20 mg l^{-1} rather well for their soils. Since the adsorptive behavior of Brilliant

Blue is highly dependent on the properties of the studied material, one has to check this for a certain case. For the staining purpose, high concentrations are preferred to guarantee the visibility of dye against the soil background. When used as a tracer for water flow in laboratory breakthrough experiments, concentrations of dye solution must be chosen such that it is high enough to enable the detection of dye breakthough and it should also be low enough in order to see tailings of the BTCs.

The sorption characteristics of Brilliant Blue to the fine sand is evaluated over a range of concentrations lower than 20 mg l^{-1}. Batch experiments were carried out with dye concentrations of 1.0, 2.0, 3.0, 5.0, 10.0, 20.0 mg l^{-1} prepared with 0.01 M $CaCl_2$ solution. Fine sand samples were dried in a oven at 105^oC for 24 h. 20g sample was equilibrated in inert polyethylene (PE) flasks with 30 ml of dye solution by shaking for 3 hours. Next, the suspension was centrifuged for 10 minutes and the supernatant was moved to test tubes. Brilliant Blue concentrations were measured with a spectrometer (Lambda 20 UV-VIS spectrometer, Perkin-Elmer) at a wavelength of 630 nm. The experiment isotherm data was analyzed with the linearized Freundlich isotherm model. The nonlinear isotherm is written as

$$C_a = KC_l^{1/n} \tag{3.5}$$

where C_a [mg kg^{-1}] is the concentration of chemical adsorbed, C_l [g m^{-3}] the concentration in the aqueous phase at equilibrium, and K [0dm^3 kg^{-1}] and $1/n$ are constants. The linearized Freundlich isotherm with $1/n$ set to 1.0 is given by

$$C_a = K_d C_l \tag{3.6}$$

where K_d is the distribution coefficient and it can be determined by fitting the model to the experimental data.

Figure 3.5 shows that the linearized Freundlich model fit measured data reasonably well. As shown in Table 3.2, the materials we investigated have pH values ranging from 6 to 8 (except the construction waste). And also because that for each experiment, in order to establish steady state in the system, 0.352 mmol l^{-1} of $CaCl_2$ was applied to flush the column. Brilliant Blue under such situation should be in bivalent anionic form, hence the adsorption to the materials should be minimized.

Before the stationary state is established, 0.352 mmol l^{-1} of $CaCl_2$ was applied and corresponding to a certain flow rate, the suction applied to the lower boundary is set such that it is equal to the readings of the sensor S2 connected to the tensiometer (Figure 3.3). As soon as the stationary state is established, i.e., the flow rate of the outflow is stable and equal to the flow rate of the inflow, 20 mg l^{-1} of Brilliant Blue solution is applied and the fraction collector starts to collect outflow samples at a specified time interval. The samples are covered as soon as possible after they are released from the reservoir to the glasses on the fraction collector and

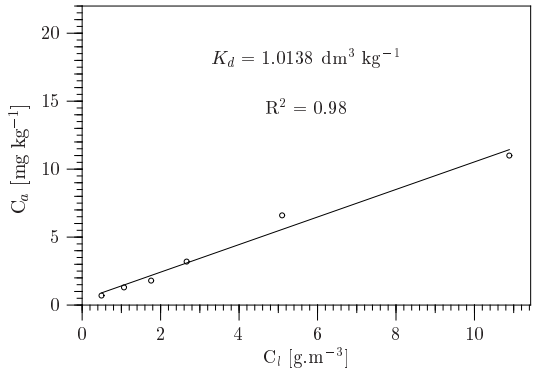

Figure 3.5: Measured adsorption isotherm of the fine sand with linear sorption isotherm. C_a [mg kg^{-1}] is the amount of chemical adsorbed, C_l [g m^{-3}] is the equilibrium concentration in the aqueous phase.

are stored in the refrigerator at 7^{o}C to avoid evaporation or any degradation if the immediate measurement can not be carried out. The dye is applied until the outflow concentration is expected to reach the input concentration. Then again the 0.352 mmol l^{-1} $CaCl_2$ is applied to displace the dye out of the column. The experiment is stopped when the dye concentration becomes very small or the tailing of the breakthrough curves (BTCs) is clearly oriented.

The samples collected are brought out of the refrigerator and are shaken to mix the solution. After they reach the room temperature, the dye concentrations are measured by the spectrometer at a wavelength of 630 nm.

To estimate the transport parameters, TAP (Transport Analysis Package) by Roth (1996b) was used. Details will be given in chapter 5.

4 Estimation of Hydraulic Parameters from MSO Experiments by Inversion

Hydraulic parameter estimation for the coarse materials* from MSO experiments using inverse technique is discussed in this chapter with respect to the goodness-of-fit, uniqueness of the problem and different possible causes of model deviation from the measurements.

4.1 The Coarse Sand

Since θ_s and θ_r have exactly opposite effects on the outflow (van Dam et al. 1992), only one of these parameters can be estimated from outflow experiments. In our case, the parameter θ_r is not optimized but fixed at a value of 0.001. Saturated hydraulic conductivity K_s was in addition measured with falling head method. Figure 4.1 shows the measured and simulated outflow curve and the deviation of the model from the measurement when all the van Genuchten-Mualem parameters were free for fitting. It shows that there is good agreement between the measured outflow curve and that calculated from the optimized hydraulic functions. The maximum model error is less than 0.02 cm. But at the early stage of drainage process, the deviation curve contains some larger values showing that there are both overestimation and underestimation of the cumulative outflow by the model. Furthermore, the model errors instead of a randomly distribution which is statistically required for a correct model, corresponding to the pressure steps, they exhibited a wavelike shape. As the sample gets drier, the deviation generally becomes smaller. As shown in Figure 4.2, when the saturated hydraulic conductivity is fixed at the measured value, instead of approaching towards a better fit, the model showed bigger positive deviations expecially in the wet stage, i.e., when K_s is fixed at the measured value, the model tends to underestimate the outflow. Similarly with the fitting in which K_s is fitted, the model errors also show a regular shape corresponding to the critical points when

*Drainage from the gravel column is too fast to allow the application of the inverse simulation of the MSO data. And the construction waste became hardened when it got wetted due to unknown chemical composition. Both results are not shown.

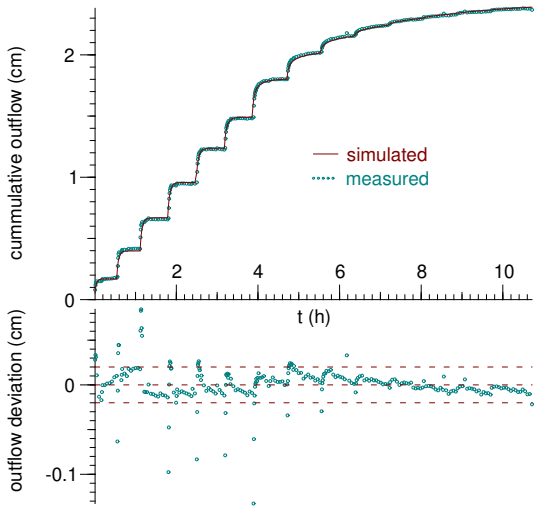

Figure 4.1: Simulated outflow curve with K_s fitted compared with the measured outflow curve with the coarse sand. The lower figure shows the residuals, i.e., the difference between the simulated and measured outflow

the pressure steps switch and almost disappears under high tension.

Looking at Table 4.1, the discrepancies in the estimated hydraulic parameters between the two fits are quite obvious, even the 95% confidence interval did not overlap. The estimated K_s is fivefold larger than the measured value. Furthermore, tortuosity τ estimated with K_s fitted almost double that estimated with K_s fixed at measurement. Durner et al. (1999a) suggested that K_s should be measured

Table 4.1: Estimated MvG parameters for the coarse sand with Ks fitted and fixed

Parameter		value	95% confidence interval lower limit	upper limit
α	K_s fitted	0.0776	0.0772	0.0780
	K_s fixed	0.0762	0.0759	0.0766
n	K_s fitted	3.12	3.06	3.18
	K_s fixed	3.65	3.59	3.71
θ_s	K_s fitted	0.307	0.303	0.311
	K_s fixed	0.281	0.279	0.284
K_s	fitted	1.8×10^3	1.6×10^2	2.0×10^3
[cm h^{-1}]	measured	$3.6\ \times10^2$		
τ	$K_s$fitted	3.41	3.25	3.57
	K_s fixed	1.81	1.75	1.88

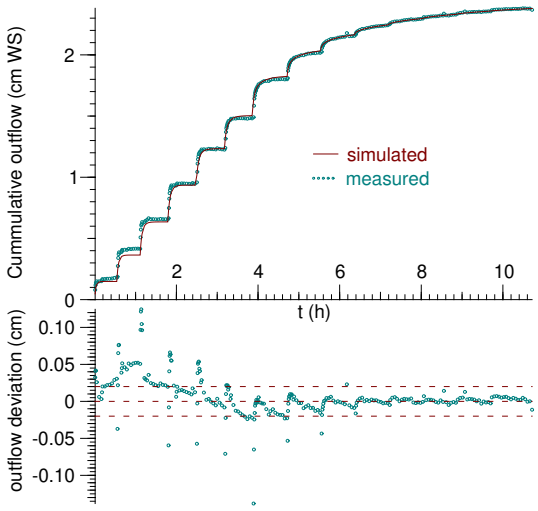

Figure 4.2: Simulated outflow curve with K_s fixed compared with the measurement with the coarse sand. The lower figure shows the residuals.

independently since accurate optimization is difficult because of low sensitivity of K_s near saturation. However, the Mualem-van Genuchten (MvG) hydraulic parameters identified by inverse modeling in combination with the MSO method have been reported to be uncorrelated with each other by Zurmühl (1996). It was found from simulation of numerical experiments with pressure at the lower boundary decrease in one-step, linear and multi-step that the MSO method is superior to the other two because it yielded independent parameters. It was also pointed out that hydraulic conductivity and the Mualem parameter τ are relatively insensitive thus difficult to be determined if the pressure range is too small. The same method adopted in the work of Zurmühl (1996) had been used earlier by Toorman et al. (1992) when the uniqueness problem of the one-step method was investigated by calculating response surfaces for the VG parameters and K_s. However, both worked with synthetic data. Here we applied the same method on our experimental data. The aim is to check whether the MvG parameters can be identified, how sensitive a certain parameter combination is to the system response and to understand the significant discrepancy between the estimated and measured saturated hydraulic conductivity.

To examine the uniqueness of the inverse problem, response surfaces for different parameters are calculated by disturbing two parameters while keeping the others fixed at their "true" values, i.e., the optimized values. Then, the simulated outflow data with different parameter sets are calculated. Deviations between the simulation and the measurement are expressed as χ^2,

$$\chi^2 = \sum_{i=1}^{k} (Q_{m_i} - Q_{s_i})^2 \tag{4.1}$$

where Q_{m_i} is the measured outflow and Q_{s_i} is the outflow simulated with disturbed parameters. In our case, the parameters are disturbed with a range of $\pm 3\sigma$ (the variance σ^2 was determined by the inverse procedure for the optimized parameters). For each parameter, 30 perturbations were taken resulting in 900 combinations for each response surface. Since the variance of K_s is as large as 102 cm h^{-1}, the perturbation steps were kept in the related cases at 1.5σ. The response surfaces are drawn with the dimensionless parameters instead of the original values.

The two-dimensional surfaces of χ^2 as a function of pairs of hydraulic parameters are shown in Figure 4.3. χ^2 surfaces for the cumulative outflow were calculated in six parameter planes (i.e. n-τ, K_s-τ, τ-θ_s, α-θ_s, θ_s-n and K_s-τ). All the response surfaces, with the exception of the K_s-τ parameter plane, show well defined global minima. For K_s-τ parameter plane, a long valley is found, indicating that many possible combinations of these two parameters would result in small deviations between simulation and the measurement. Hence, it is difficult to find a unique minimum. With the other parameters fixed at the "true" value, identification of K_s and τ would depend on the sensitivity of the optimizer and the start values. Also noises in the data set will greatly influence the estimation of K_s.

As shown in Table 4.2, the standard deviation and coefficient variance of the parameters are calculated, which were used to measure the estimation precision as well as the sensitivity of the parameters in the inverse parameter estimation. Among the five MvG parameters, α is the most sensitive and can be determined precisely. θ_s and n are also sensitive and can be estimated with high precision, while K_s and τ are insensitive parameters. Note that precision does not necessarily mean accuracy as one can find from parameter comparison in Table 4.1. Table 4.3 shows the correlation matrix for the optimized parameters for the coarse sand with K_s fitted. High correlations can be found between θ_s-τ, K_s-τ, n-θ_s, n-τ. Because of the high correlations, these parameters show high level of uncertainty.

Now we can look at Table 4.1 again for a better understanding of the differences in

Table 4.2: Optimized MvG parameters with K_s fitted for the coarse sand.

	Optimized Value	Standard deviation	Coefficient of Variation (%)
α [cm^{-1}]	0.0776	0.000179	0.23
n	3.12	0.030985	0.99
θ_s	0.307	0.002007	0.65
K_s [cm h^{-1}]	1.8×10^3	102.42	5.6
τ	3.41	0.08217	2.4

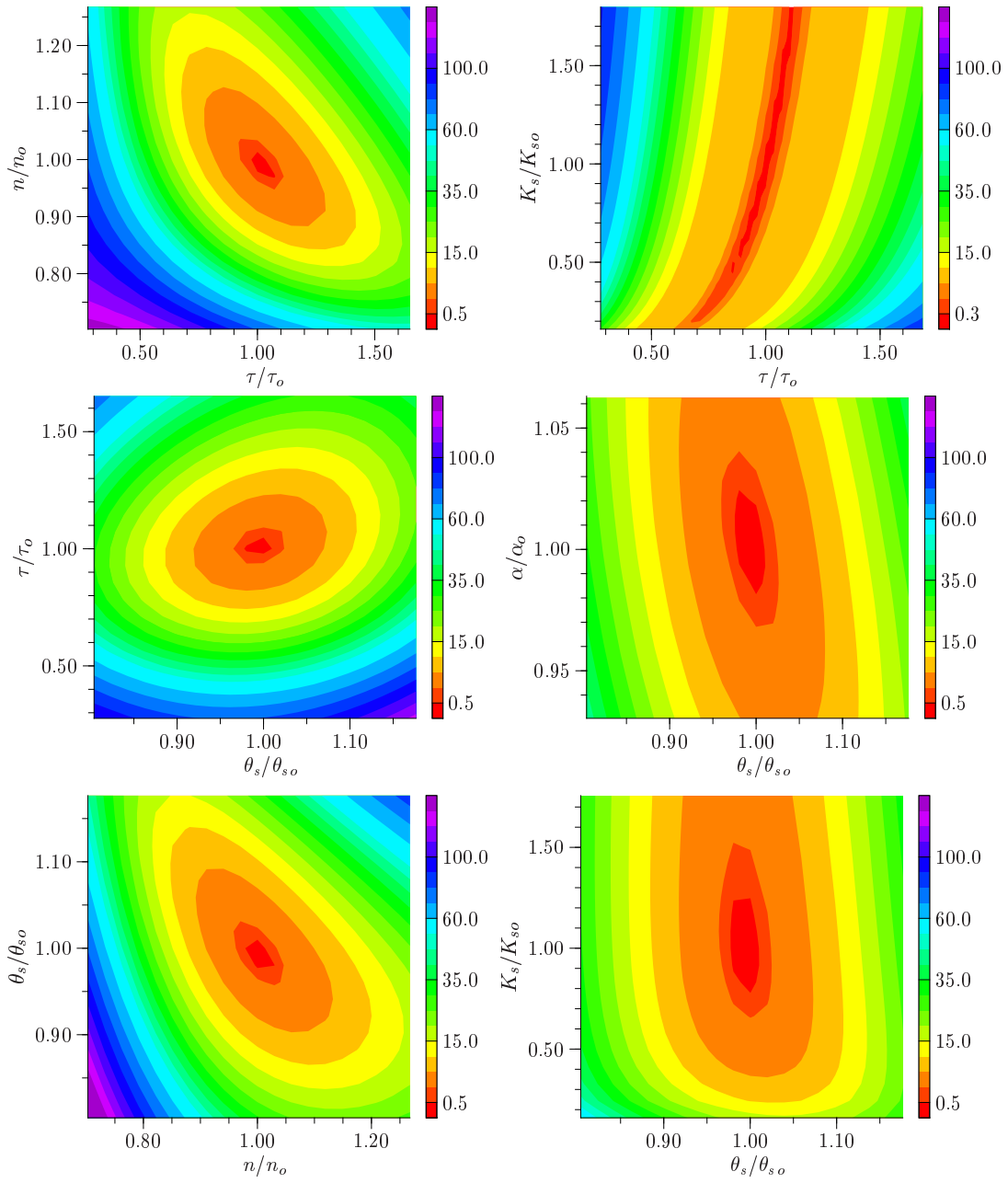

Figure 4.3: χ^2 surfaces for the coarse sand

Table 4.3: Correlation matrix for optimized MvG parameters with K_s fitted for the coarse sand

	α	n	θ_s	K_s	τ
α	1.0				
n	−0.31	1.0			
θ_s	0.15	−0.98	1.0		
K_s	0.45	−0.74	−0.68	1.0	
τ	0.22	−0.96	0.95	0.86	1.0

the estimated parameters with K_s fixed at the measured value and those obtained with K_s fitted. When K_s is free for fitting, there is more freedom and in order to minimize the deviation between simulation and the measurement, the parameters are adjusted in such a way that for all the data points, the averaged error is approaching a minimum. Since K_s is insensitive compared to the other parameters, large changes lead to only small decreases of χ^2. At the end, an unreasonably large K_s is obtained and since there is positive correlation between K_s and τ, a large τ is also obtained. Hence, when K_s is fixed at the measured value which is much smaller than the estimated value, the other parameters, e.g. a lower θ_s, a larger n and a smaller τ are understandable. In contrast to the good fit with K_s fitted, the simulated outflow curve with K_s fixed at the measured value exhibits large deviations from the observed outflow especially at the shoulder of the second pressure step. This indicates that either the independently measured K_s is inaccurate or the VG parameterization form of water retention function is inappropriate assuming Richards equation is sufficient to describe the flow behavior. Using the falling head method, PVC columns in different diameters (one is exactly the same with that for MSO measurement) were employed to test the reproducibility of measurement of K_s. Morever, the columns were filled in the same way as in the MSO experiment. It was found that although there was slight variation with the measurement values the results are generally reproducible. In this sense, it can be considered that the independent measured K_s is reliable. Therefore, only an inappropriate parameterization form of the water retention function can account for the large discrepancies between the model and the measurement, i.e., VG form in this situation may not be the right model. When fitting all the parameters, the deviations caused by an inappropriate parameterization form of the water retention function are compensated by choosing—through correlation—the "best set" of parameters. This effort leads to a fit that appears correct with actually wrong parameters. On the other hand, if the aim of the parameter estimation is to find a set of parameters that can describe the

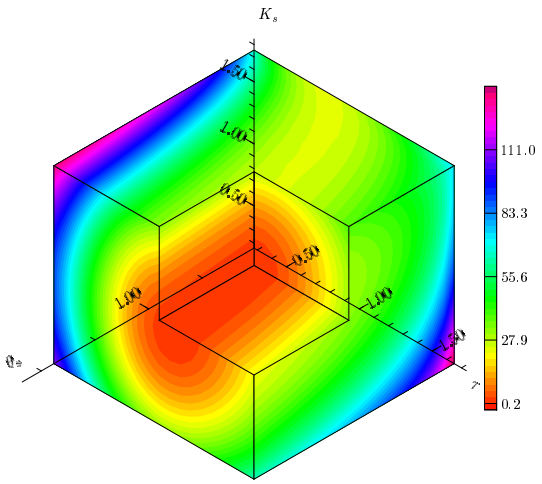

Figure 4.4: χ^2 surface for cumulative outflow in the θ_s-τ-K_s three dimensional space for the coarse sand

experimental data, it might be also reasonable to take the "best set" of parameters.

In fact, the different parameter planes given above represent only cross sections of the full five-dimensional parameter space. The χ^2 surfaces for cumulative outflow in the parameter planes can only suggest how the objective function might behave in the five dimensional continuum. But from the parameter planes it is straightforward to show whether there is a local minimum or a global minimum exists or not. The inverse parameter estimation technique is expected to be unsuccessful if the response surfaces do not display a clearly defined global minimum in the two-dimensional parameter planes. Response surfaces in spaces of more than two dimensions are difficult to display. But it contains more information. For example, Figure 4.4 is the χ^2 surface for cumulative outflow in the three dimensional parameter space.

4.2 The Fine Sand

For the fine sand, because of its light texture and less structure, there is a problem with keeping the system rigid and stable as required by Richards equation. All the columns are filled in such a way that samples are dropped from the top of the column and water moistens them by capillary rising from the bottom in order to establish an expected stable system. Excess sand above the surface was removed and the surface hence was flattened while it was found that at the end of the imbibition process, the fine sand would float up and exceed the surface by 2-3 mm. To prevent this, either preliminary runs are carried out and redundant sand is removed after each run until it stays flat, or using a metal sheet with holes on it at the surface acting as a pressure on the sand when it floats up without interfering the connection between water and atmosphere. Figure 4.5 shows three consecutive runs with the metal sheet at the surface. The sand did not float up after each run and one can find that after the first run, the system gets stable. Differences in outflow curves become very small. In this sense, we can still consider the system as rigid and stable as required by Richards equation.

Figure 4.6 shows the estimated water retention curves and unsaturated hydraulic conductivity function curves for a second and a fourth run with the same column and under the same experimental conditions. It was found that for the unsaturated

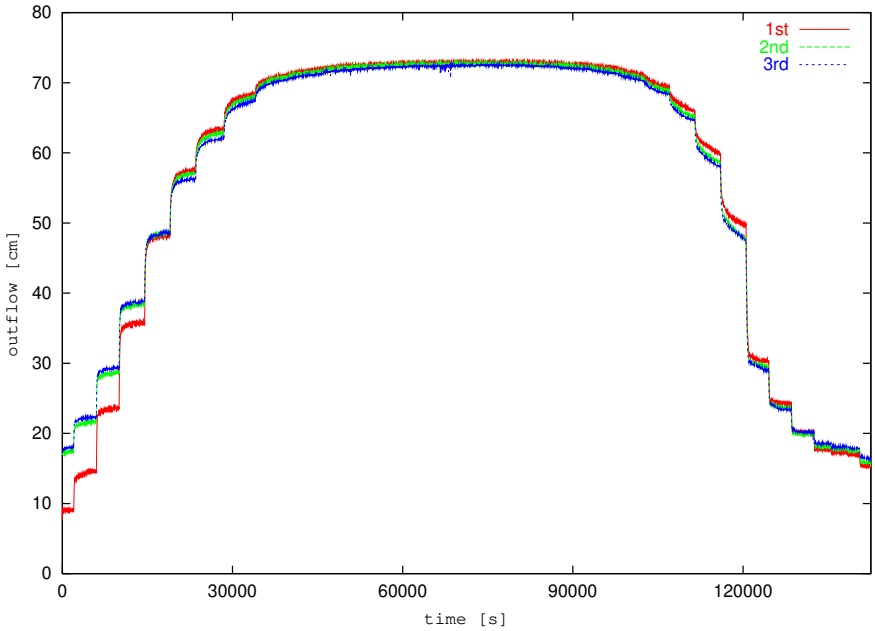

Figure 4.5: Reproducibility of multi-step outflow experiments with the fine sand—the outflow curves

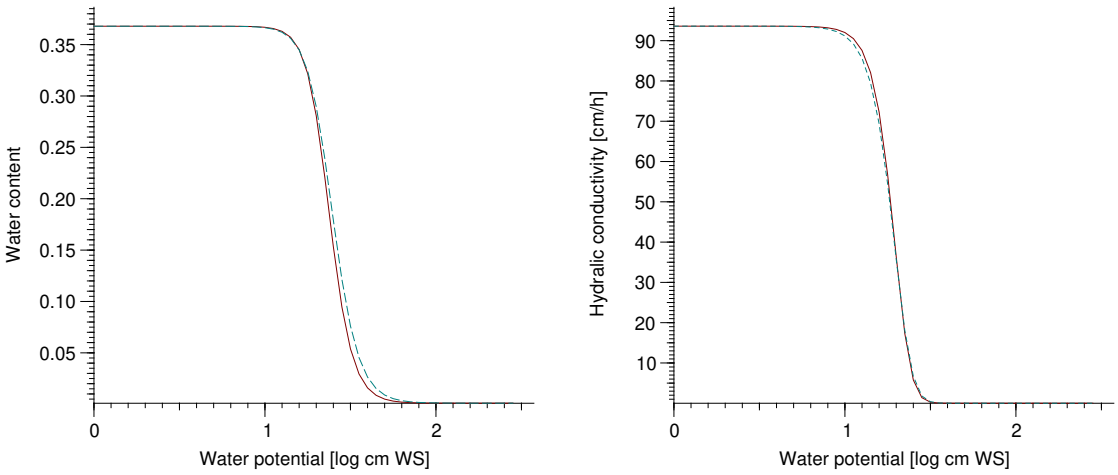

Figure 4.6: Hydraulic functions estimated from two MSO repeats with the fine sand

Table 4.4: Estimated MvG parameters for the fine sand with K_s fixed

		95% confidence interval			
Parameter	value	lower limit	upper limit	SD	CV (%)
α [cm^{-1}]	0.0434	0.0434	0.0435	3×10^{-5}	0.07
n	6.82	6.74	6.89	3.8×10^{-2}	0.56
θ_s	0.367	0.366	0.369	6.08×10^{-4}	0.17
τ	0.53	0.51	0.55	0.0106	1.99

hydraulic function except at the near saturation region, where there is little difference in $K(\psi)$, estimations from the two MSO experiments are generally consistent with each other. While for the water retention curve, at the low saturation of the curve, the difference between the two runs is getting larger up to 2% approximately.

Table 4.4 shows the estimated MvG parameters with K_s fixed at the measured value. Similar to the case of the coarse sand, α is the most sensitive parameter and can be identified with very small variance. Figure 4.7 shows one of the fitting results for the fine sand. Apparently, Richards equation using hydraulic functions expressed in MvG parameterization forms encountered some difficulty to describe the flow behavior of the system especially in the high saturation stage (e.g. at the first 3-4 pressure steps). Although the model errors again are not randomly distributed, they generally become smaller under high tension. Compared with Figure 4.2, Figure 4.7 does not exhibit a wavelike shape as that of the coarse sand. But at the early stage of the drainage process, the model errors are larger which is similar to those for the coarse sand.

As shown in Figure 4.8, the χ^2 surfaces for cumulative outflow in the different

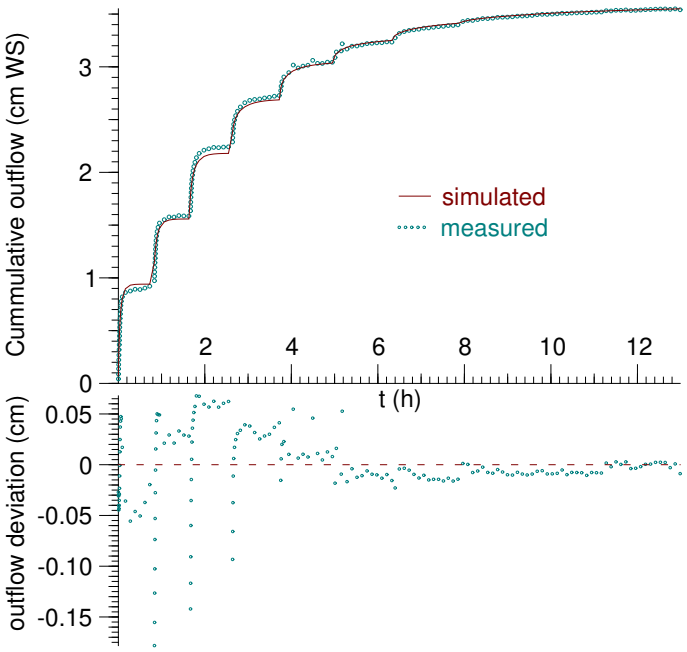

Figure 4.7: Simulated outflow curve with K_s fixed compared with the measurement for the fine sand. The lower figure shows the residuals

parameter planes (θ_s-α, n-α, θ_s-τ, n- τ, n- θ_s, τ-θ_s) show well-defined global minima for all parameter planes when the saturated hydraulic conductivity is fixed at the measured value. α is found again the most sensitive parameter to be identified. n and θ_s are also found to be able to determine with relatively low uncertainty. τ is the most insensitive among the four with the coefficient of variation of about 2% (Table 4.4). As shown in Table 4.5, α does not correlate with n and θ_s, while a high positive correlation between θ_s-τ parameter pair and high negative correlations between n-τ and n-θ_s parameter pairs were found.

There is one problem that is necessary to cause attention. Parameter estimation

Table 4.5: Correlation matrix for estimated MvG parameters for the fine sand with K_s fixed

	α	n	θ_s	τ
α	1.0			
n	0.18	1.0		
θ_s	-0.48	-0.86	1.0	
τ	-0.44	-0.95	0.90	1.0

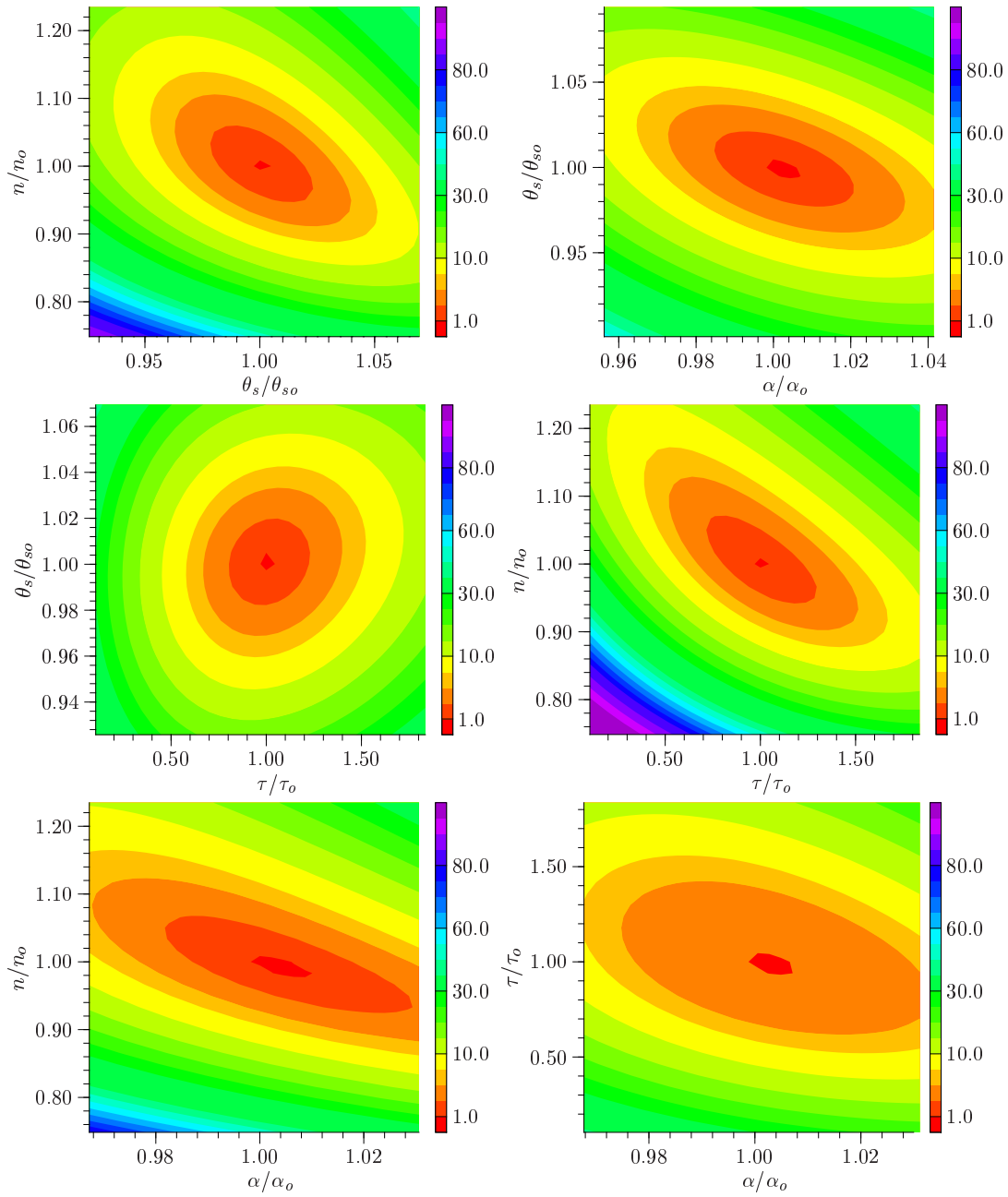

Figure 4.8: χ^2 surfaces for the fine sand

Table 4.6: Effect of data selection on the parameter estimation.

	uniform-s	more-shoulder	shoulder-most	wall-most
α	0.0431	0.0434	0.0430	0.0435
n	6.47	6.82	6.92	6.43
θ_s	0.374	0.368	0.368	0.373
τ	0.67	0.53	0.55	0.62

highly depends on the experimental data set to be simulated. For one drainage curve, different parts of data contain more or less information of a certain parameter, hence are of different sensitivity for the estimation of that parameter (Vrugt et al. 2001, Vrugt and Bouten 2002). Table 4.6 shows the parameters estimated from drainage data with different selection ways. For example, "uniform-s" denotes that the data used in parameter estimation is selected uniformly from the drainage curve. While "shoulder-most" used data mostly from "shoulders" of the drainage curve where outflow changes gradually and almost ceases and "wall-most" used data mostly from "walls" of the drainage curve where outflow changes dramatically. It was found that comparing with the "uniform-s" selection method, using more data from the "shoulders" leading to larger n value and smaller τ, which are inversely correlated with each other. The values of α and θ_s tend to be larger and smaller respectively when using more data from the "shoulders". However, the effect is not so obvious.

4.3 The Mixed Material

The grain size distribution of the mixed material is much more complicated than the others investigated here (Table 3.1). With not only fine sand, coarse sand but also from fine to coarse gravels consisting in this material, difficulties were encountered when trying to build the column with exactly the same portions of grain as listed in Table 3.1. Before taking the sample out of the container, it was mixed again manually to eliminate the heterogeneity caused by transportation. Then well-mixed material was filled into the PVC column, during which attention was paid to avoid creating artificial structures. Pressure was decreased at small steps (2 cm for the first 6 steps) to avoid losing hydraulic connections.

As shown in Figure 4.9, both the unimodal model and the bimodal model of hydraulic functions were applied to fit the MSO data. But obviously, the unimodal model for hydraulic functions has no chance to describe the complicated outflow curve. Except at the early stage of drainage, the unimodal hydraulic function model failed completely. Contrary to the unimodal model, the bimodal hydraulic function model agreed with the measurement quite well except at the third pressure step where there is first an underestimation later an overestimation of the outflow data, which was also encountered in the fitting of MSO experimental data with fine sand and coarse sand. However, except this, the deviation curve does not show the same wavelike structure as the other two materials mentioned above. Model errors distributed more randomly than other fittings.

The estimated hydraulic function curves are shown in Figure 4.10. As one can see, both the hydraulic conductivity function curve and water retention curve show a bimodal characteristic, corresponding to two different pore systems with different air entry values (α) and range of grain size distributions (n). These two different pore systems contribute to water flow by a weighting factor wi. As shown in Table 4.7, the pore systems at smaller and larger pore size are almost equally pronounced with a weight factor of approximately 0.5. The system remains at high saturation until the matric potential is reduced to the air entry value of the larger pore system. The saturation then decreases dramatically with potential. Later when matric potential is reduced to the air entry value of the smaller pore system, water content decreases again with decrease of matric potential. The hydraulic conductivity function curve shows a similar behavior. As the first to recommend bimodal hydraulic functions, Zurmühl and Durner (1996) and Zurmühl and Durner (1998) investigated the possibility of improving the goodness-of-fit for measured outflow data with bimodal functions and identifiability of the parameters of bimodal hydraulic functions. By assuming soils with different degrees of bimodality, they created synthetic multi-step outflow data and inverse modeling was applied to determine hydraulic parameters

for bimodal hydraulic functions. Through both the goodness-of-fit and parameter sensitivity analysis, they concluded that as long as the bimodality is well defined, the goodness-of-fit can be improved and also the parameters can be identified. Evaluation of optimization runs with different starting values of the parameters consistently showed that the inverse problem is unique if the derivative of the water retention curve, $\partial\theta/\partial log(-\psi)$, has two distinct maxima.

The multimodal function proposed by Zurmühl and Durner (1996) and Zurmühl and Durner (1998) is constructed by a linear superposition of weighted subcurves of

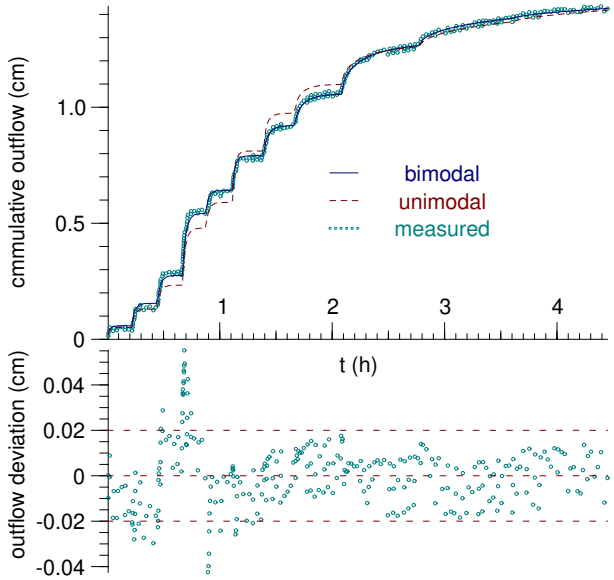

Figure 4.9: Simulated outflow curves with unimodal and bimodal hydraulic functions for the mixed material. The lower figure shows the residuals using bimodal hydraulic functions.

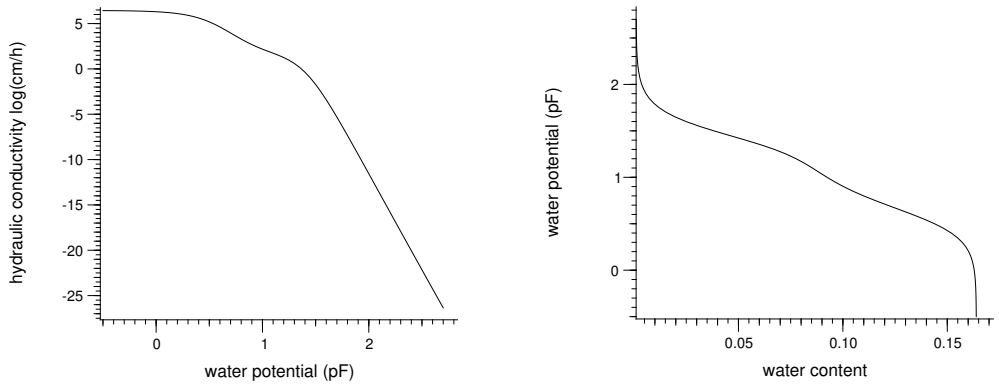

Figure 4.10: Estimated hydraulic functions $K(\psi)$ and $\theta(\psi)$ for the mixed material

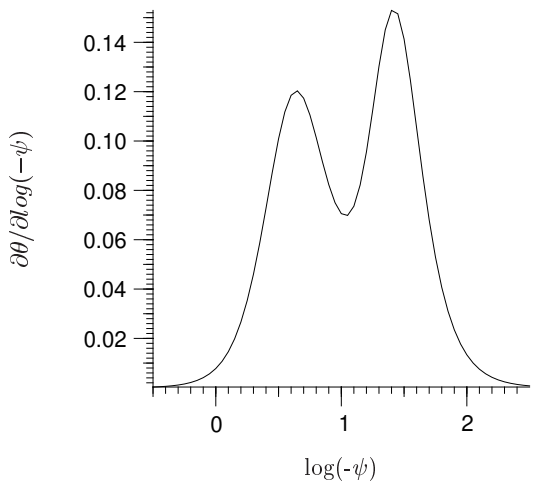

Figure 4.11: Equivalent pore size distribution of the mixed material (ψ in [cm])

the van Genuchten form:

$$\Theta(\psi) = \sum_{i=1}^{k} w_i \left[\frac{1}{1+(\alpha_i\psi)^{n_i}}\right]^{m_i} . \tag{4.2}$$

In Eq. 4.2, the integer k denotes the modality of the model (i.e., the number of pore-size density maxima), w_i [-] are the weighting factors for the subcurves, $0 < w_i < 1$ and $\sum w_i$=1, n_i, α_i, and m_i are the curve-shape parameters of the sub-curves, as in the unimodal case, $m_i = 1 - 1/n_i$.

When the retention function (Eq. 4.2) was coupled with the Mualem model (Eq. 2.8), the unsaturated hydraulic conductivity function for porous media with multimodal pore distribution density is given in the following form:

$$K(\psi) = K_s \left(\sum_{i=1}^{k} w_i \left[1+(\alpha_i|\psi|)^{n_i}\right]^{-m_i}\right)^{\tau} \cdot \left(\sum_{i=1}^{k} w_i\alpha_i \left\{1 - \left(\alpha_i|\psi|^{n_i-1}\left[1+(\alpha_i|\psi|)^{n_i}\right]^{-m_i}\right)\right\}\right)^2 / \left(\sum_{i=1}^{k} w_i\alpha_i\right)^2 \tag{4.3}$$

For bimodal function, modality $k = 2$.

In our case, as shown in Figure 4.11, the equivalent pore size distribution has two distinct maxima, hence bimodality of hydraulic function is strong in the sense of applicability of the bimodal model.

Table 4.8 shows the correlation matrix for the bimodal parameters. Except the α_1-n_1 parameter pair, correlation between parameter pairs is reduced. Statistical analysis for the estimated parameters shows that the parameters are optimized with high precision. Compared with the other parameters, uncertainty of n_2 is a little

Table 4.7: Estimated MvG parameters for the mixed material using the bimodal model with K_s fixed

		95% confidence interval			
Parameter	value	lower limit	upper limit	SD[a]	CV[b](%)
α_1	0.0387	0.0383	0.0391	0.000189	0.489
n_1	3.55	3.53	3.57	0.01047	0.295
θ_s	0.1639	0.1633	0.1645	0.00030	0.184
wi	0.51	0.50	0.52	0.00361	0.703
α_2	0.2516	0.2480	0.2553	0.00185	0.736
n_2	2.88	2.80	2.95	0.0385	1.337

[a]standard deviation
[b]coefficient of variation

Table 4.8: Correlation matrix for the optimized MvG parameters with K_s fixed for the mixed material

	α_1	n_1	θ_s	wi	α_2	n_2
α_1	1.0					
n_1	−0.92	1.0				
θ_s	−0.55	0.47	1.0			
wi	0.76	−0.74	−0.08	1.0		
α_2	−0.09	−0.02	0.63	0.53	1.0	
n_2	0.80	−0.76	−0.59	0.73	−0.02	1.0

higher, which is consistent with the χ^2 surfaces shown in Figure 4.12. The χ^2 contour lines on response surfaces in the n_1-n_2, n_2-α_2 parameter planes exhibit a curvature from small n_2 values to large n_2 values, which indicates that outflow response is sensitive to the change in the n_2 value when it is small while it becomes insensitive when it is getting larger.

Generally speaking, higher flexibility of the bimodal hydraulic functions enables a much better fit to the outflow data and more reliable parameter estimates which cannot be fulfilled by using a simple unimodal function for the mixed material. However, the disadvantage of using such a model is that there are more parameters need to be optimized, which reduces the parameter sensitivity to some extent.

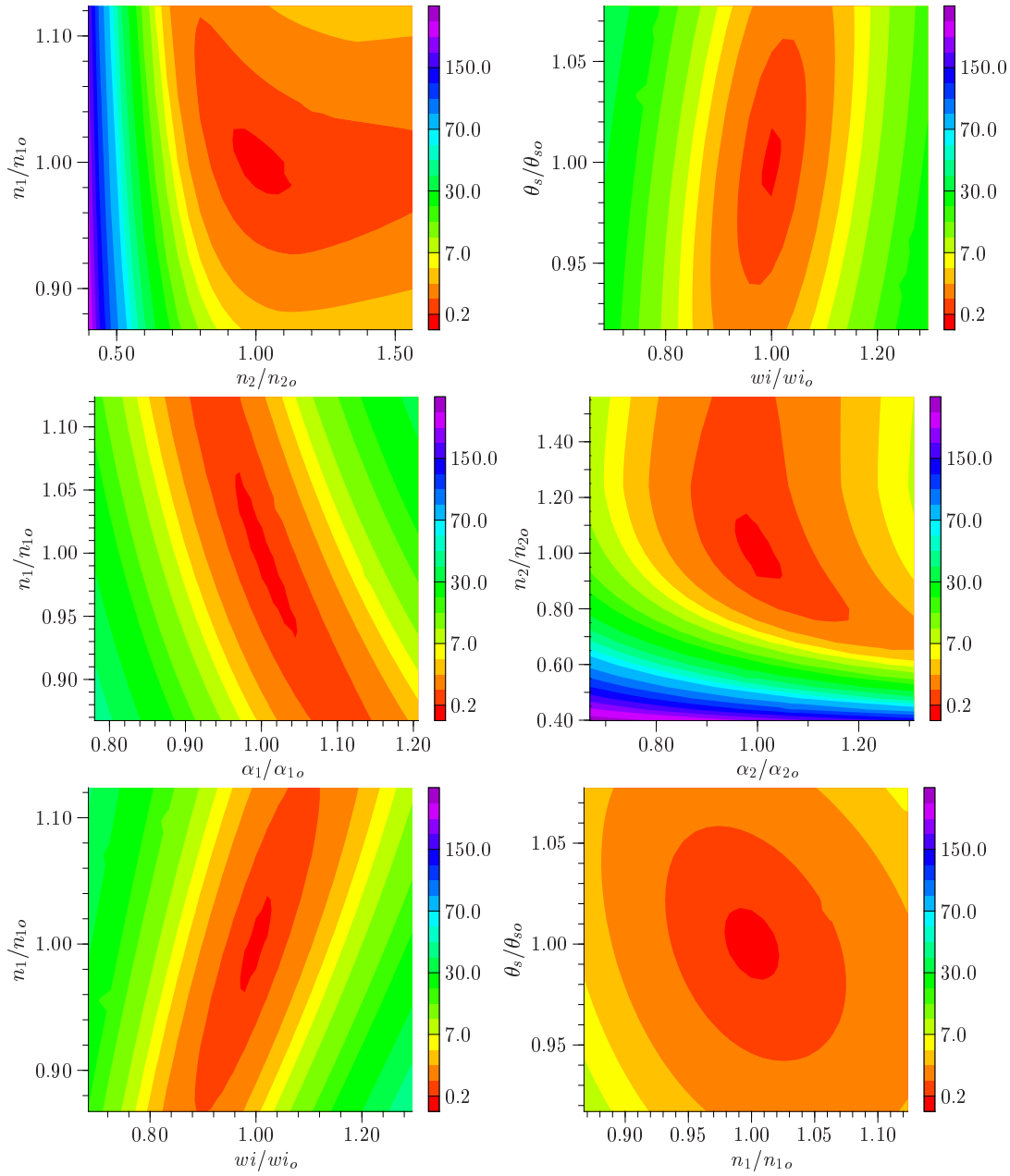

Figure 4.12: χ^2 surfaces for the mixed material

4.4 Sources for the Deviation between Simulations and Measurements

When viewed at the microscopic scale, subsurface properties and flows are highly discontinuously distributed which results in the nonlinear macroscopic hydraulic properties including water retention and hydraulic conductivity functions. Flow behavior in the macroscopic continuity is based on the representative element volume (REV) concept and is derived by volume-averaging. The classical flow concepts and quantitative analyses used today are based on this kind of volume-averaging. The empirically obtained Darcy's law and Richards equation deduced from Darcy's law and the mass conservation equation are both the results of this simplification and averaging. However, in doing so, all uncertainties of the microscopic processes were embedded in the macroscopic constitutive functions. In this section, the possible interpretations for the deviation between the simulation based on Richards equation using MvG hydraulic function models and the measurements are discussed.

As shown already in the section 4.1 (Figure 4.1, Figure 4.2), section 4.2 (Figure 4.7) and section 4.3 (Figure 4.9), with the optimized MvG hydraulic parameters, cumulative outflow calculated from Richards equation deviated from the observed value expecially in early stage of the drainage process for all the materials. Here, we classify these deviations into three groups which leads to overestimation or underestimation of the cumulative outflow at different stages of the drainage process. Note that, to separate the effects of the different sources completely needs a thourough understanding of the flow process. However, from the microscopic principle to the macroscopic phenomena, too many uncertainties exist which allow only an qualitative analysis at the moment.

The following subsection 4.4.1 traces the macroscopical Darcy's law back to the microscopical Navier-Stokes equation in order to help us understand that deviations between Darcy's law and the measurement we observe at continuum scale might be the cost of averaging and simplification of the microscopic fluid flow that follows the Navier-Stokes equation. The deduction in this subsection is attributed to Prof. K. Roth (University of Heidelberg) in his lecture notes.

4.4.1 From Navier-Stokes equation to Darcy's law–the effect of simplification

The Navier-Stokes equation for a uniform and incompressible Newtonian fluid is given in the following form (Tritton, 1988):

$$\rho \partial_t v + \rho \left[v \cdot \nabla \right] v = \rho g - \nabla p + \mu \nabla^2 v \ . \tag{4.4}$$

The kinematic form of Eq. 4.4 can be obtained by dividing it by the constant fluid density ρ, as

$$\partial_t v + [v \cdot \nabla] v = g - \frac{1}{\rho}\nabla p + \nu \nabla^2 v \tag{4.5}$$

where $\nu = \mu/\rho$ is the kinematic viscosity. The full set of Navier-Stokes equations is so complex that it is unrealistic and unrevealing to search for the general solutions. Approximations valid for certian specific circumstances are much more useful. To make systematic approximations it is necessary to have a procedure that helps us discern precisely what is small and what is not. A standard procedure is to find the scales relevant to the problem at hand. Normalization by these scales leads to dimensionless parameters which represent the relative importance of various parts of the full equations.

Introducing the dimensionless variables

$$t^{'} = \frac{t}{\tau}, \quad x^{'} = \frac{x}{l}, \quad v^{'} = \frac{v}{u}, \quad p^{'} = \frac{p}{u^2\rho} \tag{4.6}$$

and hence the derivatives $\partial_{t'} = \tau \partial_t$ and $\nabla^{'} = l\nabla$, transforms Eq. 4.5 into

$$\frac{u}{\tau}\partial_{t'} v^{'} + \frac{u^2}{l}\left[v^{'} \cdot \nabla^{'}\right] v^{'} = g\widehat{\mathrm{g}} - \frac{u^2}{l}\nabla^{'} p^{'} + \frac{\nu u}{l^2}\nabla^{'2} v^{'} \tag{4.7}$$

where $\widehat{\mathrm{g}} = \mathrm{g}/g$ is the unit vector pointing in the direction of g. Dividing by u^2/l isolates the inertial term and leads to the dimensionless form

$$\frac{1}{St}\partial_{t'} v^{'} + \left[v^{'} \cdot \nabla^{'}\right] v^{'} = \frac{\widehat{\mathrm{g}}}{Fr} - \nabla^{'} p^{'} + \frac{1}{Re}\nabla^{'2} v^{'} \tag{4.8}$$

where

$$St := \frac{u\tau}{l}, \quad Fr := \frac{u^2}{lg}, \quad Re := \frac{\rho u l}{\mu} = \frac{ul}{\nu} \tag{4.9}$$

are the Strouhal, the Froude, and the Reynolds number, respectively. Strouhal number (St) quantifies the relative importance of local acceleration with respect to that of convective acceleration. The Froude number (Fr) and the Reynolds number (Re) quantify the relative importance of inertia with respect to gravity, and viscosity respectively. Now it is easy to decide how to make approximations. For a low laminar flow, i.e., St$\ll$1, Fr$\ll$1, Re $\ll$1, we get the time dependent Stokes equation

$$\frac{1}{St}\partial_{t'} v^{'} = \frac{1}{Fr}\widehat{\mathrm{g}} - \nabla^{'} p^{'} + \frac{1}{Re}\nabla^{'2} v^{'} \ . \tag{4.10}$$

Additionally, assuming $St \gg max(Fr, Re)$), the time independent Stokes equation is

$$\mu \nabla^2 v = \nabla p - \rho g \ . \tag{4.11}$$

This time-independent stokes equation is linear. Hence, if $\{v,\ p\}$ is a solution then $\{\alpha v,\ \alpha p\}$ is also one. And since v and $-\nabla p$ are parallel we then can write

$$v\left(x;l,\mu\right) = -k(x;l,\mu)\nabla p(x;l,\mu) \tag{4.12}$$

where $k(x;l,\mu)$ is some scalar function which is typically of a very complicated form. Here we neglected gravity. Extension to gravity as an additional driving force is straightforward. We can include it by simply replacing $-\nabla p$ with the sum of pressure gradient and gravity per unit volume. We obtain the the following relation

$$v\left(x;l,\mu\right) = -k(x;l,\mu)\left[\nabla p(x;l,\mu) - \rho g\right]\ . \tag{4.13}$$

This equation shows a linear relation between the water velocity and the sum of pressure gradient and gravity per unit volume, which has the similar form with the macroscopic Darcy's law. Based on this equation and invoke averaging over REV, the macroscopic formulation—the Darcy's law can be obtained.

As we find from the deduction above, from the microscopic Navier-Stokes equation to the macroscopic Darcy's law, we assumed that inertia is negligible and external forcing time is short meaning a small Strouhal number. Whenever we apply Darcy's law or Richards equation in our continuum scale, e.g. a porous medium, we should be sure that the conditions must be fit exactly, i.e., St$\ll$1, Fr$\ll$1, Re$\ll$1. Once there is one condition that is not met, the application of Darcy's law or Richards equation will lead to deviation from the reality.

We now look at the specific case of the MSO experiment with coarse sand. As shown in Figure 4.13, the fluid velocity is calculated from outflow data. We will estimate the Strouhal number first according to $St = u\tau/l$. $l = 1.5$ mm (estimated from grain size distribution), $u = 22$ cm h^{-1}, the external acceleration time $\tau = 15 - 30$ s, which lead to a $St = 0.6 - 1.2$. This result indicates that although we cannot say how much the inertia contributes to the acceleration of the flow, at least it is hard to say that it can be completely neglected. When the criteria for neglecting the inertial term $[v \cdot \nabla]\, v$ is not satisfied, we can expect to find at least some regions where the flow is turbulent, i.e.,transient even for stationary external forcing. The direct influence of neglecting the inertia is that we expected a faster drainage while the reality is on the contrary, i.e., the model overestimated the outflow. Note that when we did the rough estimation of the Strouhal number, the characteristic velocity of the system is chosen to be equal to the highest fluid velocity, which appears very often at the instances of the pressure change. Between two pressure changes and also as the sample getting drier and drier, the velocity is getting smaller, hence leads to a smaller Strouhal number, thereby, in the drier stage of the drainage, the inertia term can be negligible. This analysis is consistent with the deviation curve which shows that at the early stage of the drainage, overestimation occurred regularly when the pressure steps change while it is not obvious later.

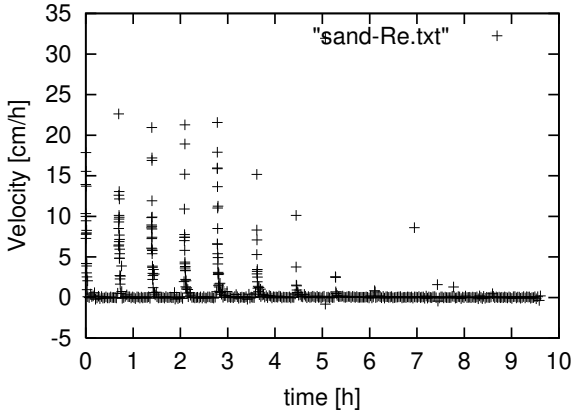

Figure 4.13: Fluid velocity calculated for the coarse sand. Not all data are used.

For the same reason, we note that from the time-dependent Stokes equation to the time-independent Stokes equation, St is assumed to be much larger than Re and Fr, which means that the external acceleration is negligible in comparison with viscosity and gravity. We again take the specific experiment for the coarse sand. The fluid velocity shown in Figure 4.13 is used for calculating the Reynolds number. Taking the highest velocity $u = 22$ cm h^{-1}, characteristic length of the material $d = 1.5$ cm, since dynamic viscosity ν/ρ_w of water is about 10^{-6} m^2 s^{-1}. Then Re can be roughly estimated, which is about 0.1. Compared this Re with St, we can find that the difference between these two is not so significant, which actually is required when deducing time-independent Stokes equation from time-dependent Stokes equation, while the latter is pre-condition for the transition from Stokes equation to Darcy's law. Large velocities appear regularly corresponding to the pressure changes as discussed above. This implies that when the pressure changes are sharp, at the beginning of the change, external force is non-negligible compared to viscosity.

Although it is hard to decide precisely the Re and the St from our data, the estimation above at least should cause attention when such coarse porous medium is under investigation. And it is possible that neglection of these factors may contribute to at least some of the model errors. Till now, we want to conclude that application of the macroscopic hydraulic equation –the Darcy's law and Richards equation which neglects the effects of the inertia and the external acceleration on water flow in coarse porous media with high hydraulic conductivity might result in overestimation of cumulative outflow for an MSO experiment with sharp changes in pressure.

4.4.2 Multiphase phenomena

The traditional Richards equation applied in the inverse parameter approach assumes that the air-phase is continuous everywhere with a pressure equal to the

atmospheric pressure and its influence on dynamics of water flow is negligible which means that no pressure gradients will build up in the gas phase. Air-water systems were then treated as one-phase (water) systems. Whereas more and more evidence indicate that the effect of air flow on water flow in many cases cannot be neglected and the condition that air continuity is established everywhere is hard to achieve. The loss of gas-phase continuity will cause deviations from atmospheric pressure since no matter under pressure or suction volumes of the entrapped air bubbles will be changed, either smaller or larger than that of continuous air-phase. Some experimental results showed that continuity of air phase could not establish until some amount of water has left the pore system. As found by Fischer et al. (1996), at a saturation above 0.58 during drainage and 0.66 during imbibition, relative permeability of gas was nonzero which indicates a non-continuous gas-phase.

Hopmans et al. (1992) used X-ray tomography to measure spatial and temporal changes in soil water distribution for two soils, a sandy soil and a sandy loam soil in one-step outflow experiments. It was found that the drainage process was influenced by the initial water content distribution. For the saturated sample, a drying front develops at the top of the sample and moves downward until air continuity is established from the top to the bottom of the sample. Only then will desorption continue at the bottom as well and the cumulative outflow is linear. This result indicated that at the early stage of drainage, air continuity, the condition needed by Richards equation is not developed. Before this condition is established, Richards equation will encounter difficulty to describe the flow behavior, in other words, flow behavior does not follow Richards equation. In these cases, transient water flow process in porous media must be regarded as a two-phase flow problem.

4.4.3 Dynamic effect in the capillary pressure-saturation relationship

For a conventional MSO experiment, no matter the outflow is induced by pneumatic pressure (van Dam et al. 1994, Eching and Hopmans 1993, Eching et al. 1994) at the upper boundary or by suction at the lower boundary, it is assumed that the capillary pressure follows the traditional capillary theory, the Young-Laplace equation,

$$\psi_c = |P_w - P_a| = \frac{2\sigma_{wa}}{r} \tag{4.14}$$

where ψ_c is capillary potential, P_w is the pressure in the water phase, P_a is the pressure in the air phase, σ_{wa} is the surface tension of the water-air phase and r is the radius of the capillary. Application of suction at the lower boundary actually changes the capillary potential by reducing the pressure in the water phase, while applying pneumatic pressure changes the capillary potential by increasing pressure

in the gas phase. These two can be put in the following form,

$$\psi_c \stackrel{?}{=} |P_a - P_{g,t}| = \frac{2\sigma_{wa}}{r} \tag{4.15}$$

where P_g and P_t are the pneumatic pressure and suction (tension) respectively. In the conventional procedure of inverse simulation of MSO experimental data, it is assumed that this relationship (Eq. 4.15) is true. While the question mark above the equal sign is suggested by Hassanizadeh et al. (2002). To be precisely speaking, it was suggested that these two are not equal unless the system is under equilibrium or steady state condition. It was demonstrated on the basis of thermodynamic theory that dynamic pressure $|P_a - P_{g,t}|$ is larger than the equilibrium capillary pressure ψ_c. Treating ψ_c equal to $|P_a - P_{g,t}|$ in the inverse simulation will cause deviations from the measurement, i.e., overestimation of outflow.

Notice that although pursued from a different point of view, dynamic effects might also result from neglecting of inertia since in the case of instantaneous or fast equilibrium, both errors caused by ignoring dynamic effects and inertia can be very small.

4.4.4 Heterogeneity

Richards equation assumes that the porous medium is homogeneous, isotropic, isothermal, and rigid and the representative elementary volume (REV) contains all the microscopic heterogeneities.

The REV concept was given by Bear (1972). He defined "Representative Elementary Volume" as the smallest volume over which there is a constant "effective" proportionality factor between the flux and the total pressure gradient or total head gradient. This proportionality factor is called the hydraulic conductivity of the REV. By definition of the REV, the hydraulic conductivity does not rapidly change as the volume to which it applies is increased to sizes larger than the REV. This is based on the conceptual notion that no heterogeneity is encountered at a scale larger than the REV.

In our cases, although attention was paid to build the column relatively homogeneous, existence of local heterogeneity is unavoidable. When there is local heterogeneity of structure, the hydraulic conductivity will change as the volume to which it applies is larger than the REV and contains this local heterogeneity. As illustrated in the sketch (Figure 4.15), such local heterogeneity will lengthen the flowpaths hence leads to the decrease of the hydraulic conductivity. Reflected from the cumulative outflow response of the system, slower increase of cumulative outflow will be expected than that under the absence of such local heterogeneity.

It is difficult to identify the local heterogeneity in the structure of the system

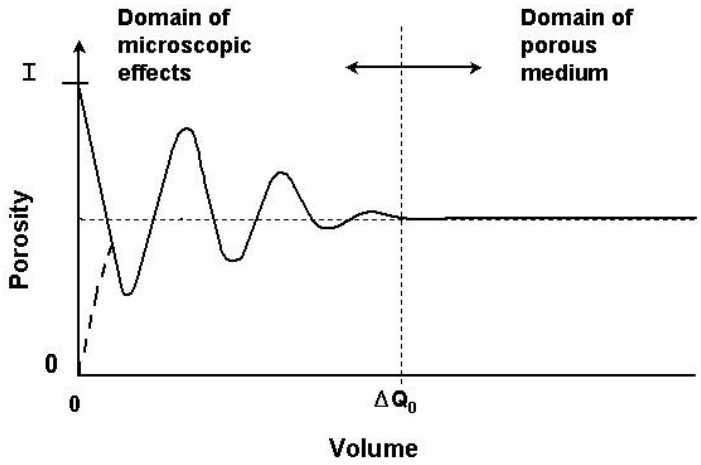

Figure 4.14: REV concept (after Bear(1972))

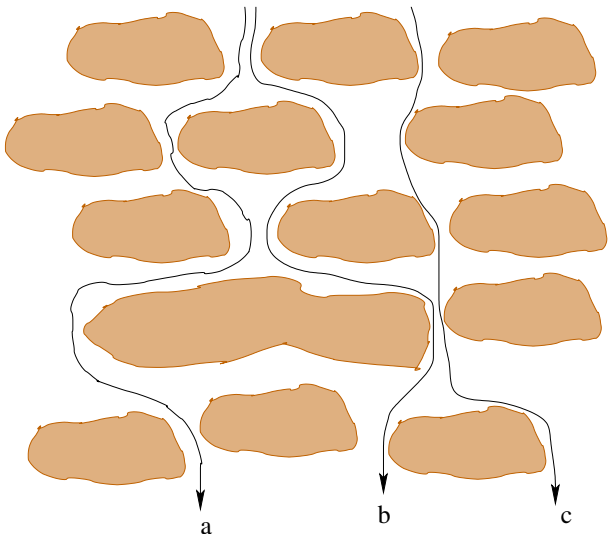

Figure 4.15: Effect of local heterogeneity–an example. Flowpaths a and b influenced by local heterogeneity are longer than c

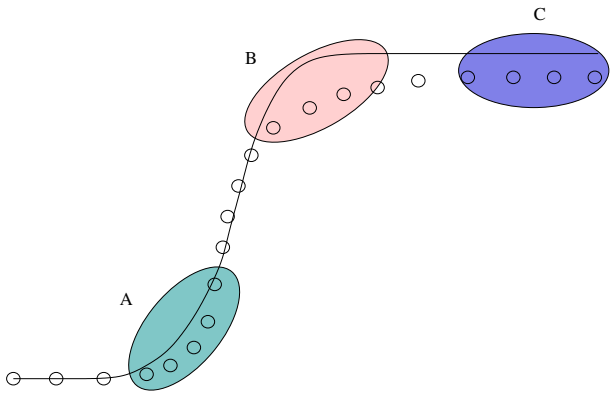

Figure 4.16: Sketch of possible sources for deviation between the model and measurement. A.non-stokes flow; B. heterogeneity, $K(\theta)$ etc. C. parameterization of water characteristic

with the outflow experiment itself. To visualize the structure of the system, X-ray tomography is suggested.

4.4.5 Parameterizations of hydraulic properties

As described in the theory part already, currently most of the parameterization models or forms available for water retention functions are basically empirical which means that no sound physical basis for the constructed θ—ψ relationship. Hence the corresponding models for the hydraulic conductivity function deduced from combining these water retention models and the Mualem model for the hydraulic conductivity function are also lack of sound physical basis. Thereby, almost all the parameters in the parameterizations of hydraulic properties are purely fitting parameters. θ_s and θ_r are of physical significance. However, the inversion can only determine the water available, i.e., $\Delta\theta = \theta_s - \theta_r$. Usually either θ_s is fixed at the measured value or θ_r is fixed at some arbitrary value. Under this situation, the requirement that the constructive relationship must represent the properties of the real pore space when applying these models in an inverse procedure is not guaranteed. Inappropriate models for hydraulic functions can be revealed by extending the pressure duration until the outflow ceases to check whether the deviation is getting smaller or continuously increasing. The latter indicate a wrong model for hydraulic properties.

To summarize this section, the possible sources and their possible active stage on one step of outflow are plotted, as depicted in Figure 4.16.

As in the whole process, deviations tend to appear in the wet stage of drainage. Note that, although illustrated here the separated sources, actually when using inverse techniques to estimate the hydraulic parameters, the total least square, the

estimated parameters, hence the hydraulic functions and the estimated outflow curve will highly depend on the selection of data points. The deviation curve will change significantly. Some factors will be highlighted and the influence of the other ones might be weakened. Whereas the procedure aims at a global minimum, it is hard to separate the influence of the different factors.

4.5 Summary

This chapter presented the results of applying the inverse method to multi-step outflow experiments to estimate hydraulic parameters in MvG parameterization forms for the coarse materials.

First, the goodness-of-fit or applicability of the inverse method coupled with MSO method is evaluated by comparing the simulated and the measured outflow data and studying the structure of the residuals, examining the χ^2 surfaces for outflow in different parameter combination planes and calculating the confidence interval and correlation relationship of the optimized parameters.

The following results were obtained:

(i) The simulations, according to conventional criteria, can generally reflect the feature of the outflow, however, the residual curves revealed insufficiency of the model;

(ii) On the one hand, χ^2 surfaces generally showed clear global minima which enables the identifiability of the hydraulic parameters. On the other hand, parameters are still correlated with each other to different extents resulting in uncertainties in parameter estimation.

By examining the residual curves, this chapter discusses the possible sources of the model deviations and classifies them into three groups according to their active stages on one step of outflow curve. The deviations may stem from neglection of the effect of inertia and external acceleration, multiphase influence, dynamic effect, heterogeneity, and parameterization of hydraulic properties.

5 Single Phase Chemical Transport through Coarse Materials with Stationary Water Flux

This chapter will present the results of the transport measurements with the coarse textured materials using Brilliant Blue as a tracer. The aims are to check whether Brilliant Blue can be used as a cost-effective tracer to investigate the transport properties of porous media and whether the traditional convection-dispersion (CD) model and the mobile-immobile (MIM) model are applicable to describe the breakthrough curves of these coarse textured porous media.

The whole chapter is organized as follows:

Section 5.1 describes the transport models employed in this work. Section 5.2 presents the results of fitting the breakthrough curves obtained with different models. These are shown from several small aspects, e.g., the general features of the BTCs of Brilliant Blue through the coarse material, fitting the breakthrough and elution limb, performance of different models and goodness-of-fit analysis of these models, etc. At the end, the chapter is summarized.

As already described in chapter 3, there are two distinct flow rates set for the transport experiments, 0.01 cm h^{-1}, referred to as low flow rate in the remainder of the chapter and 1.0 cm h^{-1} high flow rate. Transport behavior within this range can be roughly estimated although they are not linearly changing with flow rates.

5.1 Transport Models Employed

5.1.1 The convection-dispersion model

For solute transport through a homogeneous porous medium, the description for the dynamics of solute transport based on mass conservative equation and flux equation is,

$$\frac{\partial}{\partial t}\left[\theta C_w^r\right] + \frac{\partial}{\partial z}\left[j_w C_w^r - D_e \frac{\partial}{\partial z} C_w^r\right] = 0 \tag{5.1}$$

where C_w^r is the resident concentration in the water phase. For the simple case of stationary flow of water and uniform water concent, Eq. 5.1 becomes

$$\frac{\partial}{\partial t}C_w^r + V\frac{\partial}{\partial z}C_w^r - D\frac{\partial^2}{\partial z^2}C_w^r = 0 \ , \tag{5.2}$$

where $V := \frac{j_w}{\theta}$ is the pore water velocity, D the dispersion coefficient, describes the dispersive spreading of a solute plume, i.e., the variation of the velocity and it is approximated by

$$D = D_0 + \lambda|V| \tag{5.3}$$

where D_0 represents the effect of molecular diffusion and the parameter $\lambda[L]$ is the dispersivity of the porous medium and is determined by the geometry of the transport volume. Therefore the dispersion coefficient D is influenced by three factors, the molecular diffusion, fluid velocity and the characteristics of the transport volume.

The flux concentration j_s satisfies the same differential equation as the resident concentration C_w^r (Jury and Roth 1990).

Note that, the velocity of solute defined by the CD and the MIM model in the following is the average velocity for all flow paths over a representative elementary volume (REV). Therefore this average velocity does not describe velocity variation caused by heterogeneity inside an REV or at a scale smaller than REV.

The CD model is valid only when the transport of a solute has reached the Fickian regime in which the rate of solute spread grows linearly with time and the dispersive flux becomes linearly proportional to the concentration gradient. This means that a solute must travel over a large distance, or for a long enough period, to interact with many small-scale heterogeneities of the porous medium before the CD model can be applied. In the laboratory experiments, the transport distance, i.e., the length of the column must be larger than the mixing distance. For solute transport in a uniformly packed sand column under completely saturated condition, the transport distance is much larger than the mixing distance which can be estimated from the grain sizes (Padilla et al. 1999). As a result, the CD model is sufficient in this situation. However, as the porous medium desaturates, the number of flow paths decreases, and the velocity variation increases. A solute plume in an unsaturated sand column must then travel a greater distance to attain a complete mixing and to reach the Fickian regime than one in a saturated column. In many cases this distance may exceed the length of the column. As a consequence, the BTCs, in contrast to those under fully saturation, exhibit early breakthough and long tailing which cannot be described by the CD model adequately. It is called pre-Fickian regime (Padilla et al. 1999). Some empirical models have been developed to describe solute transport exhibiting such

long tailing in laboratory experiment, among which the mobile-immobile model is an influential one.

5.1.2 The mobile-immobile Model

The CD model assumes that all the water phase contributes to the transport process by convection and dispersion. However, experimental evidence and theoretical analysis prove that not all the water phase takes part in the solute convective transport. Coat and Smith (1964) (cited by Roth (1996a)) developed a mobile-immobile solute transport model within the field of petroleum engineering and later it was expanded and applied to soil columns (van Genuchten et al. 1977). In this model, water content θ is separated into mobile water phase θ_m and immobile water phase θ_{im}. As a result, solute concentration is also divided into two parts, i.e., $C_t^r = \theta_m C_m^r + \theta_{im} C_{im}^r$. In the mobile water phase solute move is due to convection and dispersion whereas in the immobile water phase solute transport results from molecular diffusion alone. For one-dimensional transport of a conservative solute, the mobile-immobile model can be written as

$$\frac{\partial}{\partial t} C_m^r + \frac{\theta_{im}}{\theta_m} \frac{\partial}{\partial t} C_{im}^r + V \frac{\partial}{\partial z} C_m^r - D \frac{\partial^2}{\partial z^2} C_m^r = 0 \ . \tag{5.4}$$

The two domains are connected by a first order rate transfer of chemical at the boundary of θ_{im} and θ_m according to

$$\theta_{im} \frac{\partial C_{im}^r}{\partial t} = \alpha (C_m^r - C_{im}^r) \tag{5.5}$$

where α is the mass transfer coefficient denoting exchange rate of the solute between the θ_m and θ_{im} phases by molecular diffusion. The dimensionless rate parameter can be defined as $W := \alpha l / j_w$ (l is the measured depth and j_w water flux). W is ranged between $[0, \infty]$. When W=0, there is no exchange, while $W \to \infty$ means the exchange is so fast that instantaneous equilibrium can be achieved. In this case, the equilibrium model—the CD model is sufficient to describe the transport process. Usually $W > 0$ so that the mean velocity of the solute is decreased due to their residence time in the immobile phase. The residence time is proportional to $\frac{\theta}{\theta_m}$ which can be defined as a retardation factor

$$R := \frac{\theta}{\theta_m} = 1 + \frac{\theta_{im}}{\theta_m} \ . \tag{5.6}$$

In this sense, the MIM model is often referred to as a model that accounts for physical nonequilibrium.

5.1.3 Solute transport process with linear kinetic interaction

The previous subsection describes the MIM model in which the total water phase is divided into two regions–the mobile region and the immobile region. Water in the immobile region does not participate in the flow. Diffusion between the two regions is the only process that the immobile region or immobile water phase is involved in. Solute molecules which enter this region by diffusion are entrapped to a certain extent because of the low mobility. This concept is constructed from a physical point of view to describe the pre-Fickian phenomenon. It assumes that the solute is nonreactive.

For solute that is not conservative and interacts with the constituents of the soil matrix or is subject to various biological or chemical processes, the transport models are getting more and more complicated depending on the complexity of the interaction processes. The simplest case is transport of solute with linear adsorption through homogeneous media with stationary water flux. The transport can be modeled as the following,

$$\partial_t C_w^r + \frac{\rho_b}{\theta}\partial_t C_s + \frac{j_w}{\theta}\partial_z C^f = 0 \tag{5.7}$$

and

$$\partial_t C_s - \alpha\left[K_d C_w^r - C_s\right] = 0, \tag{5.8}$$

where C_w^r is the resident concentration in the water phase, C_s the concentration in adsorbed phase, C^f the flux concentration and α the rate parameter, ρ_b the soil bulk density, K_d the equilibrium distribution coefficient. $R = 1 + \frac{\rho_b K_d}{\theta}$ is defined as the retardation factor.

For the convection-dispersion process, $j_w C^f = j_w C_w^r - \theta D \partial_z C_w^r$, and Eq. 5.7 becomes now

$$\partial_t C_w^r + \frac{\rho_b}{\theta}\partial_t C_s + V\partial_z C_w^r - D\partial_{zz} C_w^r = 0 \tag{5.9}$$

Compared with Eq. 5.4, Eq. 5.9 is found to have the same formula, but from a chemical point of view. Since solute adsorbed by the solid matrix is also of low mobility similar to those entrapped by immobile water in the concept of MIM model, here in the following, a model describing solute transport with convection-dispersion and additionally rate limited interaction with the matrix is sometimes also referred to as a MIM model.

5.2 Fitting of Model Functions

To solve the CD and MIM models for solute transport with stationary water flow in homogeneous porous media, Transport Analysis Package (TAP) by Roth (1996b)

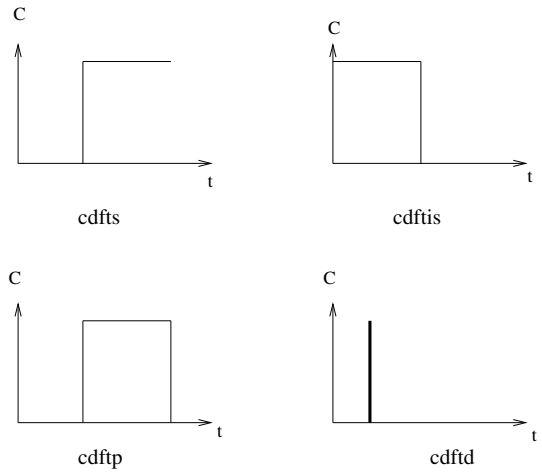

Figure 5.1: CD model with different boundary conditions. cdfts: flux concentration input as a step; cdftis: as a inverse step; cdftp: as a finite pulse; cdftd: as a dirac pulse

was employed. This package enables fitting a BTC with a model which generally consists of two parts—the transport model and the interaction model. For the transport models, analytical solutions are afforded for different boundary conditions (Jury and Roth 1990, Roth and Jury 1993), e.g. flux concentration input as a Dirac-pulse (cdftd), as a step (cdfts), as an inverse step (cdftis), and as a finite pulse (cdftp) (Figure 5.1). Since Brilliant Blue is chosen as tracer in the transport experiments and under low concentration (<20 mg l^{-1}), adsorption is linear as shown already in chapter 3 and found also by (Flury and Flühler 1995, Perillo et al. 1998), for the interaction model, a rate limited model (rl) is generally adopted in the numerical simulation. In the following, the models employed will be referred to as the combination of the transport-interaction model, e.g., cdfts-rl, when solute transport is described with the CD model with flux concentration input as step and in addition solute interaction with solid matrix is expressed with the rate limited model, cdftp-rl, for a combination of the CD model with flux concentration input as a pulse and rate limited model for describing the solute interaction with matrix. The transport parameters are estimated by minimizing the least squares sum

$$\chi^2(\mathbf{p}) = \sum_{i=1}^{N} \left[\frac{C_i - C_{mod}\left(z_i, t_i; \mathbf{p}\right)}{\sigma_i} \right]^2 \tag{5.10}$$

where C_i is the measured concentration at (z_i, t_i) and $C_{mod}(z_i, t_i; \mathbf{p})$ is the corresponding modeled concentration for the parameter vector $\mathbf{p}$. The function is minimized with the Levenberg-Marquardt algorithm in the implementation of Press et al. (1992) (cited by Roth (1996b)).

5.2.1 Characterization of BTCs of Brilliant Blue through the coarse media

Results of the transport experiments show that breakthrough curves of Brilliant Blue, which are highly asymmetric, exhibit earlier initial breakthrough than that of a conventional CD process, in which after one pore volume of infiltration, the concentration of the effluent reaches half of the input concentration, and long tailing for all the four materials (Figure 5.2). For the same material, the BTCs are more asymmetric under low flow rate than those under high flow rate. Among these four materials, BTCs of Brilliant Blue through the gravel column show the highest asymmetry, i.e., the earliest breakthough and the longest tailing. BTCs of Brilliant Blue through the fine sand column are less asymmetric. Those through the coarse sand and the mixed material column are somewhat between the gravel and the fine sand. This indicates that for a column with a certain length, the coarser the material is, the higher the risk for BTCs to skew from a typical convection-dispersion process is. Differences in the BTCs of Brilliant Blue at the high and low flow rates investigated in this study also indicate that the transport of Brilliant Blue deviates more from a typical convection-dispersion process when the flow rate is lower. This will be discussed in the following section 5.2.3. It is also interesting to find that the BTC of Brilliant Blue through the gravel column with low flow rate showed double peaks. This might be caused that preferential flow occurs during the transport process.

The BTC of Brilliant Blue for the construction waste was not obtained. After applying nearly 10 pore volumes of infiltration on this material, the dye was found to have traveled only half of the column length (by cutting the column). This is probably due to strong adsorption of Brilliant Blue to the solid matrix. Depending on pH, Brilliant Blue is either neutral or dissociates to a mono- or bivalent anion. The anionic species can possibly form ion pairs with cations like Ca^{2+} which will yield neutral or even positive charge and change the adsorption properties (Flury and Flühler 1995). As shown already in the chapter 3, this material shows an alkali characteristic with a pH value of 12. Although the exact constituents of this material are unknown, it is reasonable to suppose that strong adsorption occurred. It is then not able to use Brilliant Blue as a tracer for transport study of this material.

Figure 5.2: Breakthrough limb of BTCs of Brilliant Blue effluent for different materials under different flow rates. FS–Fine Sand; CS–Coarse Sand; GR–Gravel; MM–Mixed Material; low–0.01 cm h^{-1}; high–1.0 cm h^{-1}

5.2.2 Performance of the CD model and the MIM model in fitting BTCs of Brilliant Blue

The MIM model and the CD model are applied to fit the BTC of Brilliant Blue effluent from the fine sand column. It was found that the MIM model yielded a better fit overall than the CD model. Plots of measured versus simulated relative concentrations, in the way following Padilla et al. (1999), show that MIM-simulated C/C_0 fall on a 1:1 line (C_0 is the input concentration), whereas those from the CD model scattered from this line more (Figure 5.3). This is more clearly shown in Figure 5.4 which plots the model errors versus time. This suggests that the relative concentration measured can be well described or represented by the MIM model especially at the early breakthough and the long tailing. For the other materials, e.g., the mixed material, the results show that this difference in the fits with the MIM model and the CD model are more obvious (Figure A–9 and A–10). Hence in the following, only fits with the mobile-immobile (MIM) model are shown and discussed.

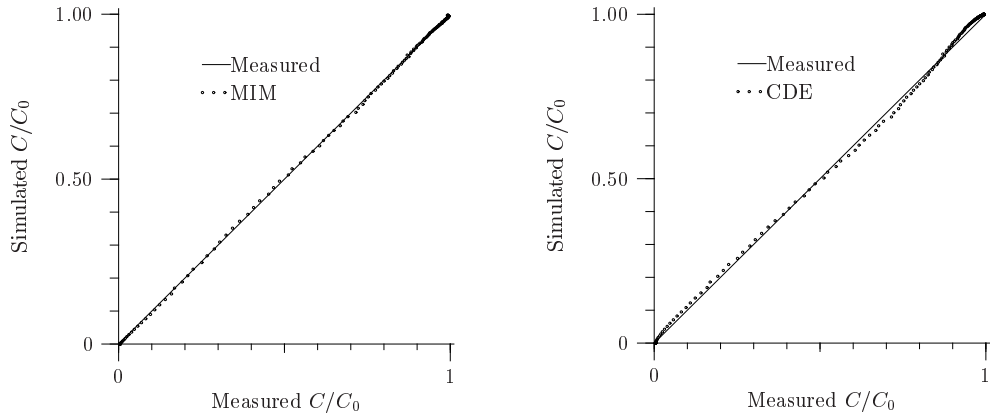

Figure 5.3: Measured versus simulated relative concentration of Brilliant Blue effluent from the fine sand column under high flow rate condition using the CD model and the MIM model

5.2.3 Effect of flow rate on the interaction between Brilliant Blue and the porous media

As depicted in the previous section, the tracer Brilliant Blue that is transported with lower flow rate shows an earlier breakthrough but a longer tailing afterwards than that with higher flow rate. These findings from the breakthrough curves (BTCs) are consistent with the estimated parameters for the interaction model (Table 5.1). It was found that under the high flow rate, the retardation factor is smaller than that under the low flow rate, which indicates that a larger portion of mobile solute

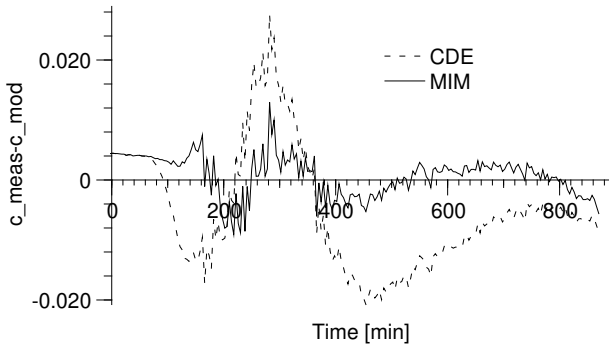

Figure 5.4: Deviations of the simulated and the measured Brilliant Blue concentration in the effluent from the fine sand column under high flow rate– comparison of performance of the MIM and CD models

molecules contributes to the flow at the high flow rate. Meanwhile, rate of exchange between mobile and immobile molecules increases dramatically with increasing flow rate with an exception of the gravel. This can be illustrated by the sketch of flow

Table 5.1: Estimated Parameters with cdfts-rl model for the rate limited interaction model for the four materials under different flow rates

		Gravel	Coarse sand	Fine sand	Mixed material
R	high	1.66	1.31	1.10	1.22
	low	1.73	1.71	1.70	1.65
α	high	1.18	0.34	0.43	1.41
$[h^{-1}]$	low	2.87×10^{-2}	2.25×10^{-3}	3.50×10^{-4}	3.30×10^{-3}
W[a]	high	11.8	3.4	4.3	14.1
	low	28.7	2.25	0.35	3.30

[a] dimensionless rate parameter

regions under different flow rate as shown in Figure 5.5. When the flow rate is high, meaning a higher water content under steady state condition, the flow occurs primarily in relatively large pores. Hence, the contact area between the solute flux and the porous media is small resulting in less chance for the adsorption or retardation. The exchange rate of solute between the adsorption region and flow region, denoted by the rate parameter α, is high due to more direct contact, which implies a good mixing under high flow rate. In other words, the time needed for the solute exchanging between the two regions, denoted by α^{-1}, is short in such case. In contrast to the situation under high flow rate, for the low flow rate, when

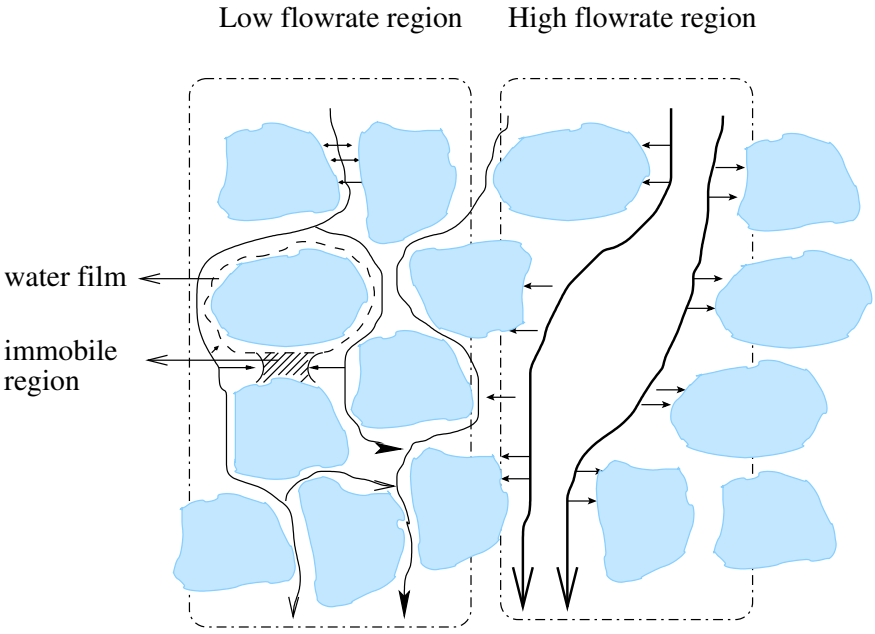

Figure 5.5: Sketch of distinct flow regions under different flow rates for steady state flow. Thicker and longer lines with arrows denoting for solute flux with high velocity; thinner and longer ones denoting solute flux with low velocity; the shorter lines with arrows direted to the solid matrix denoting the dispersion and interaction processes.

water content decreases, flux of solute takes place mainly in small pores, where the flowpaths are of higher tortuosity. The contact area increases dramatically compared with that under high flow rate, thereby adsorption increases. Since the geometry of water phases in these regions is much more complex, there are various types of exchange. The one similar to that under high flow rate is the exchange between the adsorption surface and the flux. As water content decreases, solute flux may take the flowpaths around the matrix surface, where a thin water film might then contribute as a solute deposit pool. Once solute diffuses into the water film, it will take long time to get out. Another possibility is that there is immobile water in the small pores. Solute exchange by diffusion between the immobile water phase, i.e., the stagnant region, and the mobile water phase, i.e., the dynamic region, takes also long time. For the gravel, the differences in retardation factor and rate parameter between different fluxes are not as obvious as the other three materials. This is probably due to low water content under both situations.

5.2.4 Solute breakthrough and elution

When the solute flux concentration is applied as a finite pulse, the whole BTC can be treated as two separate limbs: the solute concentration increasing limb (referred to as the breakthough limb in the following) and the decreasing limb (the elution limb), e.g., Figure 5.6 shows the two limbs of a BTC for Brilliant Blue effluent from the coarse sand column. The former is in fact a BTC for flux concentration input as a step. And the latter is the inverse step. Since the system is assumed to be linear, for the convenience of fitting, the data of the elution limb is transformed as follows:

Outcomes of the highest concentration subtracted by the real concentrations are taken as input concentrations for the model fitting, and time is shifted to start from zero. This gives us a BTC of the similar shape to that obtained from a solute transport experiment with flux concentration input as a step. Both of the two limbs are then fitted with the cdfts-rl model.

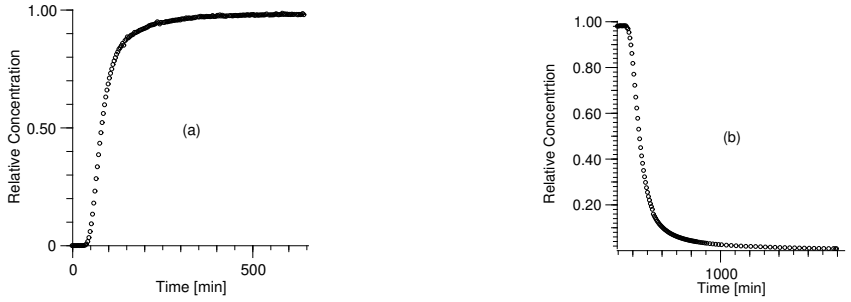

Figure 5.6: (a) Breakthrough and (b) elution limbs of a BTC for Brilliant Blue effluent from the coarse sand column

Similar to the hysteresis phenomenon that occurs very often in water flow in the drainage and imbibition processes, in the miscible experiments, transport parameters estimated from the breakthough limb and the elution limb of a BTC are also found different for the four materials investigated here (Table 5.2). To make it clear, the retardation factor and mass transfer coefficients shown in Table 5.1 for some fittings are listed again in Table 5.2. The corresponding fitting curves are shown in Figure 5.7 for the mixed material, Figure 5.8 for the fine sand, Figure 5.9 for the coarse sand and Figure 5.10 for the gravel. Having a close scrutiny of the estimated parameters shown in Table 5.2, one can find that (i) the velocities obtained for the two limbs are basically the same with each other and the slight differences are reasonable if noises in the data, weak correlation between parameters are taken into account. This is actually what one can expect from solute transport under constant flux. However, one exception is the fine sand for which the velocities estimated for the two limbs are obviously different from each other. The reasonable explanations for this might be changes in the flow rates or water content for the two limbs or correlation between

the pore water velocity V and other parameters, e.g., the retardation factor R. From the correlation matrix (will be discussed later), a strong correlation is found between V and R with a coefficient up to 0.97 from fitting of the breakthrough limb for the fine sand. This indicates that a larger V can be compensated with increasing the retardation factor. However, for the elution limb, the parameter V has no correlation with R revealed by a coefficient of -0.09. (ii) generally speaking, dispersion coefficient of the breakthrough limb is smaller than that of the elution limb. While the latter is characterized with a larger retardation factor and a smaller mass transfer coefficient than the former.

Table 5.2: Comparison of Parameters estimated with the cdfts-rl model for the breakthrough and elution limbs of BTCs of Brilliant Blue under high flow rate; "b" denoting the breakthrough limb and "e" denoting the elution limb)

		Coarse sand	Mixed material	Fine sand	Gravel
V	b	0.1225	0.1725	0.0426	0.432
[cm min^{-1}]	e	0.1236	0.1715	0.0624	0.383
D	b	7.28×10^{-2}	5.08×10^{-2}	2.35×10^{-2}	0.55
[cm^2 min^{-1}]	e	9.44×10^{-2}	6.54×10^{-2}	4.88×10^{-2}	0.69
R	b	1.31	1.22	1.10	1.65
	e	1.47	1.25	1.45	1.64
α	b	5.69×10^{-3}	2.32×10^{-2}	7.23×10^{-3}	1.97×10^{-2}
[min^{-1}]	e	3.09×10^{-3}	1.67×10^{-2}	2.07×10^{-3}	1.17×10^{-2}

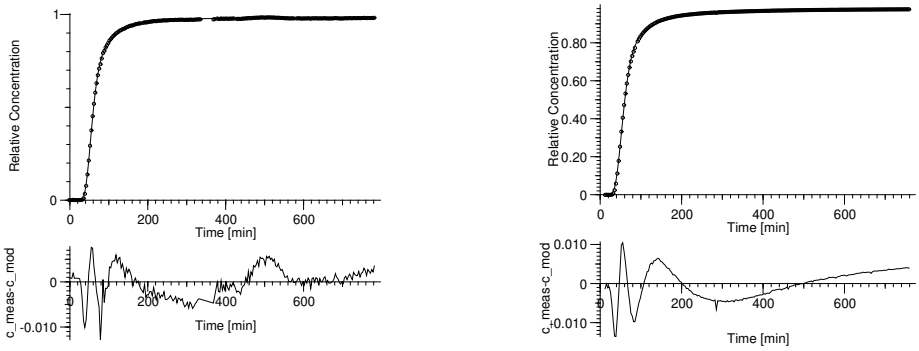

Figure 5.7: Fits of the breakthrough limb (left) and the elution limb (right) of the BTC for Brilliant Blue effluent from the **mixed material** column at high flow rate with the cdfts-rl model and the residual curves

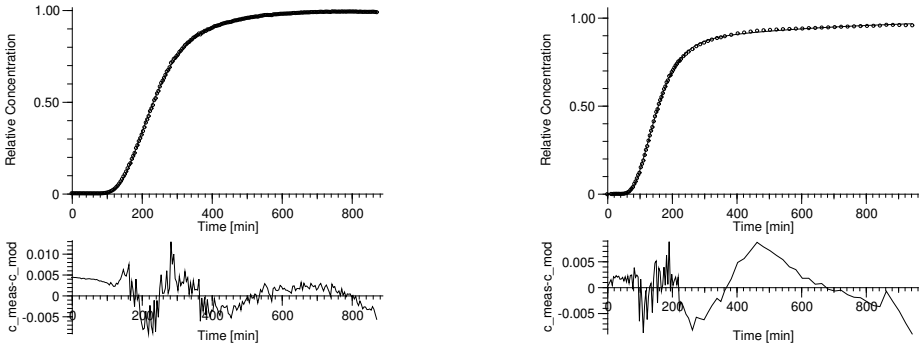

Figure 5.8: Fits of the breakthrough limb (left) and the elution limb (right) of the BTC for Brilliant Blue effluent from the **fine sand** column at high flow rate with the cdfts-rl model fixed

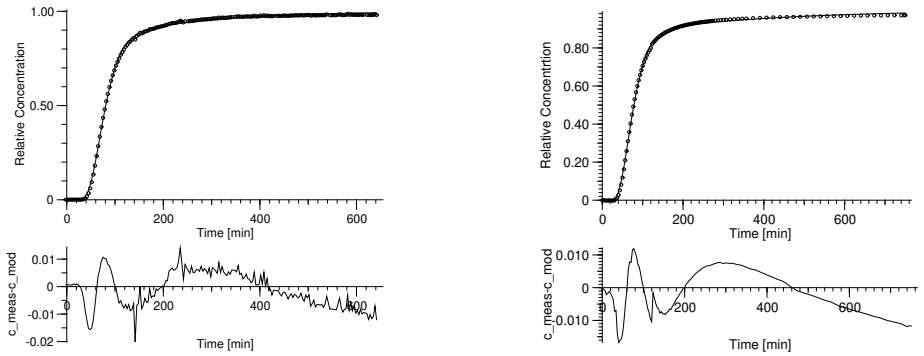

Figure 5.9: Fits of the breakthrough limb (left) and the elution limb (right) of the BTC for Brilliant Blue effluent from the **coarse sand** column at high flow rate with the cdfts-rl model and C_0 fixed

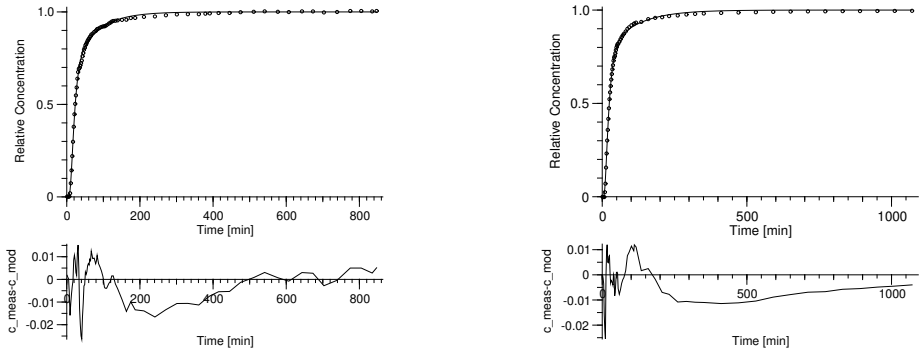

Figure 5.10: Fits of the breakthrough limb (left) and the elution limb (right) of the BTC for Brilliant Blue effluent from the **gravel** column at high flow rate with the cdfts-rl model and initial concentration fixed at C_0

The differences in these parameters imply differences in the interaction between the solute flux and the solid matrix during the breakthrough and the elution processes although it is hard to estimate how large the differences are. During the breakthrough process, simultaneously with the transport by convection, solute molecules also move towards the surface of the solid matrix by molecular diffusion. Since the surface of the solid matrix can be highly uneven, as the molecules diffuse from the outer to the inner pores around the solid surface, the resistance that they encounter will become greater, hence leading to a smaller dispersion coefficient. On the contrary, during the elution process, solute molecules diffuse from the inner pores around the solid surface to the outer ones. The resistance that the molecules encounter will become lower and lower leading to a larger dispersion coefficient. This reveals a fact that the dispersion coefficient at a certain location around the solid surface is changing nonlinearly with time. For the convenience of interpretation, the surface of the solid matrix is sketched to be even and contain two layers with molecule diffusion coefficient (Figure 5.11). Since the molecules are adsorbed mainly in the outlayer during the breakthrough process due to lower diffusion, the retardation factor is smaller and time needed for exchange between the adsorption region and the transport region is shorter due to short distance and weaker adsorbability of the solid matrix. Solute transport in the elution limb is a different story. In this case, water flow is flushing solute in the flowpaths and in the adsorption region. Molecules adsorbed by solid matrix in the inner layer have the less chance to get into the dynamic region due to longer transport distance and stronger adsorbability which is revealed by a smaller rate parameter.

Although some of the optimized parameters by fitting the cdfts-rl model to the breakthrough and elution limbs are different to some extent, for the same material, the two parts of the BTC in general exhibit similar shapes and also the structures of the residual curves are similar (Figures 5.7, 5.8, 5.9, 5.10). This implies that the primary mechanism dominating the two processes should be the same despite the slight differences mentioned above.

5.2.5 Fitting with different models

As mentioned already in section 5.2.4, one breakthrough experiment with the solute flux input as a finite pulse can be treated as two with flux input as a step. Similarly, by mathematical transformation, such data can be converted into two BTCs with dirac-pulse input for the breakthrough process and the elution process. For example, the whole BTC for Brilliant Blue effluent from the mixed material (Figure 5.12, upper figure) is transformed by taking the derivatives of the concentrations into the data shown in Figure 5.12 (lower figure). Separating the breakthrough and elution parts and upturning the latter yield two BTCs with solute flux input as a dirac-pulse

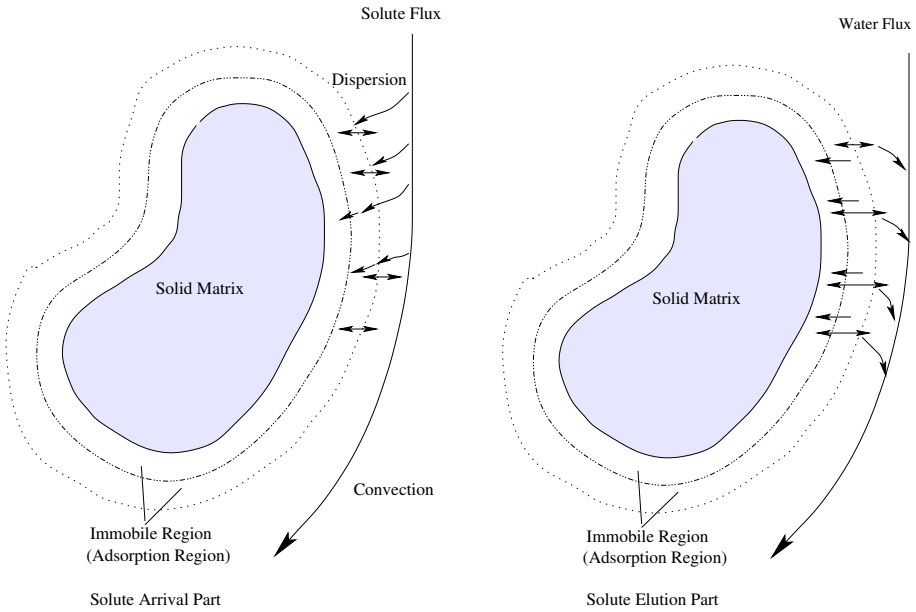

Figure 5.11: Illustration of the differences in solute breakthrough and elution during application of a pulse of solute flux

(Figure 5.15, upper figures, dots). The so-called "different models" in this section mean only such differences in solute input boundary conditions.

Figure 5.13 shows the fit with solute input as an finite pulse and rate-limited interaction of the tracer for the gravel at high flow rate. The sensitivity of the outflow concentration with respect to an individual parameter is calculated by TAP. It was found that except the initial concentration which exhibits in the whole process, a positive impact on the concentration, the other parameters all have two distinct influence effects shown in similar shapes but in the opposition of each other corresponding to the breakthrough and elution limbs of the BTC. For instance, increasing the parameter V will cause an increase of concentration at the beginning of the breakthrough limb, then the impact decreases but still in a positive direction till the concentration approaches towards the input concentration and it stays at 0, i.e., no impact on the concentration. The velocity starts to influence the concentration again when the solute pulse is stopped and displacement of solute by incoming water, i.e., the elution limb of the BTC starts. It also shows that at both moments when the solute concentration is approaching the input concentration for the breakthrough limb and when the solute concentration is approaching 0 for the elution limb, the outflow concentration is only influenced by the retardation factor R and the rate parameter α. This is actually the reason why the interaction model is employed. The retardation factor and the rate parameter account for the long tailing of the BTC.

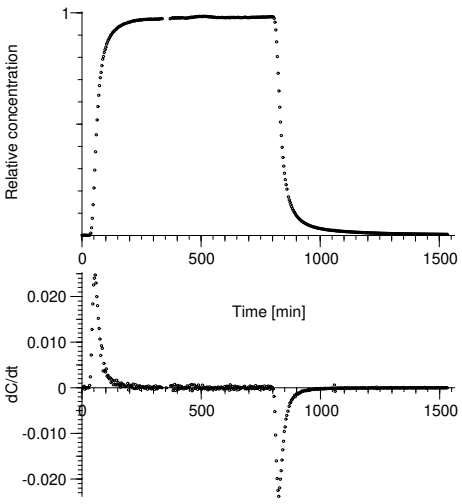

Figure 5.12: Generation of input data for the cdftd-rl model, mixed material

Compared with the cdfts-rl fitted BTC for the breakthrough limb and that for the elution limb (Figure 5.10), the cdftp-rl fitted BTC deviated from the measurement by more than 2% at the early breathough of Brilliant Blue which is a little larger than that of the cdfts-rl fitted one which is 1%. Recall that when the cdfts-rl model is fitted to the two limbs of the BTC respectively, two different sets of parameters are obtained (Table 5.2) and analysis showed that during the breakthrough and the elution processes interaction between the solute molecules and the solid matrix are different to some extent. While fitting the BTC with cdftp-rl assumes that the whole process can be described with a single set of transport parameters, which will then results in larger model errors. However, the errors are not that significant as one can find in the following section that goodness-of-fit analysis shows that the cdftp-rl model in this case is still a "correct" model from the statistical point of view.

Figure A–7 showed the fits using the cdftd-rl model for the breakthrough and elution limbs of the BTC of Brilliant Blue through the gravel column. The parameters obtained from the fittings using different models are plotted in Figure 5.14 which are different from each other. Those obtained using the cdftd-rl model show larger difference with those obtained from the cdfts-rl and the cdftp-rl models. Furthermore, with the same cdftd-rl model, parameters obtained by fitting the breakthrough and elution limbs of the BTC are significantly different from each other which is more obvious than using the cdfts-rl.

Similar results are found for the mixed material. Figure 5.7 and Figure 5.15 show the results using cdfts-rl and cdftd-rl to fit the breakthrough and elution limbs of BTCs of Brilliant Blue through the column with the mixed material respectively. It shows that the MIM model yielded a good fit to the BTCs. Both the cdfts-rl

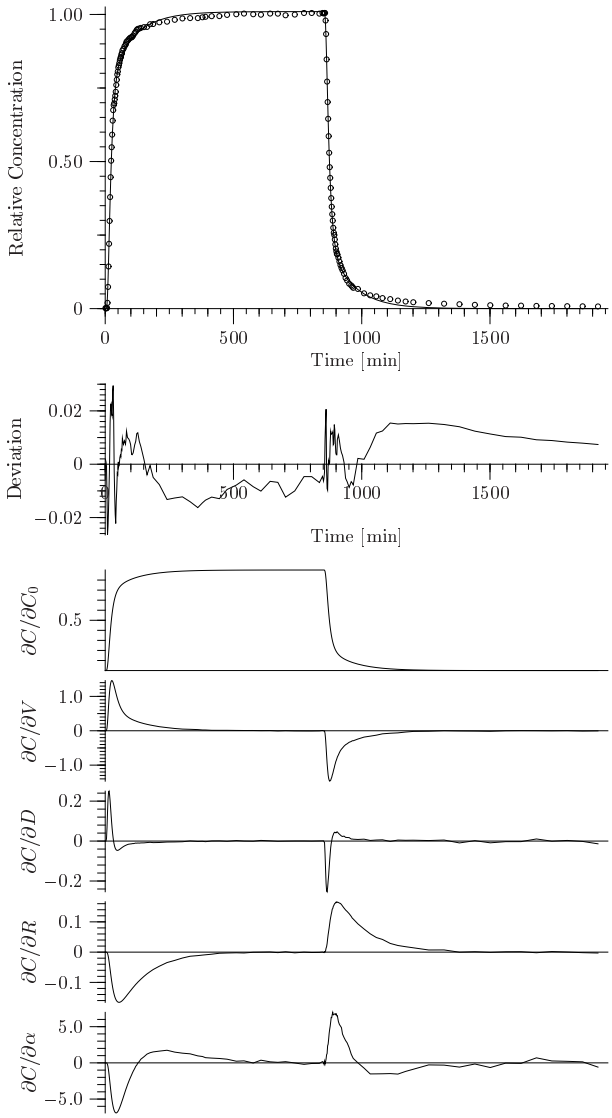

Figure 5.13: Fitting the cdftp-rl model to the BTC of Brilliant Blue effluent from the gravel column with high flow rate, initial concentration is fitted and the sensitivity of the parameters

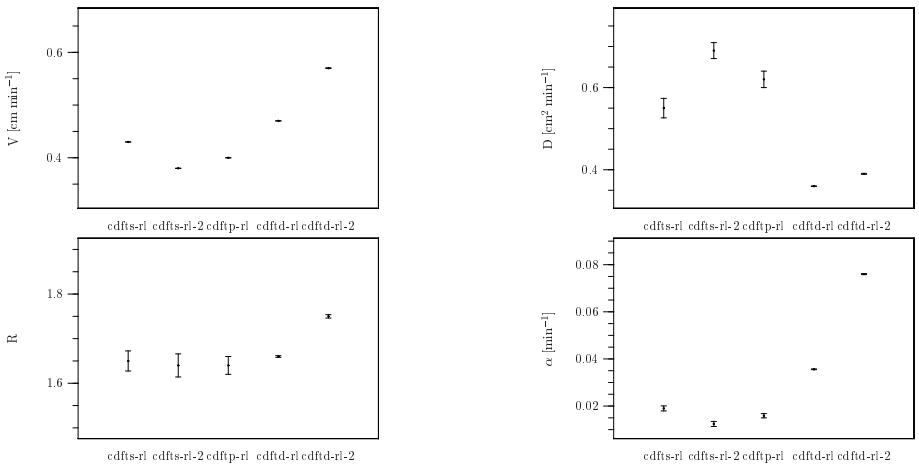

Figure 5.14: Parameter obtained using different flux concentration input for the gravel at high flow rate

and the cdftd-rl models can describe the BTCs in a general sense. For the cdfts-rl model, the estimation errors are limited within 1.2%. The parameters obtained using different flux concentration input of this mixed material are plotted in Figure 5.16. Again similar to that found for the gravel, the parameters obtained with different models are also different for the mixed material. The fitted parameters using the cdfts-rl and cdftp-rl models are closer to each other while fitting with cdftd-rl yielded significantly different parameters. Generally speaking, the cdfts-rl model agrees with measured data best and cdftp-rl comes the second with larger deviations especially at the breakthough of Brilliant Blue. To summarize the results from the gravel and the mixed material cases, the CD model with different flux concentration input conditions and rate-limited interaction of the tracer yielded different parameters. As already discussed in section 5.2.4, the difference between the parameters fitted by applying the cdfts-rl model to the breakthrough and elution limbs may be caused by difference in interaction between the solute molecules and the solid matrix. This explains also why the cdftp-rl model simulation deviates from the measurement more than the cdfts-rl model does. However, applied to the same data set, the cdftd-rl model was not expected to yield different parameters with those obtained from the cdfts-rl since the mathematical transformation should not influence the estimation of the parameters. The reasonable interpretation for this discrepancy is that taking derivatives of the concentrations when generating input data for the cdftd-rl model yields more noises in the data set caused by fluctuation of the original concentration which disturbs the model simulation. This is shown clearly from the Figures 5.15 and A–2 especially for the breakthrough process.

Another phenomenon which needs to be paid attention to is that the largest devia-

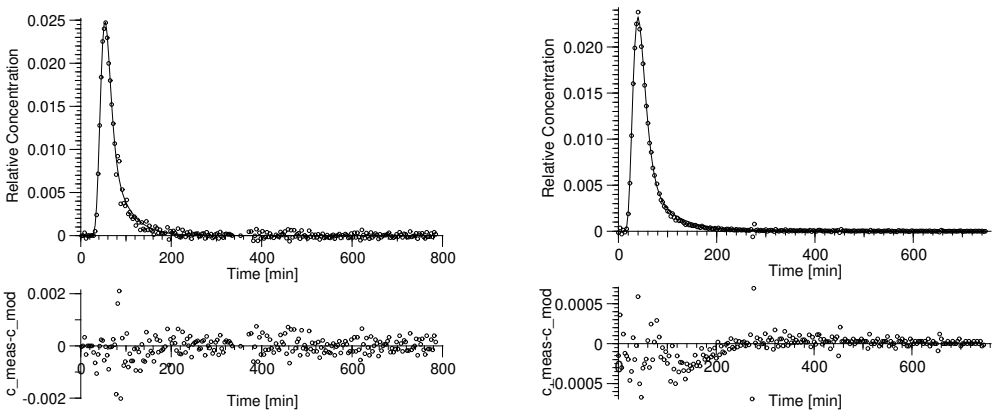

Figure 5.15: Fits of the breakthrough limb (left) and the elution limb (right) of the BTC for Brilliant Blue effluent from the mixed material column at high flow rate with the cdftd-rl model and C_0 fixed

tions between the model and measurement occur usually at the early breakthough in both breakthrough and elution limb of the BTC. This indicates that application of convection-dispersion theory encounters difficulties at these points. More intensive sampling at these periods can improve the model simulation but it cannot solve this problem completely.

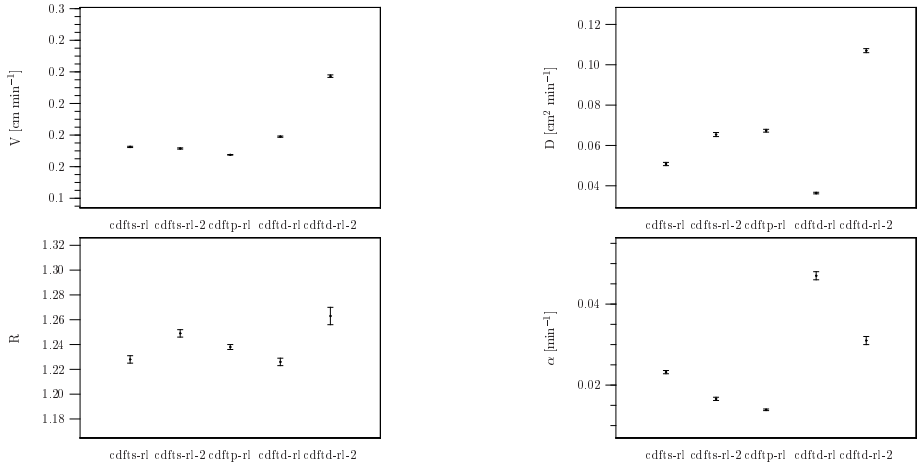

Figure 5.16: Parameters obtained using different flux concentration input for the mixed material at high flow rate

5.2.6 Dye transport with low flow rate through the fine sand column

Dye transport with low flow rate through the fine sand column is a special case. After nearly 40 days, the outflow concentrations neither increased still obviously like the case of the coarse sand (Figure A–3) nor reached the input concentration. As shown in Figure 5.17, the concentration of the effluent almost kept stable at a relative concentration of about 0.91. Fitting this BTC with the cdfts-rl model with C_0 fixed at the input concentration 1.0 yielded a good fit. But the uncertainties of the estimated parameters are really high, especially those of the retardation factor and the rate parameter, which indicates that interaction of the dye with the solid matrix cannot be described with a rate-limited adsorption isotherm. While fitting the BTC with the CD model with C_0 fitted yielded the similar, or even better fit, and the precision of the parameters are acceptable. This implies the possibility that the dye during transport process might be adsorbed by sand irreversibly or there is decay of the dye inside the column since the input concentration was measured again after the experiment resulting in a value about 1.0 as the original one.

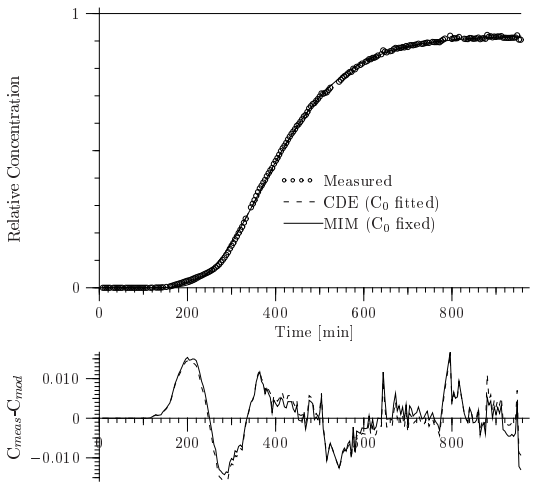

Figure 5.17: Dye transport through the fine sand column with low flow rate, fitted with the cdfts model with C_0 fitted and the cdfts-rl model with C_0 fixed

5.2.7 Confidence intervals for estimated parameters and estimation of goodness-of-fit for the model

The estimated parameters can be used or the model can be considered to be applicable only when they are statistically significant. The Levenberg-Marquardt algorithm returns the covariance matrix $cov_{\vec{p_{est}}}$ and the matrix of correlation coefficients $corr_{\vec{p_{est}}}$ for the estimated parameter vector $\vec{p}_{est}$. As an example the results of the es-

timation of $\vec{p}_{est} = (v, D, R, \alpha)$ for Brilliant Blue transport through the gravel column with high flow rate as shown in Figure 5.10 are given in Table 5.3

Table 5.3: Statistical information excerpted from output of Levenberg-Marquardt algorithm on parameters estimated from fit of a BTC of Brilliant Blue effluent from the gravel column at high flow rate with cdfts-rl model

Parameter	Value	SD	CV
V [cm min^{-1}]	4.3×10^{-1}	6×10^{-3}	0.015
D [cm^2 min^{-1}]	5×10^{-1}	2×10^{-2}	0.043
R	1.6	2×10^{-2}	0.013
α [min^{-1}]	1.9×10^{-2}	1.0×10^{-3}	0.054

This gives the precision of the estimated parameters. The matrix of correlation coefficients, given by Table 5.4, shows to what extent the estimated parameters correlate with one another. Generally speaking, the precision of the estimated parameters, although there is correlation between some parameter combinations, is acceptable. However, no information is given by these quantities on whether the model fitting is successful or not, i.e., whether the model chosen is correct for description of the data. There are quite a few methods to evaluate a model fitting. Usually this is done by calculating the χ^2 (Eq. 5.10), which is the sum of the square of the difference between the model and the measurement divided by the measurement variance. The so-called goodness-of-fit is then measured by the value of χ^2 at the minimum and the number of degrees of freedom (the difference between the number of data points N and the number of the parameters M) $\nu = N - M$. The

Table 5.4: Correlation matrix for the optimized parameters from a fit of the BTC of Brilliant Blue effluent from the gravel column at high flow rate with cdfts-rl model

	V	D	R	α
V	1.0	−0.80	0.78	0.73
D	−0.80	1	−0.71	−0.51
R	0.78	−0.71	1	0.23
α	0.73	−0.51	0.23	1

goodness-of-fit is given by the value of the incomplete gamma function

$$P\left(\frac{\nu}{2}, \frac{\chi^2_{min}}{2}\right) = \frac{1}{\Gamma\left(\chi^2_{min}/2\right)} \int_0^{\nu/2} e^{-t} t^{\chi^2_{min}/2-1} dt \ . \tag{5.11}$$

Typically the goodness-of-fit is believable for values larger than 0.1 (Press et al. 1992). If the value is too small, then either the model is wrong, or the measurement error σ_i is not estimated correctly. There is also a possibility that the measurement error is not normally distributed. On the other hand, if the value is too large, too near to 1, then it might be that the measurement error is overestimated. If the measurement error is such that C_i is a Gaussian random variable with mean $\bar{C}_i$ and variance σ_i and if the model is correct, then for the correct parameter vector $\mathbf{p}^*$, $\chi^2(\mathbf{p}^*)$ is a χ^2-distributed random variable with an expectation $\langle\chi^2\rangle \approx N - M$ and a standard deviation $\sqrt{2\nu}$. This is a rule of thumb to judge a "typical" value of χ^2 for a "moderately" good fit.

In this study, the measurement errors are estimated from either the concentrations of the first several samples, or the fluctuations of the concentrations on the shoulder of the BTCs. It was found that using the cdfts-rl model generally provided best fits for the BTCs. Calculated goodness-of-fits (Table 5.5) are also consistent with the results shown in the previous sections.

Table 5.5: Calculated Goodness-of-Fit for Different Models ("/": concentration data not available; "†": value is too small)

Material		cdfts-rl		cdftp-rl	cdftd-rl
		b[a]	e[b]		
Coarse sand	h[c]	0.95	0.79	0.93	†
	l[d]	0.28	/	/	/
Gravel	h	0.36	0.42	†	†
	l	0.15	0.97	†	†
Mixed material	h	0.60	0.32	†	0.30 (e)
	l	0.36	†	0.13	†
Fine sand	h	0.98	0.78	†	†

[a] breakthrough
[b] elution
[c] high flow rate
[d] low flow rate

5.3 Summary

Using Brilliant Blue as a tracer, breakthrough experiments with two distinct stationary water fluxes were carried out with the coarse textured materials. The BTCs obtained were simulated with the traditional CD and the MIM model to estimate transport parameters. The following results are obtained:

(i) Compared with a standard BTC from a convection-dispersion process, the BTCs of Brilliant Blue effluent from the coarse textured media are highly asymmetric which are featured with earlier breakthrough and long tailing which was not expected for the coarse materials indicating that under the used experimental conditions the solute transport did not reach a Fickian regime, therefore the physical non-equilibrium MIM model or the chemical non-equilibrium model yielded better fits for the experimental data under such situation.

(ii) "Hysteresis" phenomenon was found for the solute transport which was revealed by different parameter values, especially those of the dispersion coefficient and the rate parameter, for the breakthrough and the elution limbs of the BTCs.

(iii) Goodness-of-fit was calculated for the MIM model with different flux input conditions as a criterion of a "correct" model to describe the BTCs. The MIM model with step input of solute flux generally gave the best fit.

(iv) Flow rate showed an influential impact on the interaction between the Brilliant Blue molecules and the solid matrix. For transport with low water flux, Brilliant Blue is retarded to a larger extent than with high flux and the exchange rate between the mobile phase and the immobile phase is dramatically reduced.

6 Summary and Outlook

In the present work, the hydraulic properties and transport properties of some coarse textured materials were studied. A state-of-the-art method, the inverse approach coupled with laboratory multi-step outflow experiments was applied to estimate hydraulic parameters of the coarse textured materials. Using the outflow experimental setup and Brilliant Blue as a tracer, steady-state transport experiments were conducted, and the conventional transport models were fitted to the BTCs to estimate transport parameters.

6.1 Hydraulic Parameter Estimation with Inversion

The application of the inverse technique to MSO experimental data to estimate hydraulic parameters is not as simple as it seems to be. Although the simulated outflow curves seemed to have captured the feature of the flow behavior, structures of the residuals revealed the existence of indistinct factors causing discrepancies between the model and the measurement. These deviations of the Richards equation, the underlying process model, with the invoked model for the hydraulic functions, the MvG models, from the measurement are found mostly at high saturations and show a global structure related to the pressure changes. These findings lead to the discussion of the sources of these model errors.

χ^2 surfaces for outflow showed clear global minima in most of the parameter planes indicating the identifiability of the parameters using the inverse method. However, parameters are found to correlate with each other to varied extents which resulted in some uncertainties in the parameter estimation. Insensitive parameters like saturated hydraulic conductivity cannot be determined well. Optimization of such parameters may yield unreliable values as found for the coarse sand.

For materials with complicated pore systems, simple unimodal hydraulic models cannot describe the flow behavior. Instead, bimodal or even multimodal hydraulic models with higher flexibility can yield better fit and more randomly distributed model errors which are verified by using the bimodal hydraulic models for the mixed material case. On the other hand, an obvious disadvantage with using multimodal

hydraulic models is that with more parameters needed to be optimized, the parameter sensitivity may be reduced.

By scrutinzing the residuals and based on the related reports, we discussed the possible explanations for the model deviations. One important reason resulting in the model errors is considered to be that the assumptions for application of Richards equation were not met in the measurements. Richards equation assumes that the porous medium is homogeneous, rigid and the air-phase is continuous and the air-phase pressure is equal to the atmospheric pressure anywhere in the system. Furthermore, Richards equation is in fact an equilibrium equation. It implies that the system can reach equilibrium instantaneously when it is subjected to the external force. However, for the coarse materials, local heterogeneity is hard to avoid. Fast drainage in the larger pores easily leads to the loss of continuous air-phase hence, instantaneous equilibrium is difficult and there may be entrapped air bubbles and pressure inside them may be different from the atmospheric pressure. Obviously, these conditions in the real measurements do not satisfy the prerequisites of Richards equation. In addition, invoking an inappropriate hydraulic parameterization may also account for some errors.

6.2 Transport Behavior of Brilliant Blue with Stationary Water Flux

In chapter 5, results from transport experiments were shown. As a cost-effective tracer for water flow, Brilliant Blue was used in the breakthrough experiments to estimate transport parameters for the coarse textured materials.

Highly asymmetric BTCs were obtained with those for the coarser materials skewed more than those for the finer ones.

Fitting the breakthrough and elution limbs of the BTCs, respectively, yielded different parameter values especially for those of the dispersion coefficient and of the rate parameter. This phenomenon was interpreted as a consequence of variably effective diffusion which is generally larger in outer pores around the solid surface and smaller in the inner ones.

The interaction between Brilliant Blue and the solid matrix was found to be different under high and low fluxes for each material. This was revealed by a larger retardation factor and a smaller rate parameter under high flux. Since the experiments were running under steady-state, it is attributed to the less contact between the solute molecules and the matrix surface at higher flux under which condition solute transport is dominated by that in larger pores or flow paths. At a low flux, water content is reduced and larger pores are empty. Hence, solute transport takes place prevailing in the smaller pores with higher tortuosity therefore larger resis-

tance, which is reasonable to find a larger retardation factor and smaller exchange rate.

Finally, the performance of the MIM model with different flux input was evaluated by the calculated goodness-of-fit. The results showed that generally the physical nonequilibrium MIM model can describe the BTCs of Brilliant Blue effluent through the coarse materials well especially with flux input as a step.

However, no conclusion can be drawn from the designed experiments with respect to whether the transport process is a convection-dispersion process or not since solute concentrations were only measured at one depth. Still for the purpose of description of the BTCs, the MIM model seems sufficient.

6.3 Outlook

This work investigated hydraulic and transport properties of several coarse textured materials. However, the extension of the presented results and problems to other porous media may be possible. With respect to estimation of hydraulic parameters using the inverse method coupled with MSO experiments, inconsistencies were found mostly at high saturations and were attributed to the failure of assumptions of the process model, the Richards equation. Another possible reason is the inappropriate hydraulic parameterization. Against these problems, future work can be improved from the following different aspects:

On the experimental side, the sample must be carefully prepared and the initial condition, e.g., initial saturation must be accurately determined. The pressure changes at the upper or lower boundary must be carefully decided to avoid loss of air-continuity due to sharp changes in pressure and hence nonequilibrium during the drainage. In case of non-negligible effect of air-phase, a two-phase flow model must be adopted.

Limited by time, this work did not explore different parametric hydraulic models. Since most of the models for soil water characteristic lack physical basis, anyway, a selected model may happen to have the flexibility to capture the feature of the water characteristic under investigation and it is also possible that the constitutive relationship is too far from the real relationship between water content and matric potential. Examining different models and choosing the suitable one for a certain material can eliminate the model errors caused by inappropriate hydraulic parameterization. On the other hand, most hydraulic conductivity models are coupled with the water characteristic model. Hence, the parameters that determine the shape of the water retention curve also determine the shape of the hydraulic conductivity curve, which will apparently reduce the fitting capability of the models. Therefore, using models for hydraulic conductivity and water characteristic without coupling

them together may improve the fitting.

The last but not the least point is to determine soundly which parameters to be optimized and which part of data contains most information for a certain parameter, i.e., the model is most sensitive to changes in this parameter. This work only compared the parameters estimated using different selected data sets and found that using more data from "shoulders" of the outflow curve leading to a larger n and smaller τ compared with using uniformly selected data. The parameters θ_s and α were not influenced significantly. More comprehensive work in this direction actually has been carried out by Vrugt et al. (2001) and Vrugt and Bouten (2002). They developed a sequential optimization methodology to find the most informative subsets for different parameters which is found effective.

Bibliography

Aeby, P., J. Forrer, C. Steinmeier, and H. Flühler. 1997. Image analysis for determination of dye tracer concentrations in sand columns. Soil Sci. Soc. Am. J. 61:33–35.

Brooks, R., and A. Corey. 1966. Properties of porous media affecting fluid flow. J. Irrigation and Drainage Div., Proc. Am. Soc. Civil Eng. (IR2) 92:61–88.

Chahal, R., and R. Yong. 1965. Validity of the soil characteristics determined with the pressured apparatus. Soil Sci. 99:98–103.

Crescimanno, G., and M. Iovino. 1995. Parameter estimation by inverse method based on onestep and multistep outflow experiments. Geoderma 68:257–277.

Dijk, P., and B. Berkowitz. 1999. Investigation of flow in water-saturated rock fractures using nuclear magnetic resonance imaging (NMRI). Water Resour. Res. 35:347–360.

Doering, E. 1965. Soil water diffusivity by one-step method. Soil Sci. 99:322–326.

Durner, W., B. Schultze, and T. Zurmühl. 1999a. State-of-the-art in inverse modeling of inflow/outflow experiments. *In* M. Genuchten, F. Leij, and L. Wu. (ed.) Characterization and measurement of the Hydraulic Properties of Unsaturated Porous Media. University of California, Riverside, CA. p. 661–681.

Durner, W., E. Priesack, H.-J. Vogel, and T. Zurmühl. 1999b. Determination of parameters for flexible hydraulic functions by inverse modeling. *In* M. Genuchten, F. Leij, and L. Wu. (ed.) Characterization and measurement of the Hydraulic Properties of Unsaturated Porous Media. University of California, Riverside, CA. p. 817–829.

Eching, S., and J. Hopmans. 1993. Optimization of hydraulic functions from transient outflow and soil water pressure data. Soil Sci. Soc. Am. J. 57:1167–1175.

Eching, S., J. Hopmans, and O. Wendroth. 1994. Unsaturated hydraulic conductivity from transient multistep outflow and soil water pressure data. Soil Sci. Soc. Am. J. 58:687–695.

Fischer, U., R. Schulin, and M. Keller. 1996. Experimental and numerical investigation of soil vapor extraction. Water Resour. Res. 32:3413–3427.

Flury, M., and H. Flühler. 1995. Tracer characteristics of Brilliant Blue FCF. Soil Sci. Soc. Am. J. 59:22–27.

Flury, M., H. Flühler, W. Jury, and J. Leuenberger. 1994. Susceptibility of soils to preferential flow of water: a field study. Water Resour. Res. 30:1945–1954.

Forrer, I., A. Papritz, R. Kasteel, and H. Flühler. 2000. Quantifying dye tracer contents in field transport studies by image analysis. Europ. J. Soil Sci. 51:313–322.

Gardner, W. R. 1956. Calculation of capillary conductivity from pressure plate outflow data. Soil Sci. Soc. Am. Pro. 20:317–320.

Gardner, W. R. 1958. Some steady state solutions of unsaturated moisture flow equations with application to evaporation from a water table. Soil Sci. 85:228–232.

Hassanizadeh, S., M.A.Celia, and H.K.Dahle. 2002. Dynamic effect in the capillary pressure-saturation relationship and its impacts on unsaturated flow. Vadose Zone Journal 1:38–57.

Hopmans, J., T. Vogel, and P. Koblik. 1992. X-ray tomography of soil water distribution in one-step outflow experiments. Soil Sci. Soc. Am. J. 56:355–362.

Hopmans, J. W., and J. Šimůnek. 1999. Review of inverse estimation of soil hydraulic properties. *In* M. Genuchten, F. Leij, and L. Wu. (ed.) Characterization and measurement of the Hydraulic Properties of Unsaturated Porous Media. University of California, Riverside, CA. p. 643–659.

Hwang, S. I., and S. E. Powers. 2003. Estimating unique soil hydraulic parameters for sandy media from multi-step outflow experiments. Adv. Water Res. 26:445–456.

Inoue, M., J. Šimůnek, J. Hopmans, and V. Clausnitzer. 1998. In situ estimation of soil hydraulic functions using a multistep soil-water extraction technique. Water Resour. Res. 34:1035–1050.

Jawitz, J. W., M. D. Annable, and P. S. C. Rao. 1998. Miscible fluid displacement stability in unconfined porous media: Two-dimensional flow experiments and simulations. J. Contam. Hydrol. 31:211–230.

Jury, W., and K. Roth. 1990. Transfer Functions and Solute Movement through Soils. Theory and Applications. Birkhäuser Verlag., Basel, Switzerland.

Jury, W. M., W. R. Gardner, and W. H. Gardner. 1991. Soil Physics. 5th. John Wiley & Sons, New York, United States of America.

Kastanek, F., and D. Nielson. 2001. Description of soil water characteristic using cubic spline interpolation. Soil Sci. Soc. Am. J. 65:279–283.

Kasteel, R., H.-J. Vogel, and K. Roth. 2002. Effect of non-linear adsorption on the transport behaviour of brilliant blue in a field soil. Europ. J. Soil Sci. 53:231–240.

Klute, A., and C. Dirksen. 1986. Methods of soil analysis. chapter Hydraulic conductivity and diffusivity: Laboratory methods. p. 687–734. Part 1. Physical and Mineralogical Methods. 2nd edn. American Society of Agronomy, Madison, Wisconsin.

Kool, J., and J. Parker. 1988. Analysis of the inverse problem for transient unsaturated flow. Water Resour. Res. 24:817–830.

Kool, J., J. Parker, and M. van Genuchten. 1985. Determining soil hydraulic properties from one-step outflow experiments by parameter estimation: I. theory and numerical studies. Soil Sci. Soc. Am. J. 49:1348–1354.

Kosugi, K. 1996. Lognormal distribution model for unsaturated soil hydraulic properties. Water Resour. Res. 32:2687–2703.

Mualem, Y. 1976. A new model for predicting the hydraulic conductivity of unsaturated porous media. Water Resour. Res. 12:593–622.

Padilla, I., T.-C. Yeh, and M. Conklin. 1999. The effect of water content on solute transport in unsaturated porous media. Water Resour. Res. 35:3303–3313.

Parker, J., J. Kool, and M. van Genuchten. 1985. Determining soil hydraulic properties from one-step outflow experiments by parameter estimation: II. Experimental studies. Soil Sci. Soc. Am. J. 49:1354–1359.

Peck, A. 1960. Change of moisture tension with temperature and air pressure: Theoretical. Soil Sci. 89:303–310.

Perillo, C., S. Gupta, E. Nater, and J. Moncrief. 1998. Flow velocity effects on the retardation of FD&C Blue no.1 Food dye in soil. Soil Sci. Soc. Am. J. 62:39–45.

Press, W., S. Teukolsky, W. Vetterling, and B. Flannery. 1992. Numerical Recipes in C. The Art of Scientific Computing. 2nd. Cambridge University Press.

Robinson, D., S. Jones, J. Wraith, D. Or, and S. Friedman. 2003. A review of advances in dielectric and electrical conductivity measurement in soils using time domain relectometry. Vadose Zone Journal 2:444–475.

Rogasik, H., J. Crawford, O. Wendroth, I. Young, M. Joschko, and K. Ritz. 1999. Discrimination of soil phases by dual energy x-ray tomography. Soil Sci. Soc. Am. J. 63:741–751.

Roth, K. 1996a. Lecture notes in Soil Physics. University of Hohenheim.

Roth, K. 1996b. Transport Analysis Package.

Roth, K., and W. Jury. 1993. Linear transport models for adsorbing solutes. Water Resour. Res. 29:1195–1203.

Russo, D. 1988. Determining soil hydraulic properties by parameter estimation: On the selection of a model for the hydraulic properties. Water Resour. Res. 24:453–459.

Stoffregen, H., U. Yaramanci, T. Zenker, and G. Wessolek. 2002. Accuracy of soil water content measurements using ground penetrating radar: comparison of ground penetrating radar and lysimeter data. J. Hydrol. 267:201–206.

Toorman, A., P. Wierenga, and R. Hills. 1992. Parameter estimation of hydraulic properties from one-step outflow data. Water Resour. Res. 28:3021–3028.

van Dam, J., J. Stricker, and P. Droogers. 1992. Inverse method for determining soil hydraulic functions from one-step outflow experiments. Soil Sci. Soc. Am. J. 56:1042–1050.

van Dam, J., J. Stricker, and P. Droogers. 1994. Inverse method to determine soil hydraulic functions from multistep outflow experiments. Soil Sci. Soc. Am. J. 58:647–652.

van Genuchten, M. T. 1980. A closed-form equation for predicting the hydraulic conductivity of unsaturated soils. Soil Sci. Soc. Am. J. 44:892–898.

Vrugt, J. A., W. Bouten, and A. H. Weerts. 2001. Information content of data for identifying soil hydraulic parameters from outflow experiments. Soil Sci. Soc. Am. J. 65:19–27.

Vrugt, J., and W. Bouten. 2002. Toward improved identifiability of hydrologic model parameters: the information content of experimental data. Water Resour. Res. 38:doi:10.1029/2001WR001118.

Weerts, A., W. Bouten, and J. M. Verstraten. 1999. Simultaneous measurement of water retention and electrical conductivity in soils: Testing the mualem-friedman tortuosity model. Water Resour. Res. 35:1781–1787.

Wildenschild, D., J. Hopmans, C. Vaz, M. Rivers, and D. Rikard. 2002. Using X-ray computed tomography in hydrology: systems, resolutions, and limitations. J. Hydrol. 267:285–297.

Wildenschild, D., J. W. Hopmans, and J. Šimůnek. 2001. Flow Rate Dependence of Soil Hydraulic Characteristics. Soil Sci. Soc. Am. J. 65:35–48.

Yeh, W.-G. 1986. Review of parameter identification procedures in groundwater hydrology: The inverse problem. Water Resour. Res. 22:95–108.

Zachman, D., P. Duchateau, and A. Klute. 1981. The calibration of Richards equation for a draining column by parameter identification. Soil Sci. Soc. Am. J. 45:1012–1015.

Zurmühl, T. 1996. Evaluation of different boundary conditions for independent determination of hydraulic parameters using outflow methods. *In* J. Gottlieb, and P. DuChateau. (ed.) Parameter identification and inverse problems in hydrology, geology and ecology. Kluwer Academic Publishers. Netherlands. p. 165–184.

Zurmühl, T., and W. Durner. 1996. Modeling transient water and solute transport in a biporous soil. Water Resour. Res. 32:819–829.

Zurmühl, T., and W. Durner. 1998. Determination of parameters for bimodal hydraulic functions by inverse modeling. Soil Sci. Soc. Am. J. 62:874–880.

Appendix

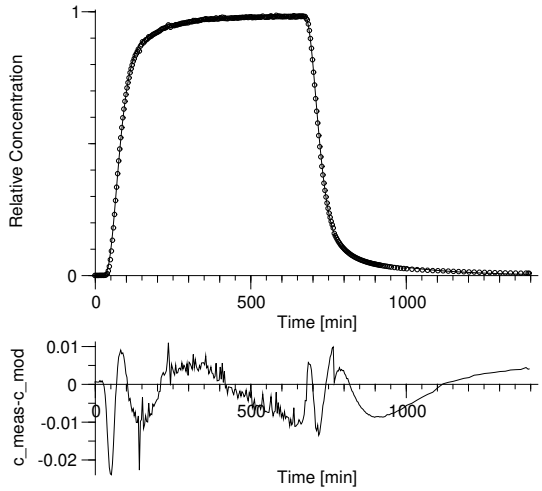

Figure A–1: Fit of the whole BTC for Brilliant Blue effluent from the coarse sand column at high flow rate with the cdftp-rl model, C_0 fixed

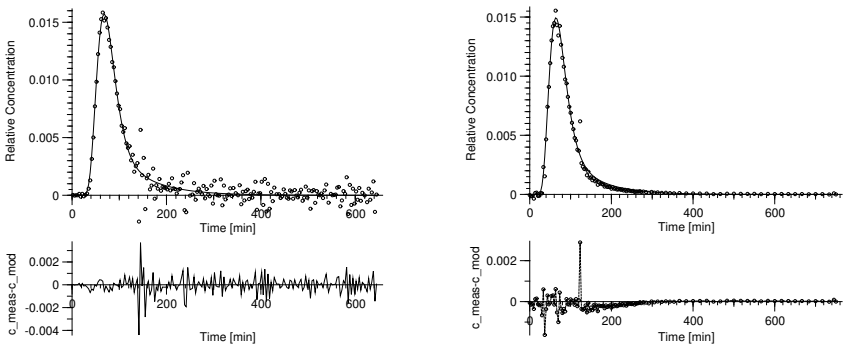

Figure A–2: Fits of the breakthrough limb (left) and the elution limb (right) of the BTC for Brilliant Blue effluent from the coarse sand column at high flow rate with the cdftd-rl model C_0 fixed—more noises generated especially for the breakthrough limb

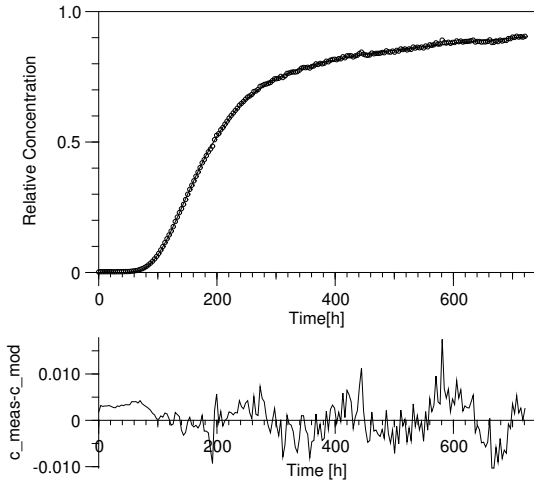

Figure A–3: Fit of the breakthrough limb of the BTC for Brilliant Blue effluent from the coarse sand column at low flow rate with the cdfts-rl model C_0 fixed, the solid line denoting the input concentration

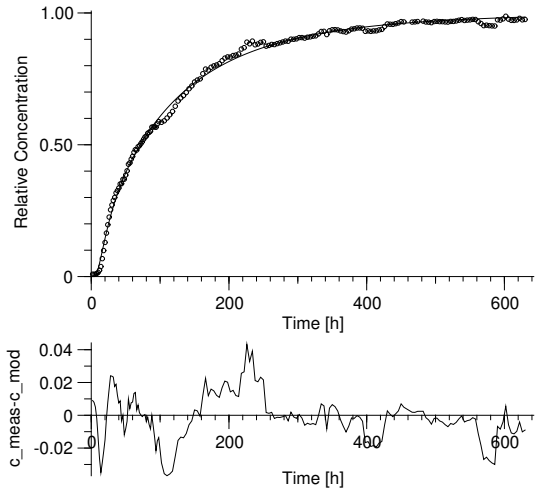

Figure A–4: Fit of the breakthrough limb of the BTC for Brilliant Blue effluent from the gravel column at low flow rate with the cdfts-rl model, C_0 fixed

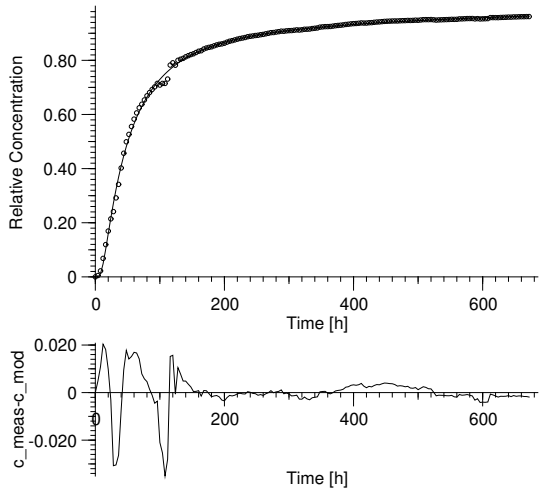

Figure A–5: Fit of the elution limb of the BTC for Brilliant Blue effluent from the gravel column at low flow rate with the cdfts-rl model, C_0 fixed

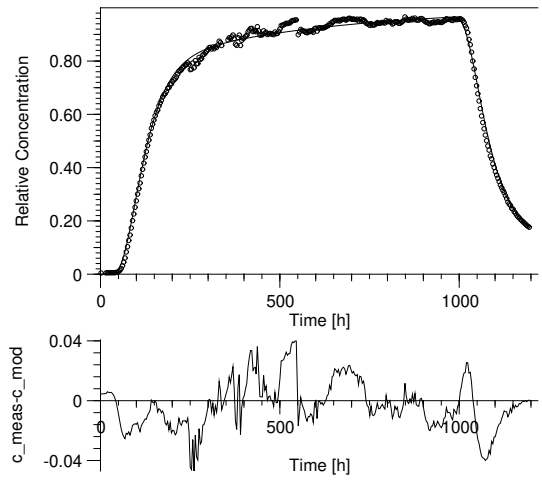

Figure A–6: Fit of the whole BTC for Brilliant Blue effluent from the mixed material column at low flow rate with the cdftp-rl model, C_0 fixed, solid line denoting the input concentration and the disturbance are caused by external disturbance

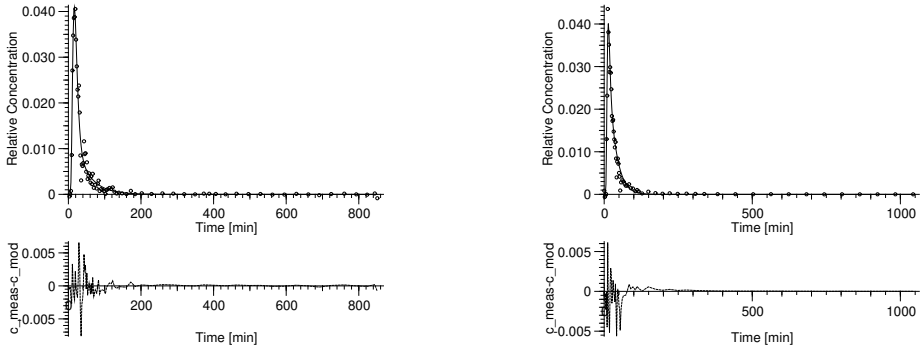

Figure A–7: Fit of the breakthrough limb (left) and the elution limb (right) of the BTC for Brilliant Blue effluent from the gravel column at high flow rate with the cdftd-rl model, C_0 fixed

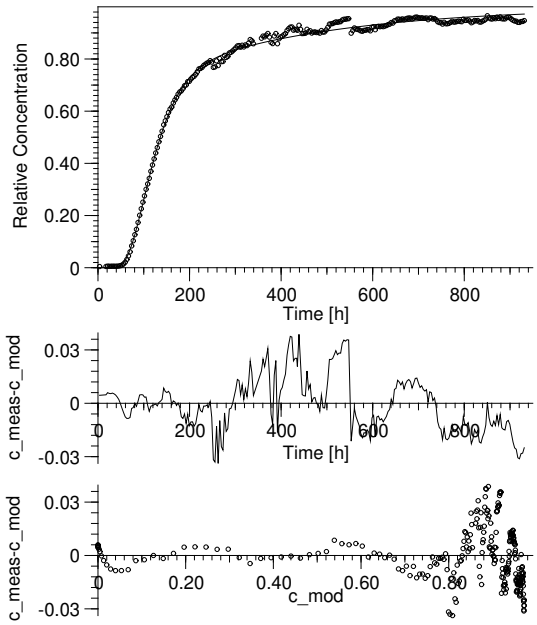

Figure A–8: Dye transport in the mixed material with low flow rate, fitted with cdfts-rl model, C_0 fitted

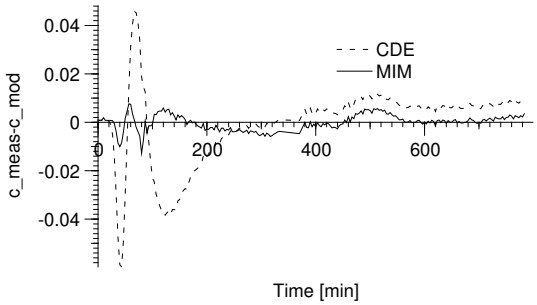

Figure A–9: Dye transport in the mixed material with high flow rate, deviations of the MIM and CD model from the measurement, C_0 fitted

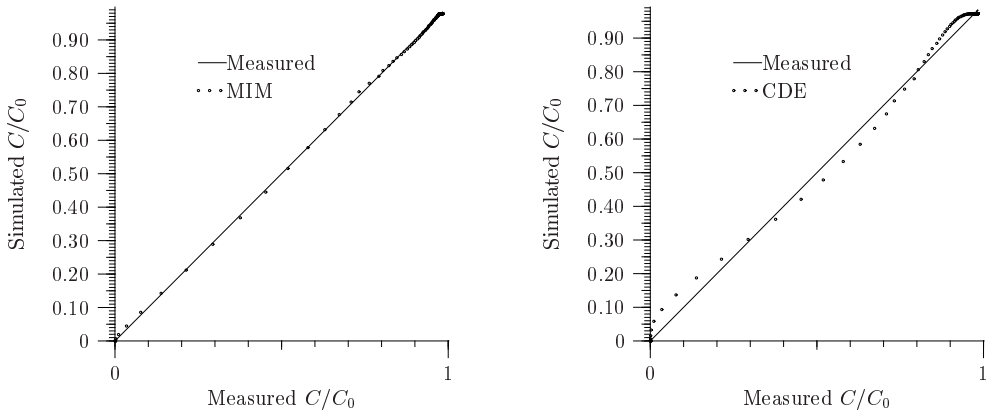

Figure A–10: Measured versus simulated relative concentration of Brilliant Blue effluent from the mixed material column under high flow rate condition using the CD model and the MIM model

ACKNOWLEDGEMENTS

I would like to acknowledge many people for helping me during my doctoral work. Expecially I want to thank my supervisor, Prof.Dr. Kurt Roth who offered me the chance to study in Germany, encouraged me to develop independent thinking and research skills throughout my academic work. I deeply thank him for the generous time, patient guidance and heuristic discussions.

I would like to thank Dr. Hans-Jörg Vogel for the introduction to laboratory experiments and numerical modeling and many valuable discussions. I could not forget every time I met trouble how he patiently helped me.

I am grateful to the soil physics group at IUP for the warm and friendly atmosphere during the last two years. I would like to thank especially Ute Wollschläger, Andreas Bayer, Holger Gerhards, Fereidoun Rezanezhad, Michael Stöhr, Volker Schultz, Anita Schmidt for their all-aspect help which cannot be enumerated here. Without the help of Andreas, Ute and Holger, I couldn't have the abstract of my thesis translated into German. I appreciate especially that Ute and Andreas spare their time proofreading my thesis.

I owe one special note of gratitude to my friends Haiwen Ge and Bingchao Song for their help in programming and computer problems.

I extend many thanks to Roswitha Marioth, the coordinator of the International Postgraduate Program. Without her arranging me to take German courses I could not have gained my basic German knowledge. I thank her for the warm care.

Last but not the least, I want to thank my husband Xiaozhong Qin and my daughter Yimei for their persevering and loving support.